DEVELOPMENT OF ANION–EXCHANGE MEMBRANES FOR ELECTROCHEMICAL APPLICATIONS

A THESIS

Submitted to the University of Calicut

for the award of the degree of

DOCTOR OF PHILOSOPHY

by

Moly P. P.

Department of Chemistry

Christ College

Irinjalakuda

MARCH 2018

DECLARATION

I, Moly P. P. hereby declare that the thesis entitled **"Development of anion–exchange membranes for electrochemical applications"** is a bonafide record of research work done by me under the guidance of Dr. V. T. JOY, Assistant Professor, Department of Chemistry, Christ College, Irinjalakuda for the award of the degree of Doctor of Philosophy in Chemistry of the University of Calicut and this thesis contains no material previously submitted for a degree, diploma, fellowship or other similar title of any other University.

Christ College, Irinjalakuda Moly P. P.

Date:

THESIS CERTIFICATE

This is to certify that the thesis entitled "**Development of anion–exchange membranes for electrochemical applications"** submitted by **Moly P. P.** to University of Calicut, for the award of the degree of Doctor of Philosophy is a bonafide record of research work carried out by her under my supervision. The contents of this thesis, in full or parts have not been submitted to any other institute or University for the award of any degree or diploma.

Irinjalakuda
Date

Research Guide
Dr. V. T. JOY
Assistant Professor
Department of Chemistry
Christ College, Irinjalakuda.

ACKNOWLEDGEMENTS

"Nothing is impossible for God"

God Almighty has showered his abundant grace on me and my work throughout the hectic journey of my research. I bow my head in gratitude before the kindly light which led me through this arduous path.

My sincere gratitude and indebtedness towards my guide and mentor, Dr. V. T. Joy, Assistant Professor, Department of Chemistry, Christ College, Irinjalakuda, is to be marked here for giving me an opportunity to work with him in the area of electrochemistry. His valuable guidance and support have been of great aid for my research work.

I express my heartfelt gratitude and tribute to Late Rev. Fr. Dr. Jose Thekkan C. M. I., former Principal, Christ College, Irinjalakuda for his love and prayers. A great teacher and spiritual guide, Rev. Fr. Jose Thekkan, had blessed me with boundless support and care. I place my gratitude before his fond memory.

I am grateful for the support and help extended by Dr. Mathew Paul Ukken, Head of Dept. of Chemistry and all the former heads of the Dept. of Chemistry, Christ College. I also thank all my teachers and non teaching staff members and students of Christ College, Irinjalakuda, for their support and encouragement given to me throughout my research.

It is with immense pleasure that I thank my dear friends, the research group at Christ College, Irinjalakuda, for their whole hearted support and friendship.

My family had been of tremendous support to me during all the difficult stages of my research work. I thank my parents, brothers, and parents, sisters, brothers in law at this point.

The unending support and consideration vested upon me by my husband Pius is unforgettable. My gratefulness to him is never-ending.

I also express my humble gratitude to the Principal and all the staff members of Little Flower College, Guruvayoor for the support and prayers extended to me for

availing faculty development programme and helping me to complete my research work in time.

I express my sincere gratitude to University of Calicut for providing all support for my research work. I gratefully acknowledge University Grants Commission of India for the financial support under Faculty Development Programme.

Moly P. P.

ABSTRACT

KEYWORDS: Nanoparticles, Crystal structure, X-ray diffraction, Anion-exchange membranes, Ion exchange Capacity, Ionic Conductivity, AC impedance analysis, galvanostatic charge-discharge, redox flow batteries.

In response to the needs of modern society and emerging ecological concerns, efficient, environmental friendly and economically viable energy conversion and storage systems are to be developed. Nowadays, modern electro-chemical energy conversion/storage technologies, such as fuel cells and redox flow batteries are capable of fulfilling these requirements. Over the past decade, the development of ion-exchange membranes has attracted great attention due to their increasing industrial applications. Ion-exchange membranes are the key component in batteries and fuel cells, as well as in many other electrochemical devices. The function of a membrane is to prevent cross mixing of the positive and negative electrolytes, while still allowing the transport of ions to complete the circuit during the passage of current. The membranes must have good ionic conductivity, chemically stability and mechanical strength to avoid damage during long term operations. Materials fulfilling these criteria involve complex reaction routes and are very expensive.

The work described in this thesis consists of synthesis and characterization of inorganic and organic anion-exchange materials and the development of heterogeneous and homogeneous anion exchange membranes. The composition of the ion-exchange material was optimized for best electrochemical performances. The electrochemical performance of the membranes prepared in this work was tested by studying the galvanostatic charge-discharge cycles of an all-iron redox flow cell.

Chapter 1 gives an overview of the importance of ion-exchange membranes in the electrochemical applications. This chapter also includes a brief description of the development of ion-exchange membrane technology, classification of ion-exchange membranes, transport mechanisms in anion-exchange membranes, chemical stability of anion-exchange membranes, strategies for improving the chemical stability of AEMs, AEM fabrication methods and the applications of anion-exchange membranes in electrochemical devices like flow batteries and fuel cells.

Chapter 2 deals with experimental techniques that are employed for the characterization of the anion-exchange materials and membranes developed in the present work. These techniques include FI-IR, SEM, TEM, XRD, EDAX, TGA, and TS measurements. The procedures for the measurement of ion-exchange capacity, water uptake, alkaline stability, oxidative stability methanol permeability, ionic conductivity of the membranes by AC impedance measurements are also described. The study of electrochemical performance of an all-iron flow battery during the galvanostatic charge-discharge cycles using the anion-exchange membranes developed in the present work as separators are also described.

Chapter 3 presents synthesis and characterization of calcium titanate (perovskite) nanopowder as anion-exchange material by precipitation from a solution of potassium titanyl oxalate and calcium chloride in ammoniacal medium followed by filtration, drying and calcination. The XRD pattern showed the formation of phase pure orthorhombic calcium titanate. The crystalline nature of the particles was also exhibited by HRTEM image. Selected area electron diffraction (SAED) pattern shows the crystalline nature of the material. Morphological features investigated with SEM, reveals that the $CaTiO_3$ nanoparticles are having spherical shape.

Chapter 4 describes the preparation of calcium titanate incorporated polyvinyl alcohol nanocomposite anion-exchange membranes. The $CaTiO_3$ was synthesized by a new co-precipitation method as described in chapter 3. The PVA/$CaTiO_3$ nanocomposite membranes were fabricated by solution casting method from a well dispersed suspension of $CaTiO_3$ in PVA and characterized by techniques like FT-IR, TGA, SEM, AC impedance analysis and tensile strength measurements. The membranes possess ionic conductivity of 66 mS cm^{-1} at room temperature. The electrochemical performance of an all-iron redox flow cell was studied using galvanostatic charge-discharge tests using the above nanocomposite membrane as separator and a coulombic efficiency of 75% and more were observed during repeated charge-discharge cycles.

Chapter 5 presents the fabrication and characterization of of a stable anion exchange membrane by chemical modification of polyvinyl alcohol by oxidation of PVA to polyvinyl ketone with $KMnO_4$ followed by guanidination reaction and cross-linking

with glutraldehyde. Through this approach chemically stable, mechanically robust membranes with good ionic conductivity were developed. The characterization of the membrane was done using ATR FT-IR spectroscopy, SEM, TGA, AC impedance analysis, and tensile strength measurements. The physical properties of the membranes like water up-take, ion exchange capacity, methanol permeability and chemical stability were also measured. It was found that the membranes possess high ionic conductivity of approximately 71mS cm^{-1} at room temperature.

Chapter 6 deals with development and characterization of anion-exchange membranes for electrochemical devices by chemical functionalization of phenol-formaldehyde resins. The anion-exchange material was synthesized by polycondensation of phenol, formaldehyde and guanidine. The anion-exchange membranes were prepared by effectively incorporating the anion-exchange material into the matrix of PVC polymer. FT-IR spectroscopy was used to characterize the chemical structure of the synthesized anion-exchange material and the membranes. The characterization of the membranes were done using TGA, SEM, AC impedance, IEC, water uptake, methanol permeability test and alkaline stability tests. The membranes possess ionic conductivity of the order of 70 mS cm^{-1} at room temperature. The electrochemical performance of an all-iron redox flow cell was studied using galvanostatic charge-discharge tests using the above membrane as separator and the system exhibited a columbic efficiency of 80% and more were observed during the repeated charge-discharge cycles.

LIST OF FIGURES

Page No.

TABLE OF CONTENTS

CHAPTER 1

INTRODUCTION

1.1 Green energy resources: Need and prospects

Over the last decade, a growing demand on the deployment of efficient and cost effective renewable energy resources has been observed as a result of several factors. One of them is global environmental issues due to the emission of green house gases (GHGs). A second factor is the limited availability of fossil fuels including coal and oil [1]. Energy is directly related to the key global challenges such as poverty alleviation, climate change, global environmental issues and food security [2,3].

In 1988, two UN bodies—UNEP (United Nations Environment Programme) and the World Meteorological Organization (WMO)—came together to establish the Intergovernmental Panel on Climate Change (IPCC). The Panel consisting of thousands of leading scientists and experts contributing on a voluntary basis, reviews scientific research on the issue, with a view to find solution for issues associated with energy and environment. In recognition of its work, the Panel was awarded the 2007 Nobel Peace Prize, together with former United States Vice President Albert Arnold Gore, Jr. [4]. A transition to renewable and low-carbon forms of energy is being widely debated as a means of securing a sustainable future for the development of the society. Global demand for energy is rising fast as the population increases, especially in countries such as China and India. The International Energy Agency (IEA) says the world's energy needs could be 50% higher in 2030 than they are today [5].

In 1997, in Kyoto, Japan, more than 150 industrialized nations agreed to reduce their greenhouse gas emissions, as part of an international agreement on climate change called the Kyoto Protocol. Based on the protocol and the report of the IPCC on carbon capture and storage, there is an emerging need to reduce the emission of CO_2 to the atmosphere [2,6].

The most used sources of renewable energy include biofuels, photovoltaics, wind, ocean currents, geothermal, tidal and hydroelectric power [7]. Among these resources most abundant and sustainable energy sources are considered to be solar and wind power. To be competitive with existing energy resources, renewable energy needs to be cost effective and reliable. However, successful incorporation of these resources into the existing infrastructure is difficult due to the lack of an efficient means for energy storage [8]. In response to the needs of modern society and emerging ecological concerns, efficient, environmental friendly and economically viable energy conversion and storage systems are to be developed. Nowadays, modern electro-chemical energy conversion/storage technologies, such as fuel cells and redox flow batteries are believed to be capable of fulfilling these requirements [9,10].

1.2. Ion exchange membranes

Ion-exchange membranes (IEMs) have potential applications in various fields to overcome the problems related to energy crisis and environmental pollution. IEMs are found to be a key component in electrochemical technologies such as polymer electrolyte membrane fuel cells [11,12], redox flow batteries [10,13], hydrogen production through water electrolysis [14], water treatment [15,16] and gas purification [17]. The function of a membrane is to prevent cross-mixing of the positive and negative electrolytes, while still allowing the transport of ions to complete the circuit during the passage of current [18,19].

1.3. Development of membrane technology

The study of semipermeable membranes by Ostwald in 1890 lead to the development of ion-exchange membrane based process and found that a membrane can be impermeable to any electrolyte only if it is impermeable either for its cation or its anion [20,21]. The basic studies related to IEMs were started by Michaelis and Fujita in 1925 by using homogeneous, weak acid collodium membranes [22]. Amphoteric membrane containing both negatively and positively charged ion exchange groups were presented by S¨ollner in 1930 [23]. Around 1940, ion-exchange membranes based on phenol-formaldehyde resins were developed for industrial purposes from phenol sulfonic acid and formaldehyde solution [24]. Meyer and Strauss developed an

electrodialysis process in which anion-exchange and cation exchange membranes were arranged in alternating series to form many parallel solution compartments between two electrodes [25]. Electrodialysis based on IEMs became an industrial process for demineralization and concentration of electrolyte solutions. In 1960s, Asahi Co. developed methods for salt production from sea water with ion-exchange membranes [26]. In 1970s, Dupont successfully developed a chemically stable cation exchange membrane Nafion, based on sulfonated polytetra-fluoroethylene, which finds application in the chloralkali production industry and energy storage and conversion system [27,28]. The basic chemical structure of ion-exchange membrane consists of hydrophobic substrates, immobilized ion-functionalized groups, and movable counter-ions. The ion-functionalized groups attached onto the polymer backbone will release cations or anions in aqueous medium depending on the functional groups attached [29].

1.4 Classification of Ion-exchange membranes

Classification of ion-exchange membranes are based on

1. Ion-exchange groups attached
2. Materials constituting the membranes
3. Microstructure of the membranes

1.4.1 Classification based on the ion-exchange groups attached

Ion-exchange membranes are classified into anion-exchange membranes and cation-exchange membranes depending on the nature of ion-exchange groups attached to the polymer backbone [29,30].

1. Cation-exchange membranes:

These types of membranes have cation-exchange groups (anionic charged groups) such as sulfonic acid, carboxylic acid, phosphoric acid, hydroxyl groups of phenol, thiol, perfluorotertiary alcohol groups etc., fixed to the polymer backbone of the membrane that provide a negative fixed charge in aqueous or mixed water and organic solvent solutions and allows only cations to selectively permeate through the membrane.

2. Anion-exchange membranes:

These type of membranes have anion-exchange groups (cationic charged groups), like quarternary ammonium, guanidium, phosphonium, sulfonium etc. fixed to the polymer backbone of the membrane that provide a positive fixed charge in aqueous or mixed water and organic solvent solutions and allows only anions to selectively permeate through the membrane.

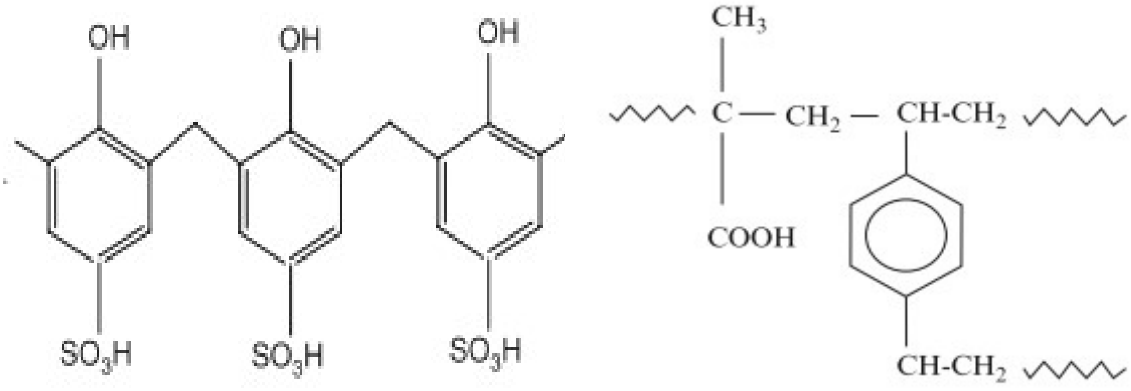

Fig. 1 Chemical structures of cation-exchange membranes [31]

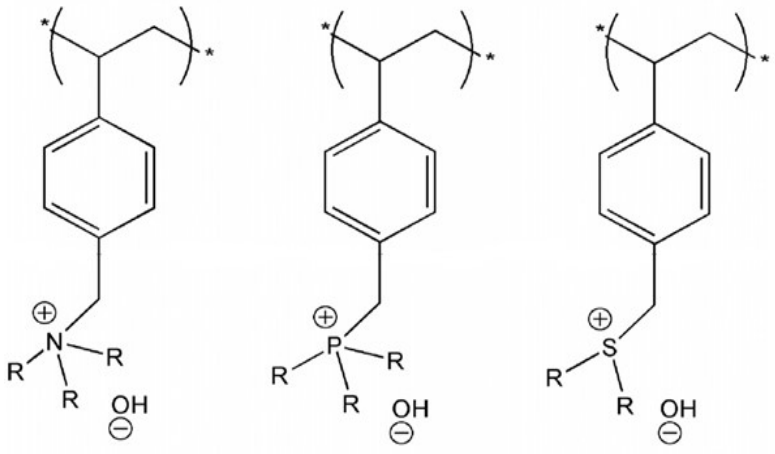

Fig. 2 Chemical structure of anion-exchange membranes [9]

3. Amphoteric ion-exchange membranes, in which both cation and anion-exchange groups exist at random throughout the membranes.

1.4.2 Classification based on the materials

Materials used for IEMs are generally classified into different membrane systems as follows [32]

1. Perfluorinated and partially fluorinated polymer backbones.

Fluorine-containing polymers are commonly used due to their chemical stability, thermal stability and easily tunable properties using radiation grafting method. The fluoropolymer backbones used as membrane materials for fuel cells can be divided into two categories [33].

(1) perfluorinated polymers
(2) partially fluorinated polymers

A perfluorinated compound is an organo-fluorine compound containing only C-F and C-C bonds and no C-H bonds but contains other hetero atoms. Currently used polymer membranes in portable fuel cell applications have perfluorinated structures with attached sulfonic acid groups. The perfluorinated polymer, Nafion, is most extensively used and produced by DuPont. Similar polymers are Flemion by Asahi Glass and Aciplex-S produced by Asahi Chemical. Poly(tetrafluoro ethylene -co-hexafluoro propylene), poly(tetrafluoro ethylene-co-perfluoro propyl vinyl ether) (PFA), and poly(tetrafluoro ethylene) (PTFE) are the other commonly used perfluorinated polymers.

Partially fluorinated polymers include poly(vinylidene fluoride-co-hexafluoro propylene) (PVDF-co-HFP), poly(vinyl fluoride) (PVF), poly(vinylidene fluoride) (PVDF), poly(ethylene-alt-tetrafluoro ethylene) (ETFE), and poly(chlorotri-fluoro ethylene) (PCTFE).

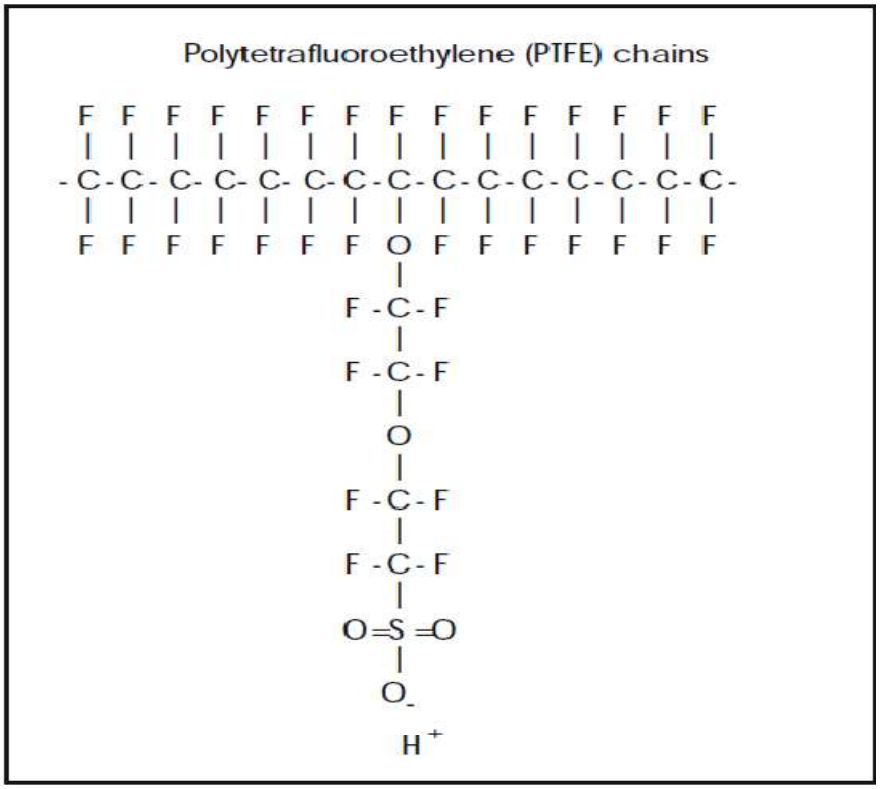

Fig. 3 Chemical structure of Nafion membrane

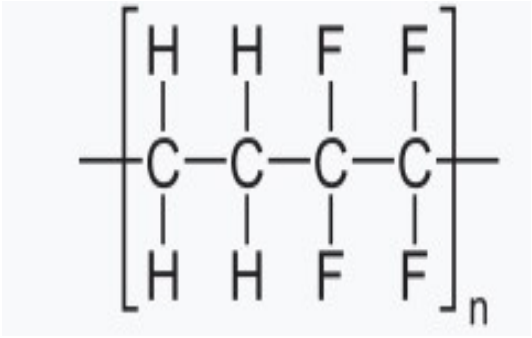

Fig. 4 Chemical structure of ethylene tetrafluoroethylene (ETFE)

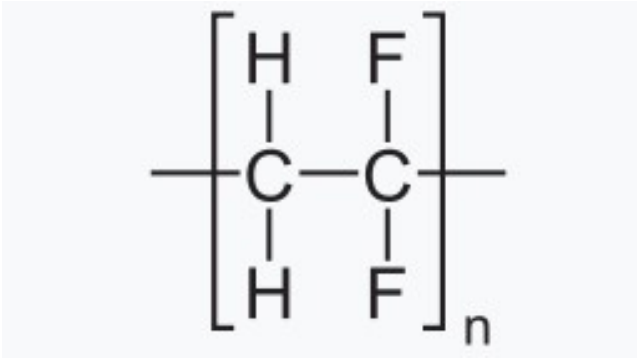

Fig. 5 Chemical structure of poly(vinylidene fluoride)

3. Non-fluorinated membranes with aromatic backbone

Aromatic hydrocarbons can be modified with suitable functional groups to render them suitable for conduction of ions. This type of membranes include sulfonated poly ether ketones (SPEEK) consisting of polyarylenes linked through varying sequences of ether (E) and ketone (K) units to give ether rich SPEEK. Poly(phenylene sulfide) (PPS) and poly(phenylene oxide) (PPO) can be sulfonated in concentrated sulfuric acid to get SPPS and SPPO [34]. Low cost ion-exchange membranes can be produced from sulfonated polystyrene. This material is composed of sulfonated styrene copolymers, obtained by sulfonating styrene-(ethylene-butylene)-styrene (SEBS) copolymer [35].

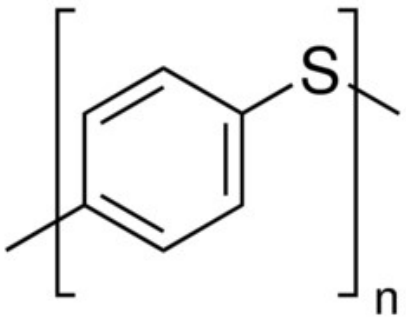

Fig. 6 Chemical structure of Poly(phenylene sulfide)

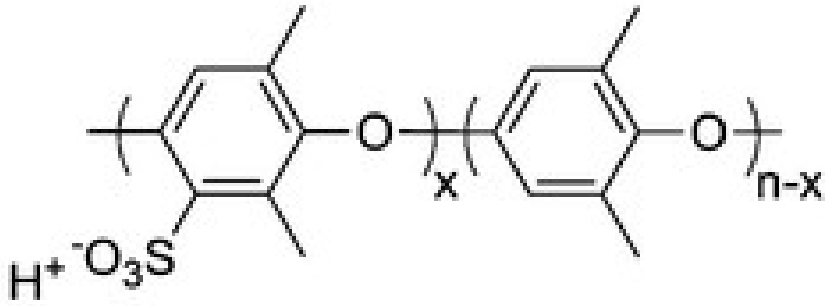

Fig. 7 Chemical structure of Sulfonated poly(phenylene oxide)

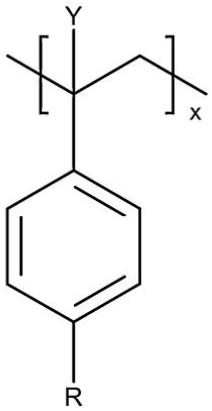

Fig. 8 Basic structure of chemically modified polystyrene

4. Non-fluorinated hydrocarbons

The most promising alternative materials that are capable of producing low cost membranes are non-fluorinated hydrocarbons. These include polymer films of polyethylene (PE), polypropylene (PP), and polyvinyl chloride (PVC).

5. Acid–base blends.

Acid–base blends used as membrane materials are prepared by incorporating an acid component into an alkaline polymer base to promote ionic conduction. Acid–base blends can maintain high conductivity at elevated temperatures without suffering from dehydration effects of Nafion. For example polybenzimidazole doped with phosphoric

acid (PBI/H_3PO_4), polybenzimidazole doped with sulphuric acid (PBI/H_2SO_4), sulfonated polyether ether ketone (SPEEK)/PBI can be used as membrane materials.

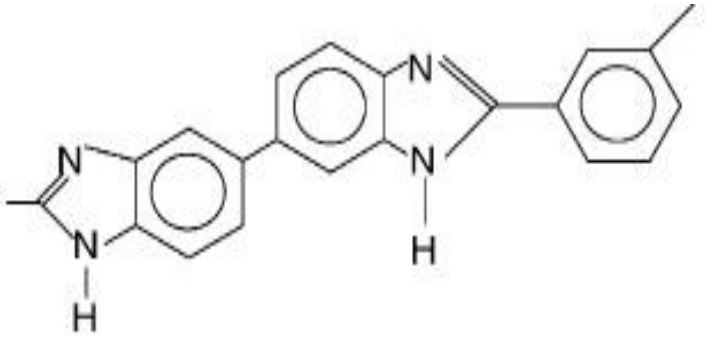

Fig. 9 Chemical structure of polybenzimidazole

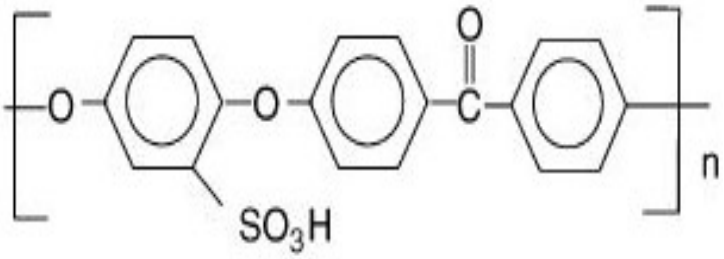

Fig. 10 Chemical structure of sulfonated polyether ether ketone (SPEEK)

1.4.3 Classification based on the microstructure:

Based on the microstructure, ion-exchange membranes are classified into two categories

1. Heterogeneous membranes
2. Homogeneous membranes

In heterogeneous membranes the ion-exchange groups are distributed throughout a polymer matrix which provides a mechanical support. Membranes based on polyethylene oxide (PEO) polymers with oxyethylene chains, containing KOH is one of the most extensively studied heterogeneous anion-exchange membrane [9].

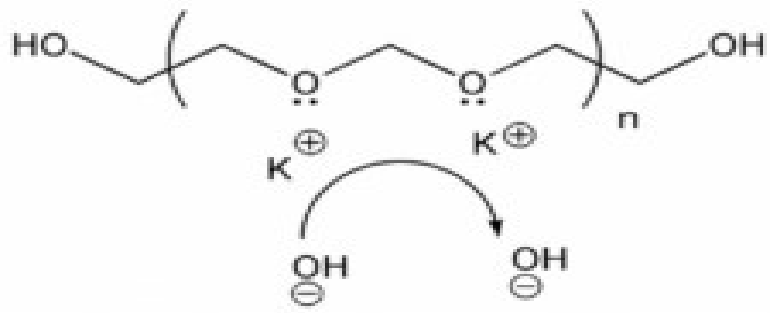

Fig. 11 Chemical structure of polyethylene oxide (PEO) polymers doped with KOH

In homogeneous membrane, the ion-exchange groups are covalently bound to the polymer backbone forming a one-phase system. These membranes contain ionic sites such as quaternary ammonium groups grafted on the skeleton of the polymer chain. A mobile counter ion is associated with each ionic function in order to preserve the electro-neutrality of the polymer. These types of membranes are fabricated by following methods [36].

1. Preparation of membranes by polycondensation reaction

Under this category, at least one of the monomers must contain a moiety that can be made cationic or anionic. The first membrane made by polycondensation of monomer followed by cross-linking with formaldehyde was of phenolsulfonic acid. The preparation scheme is presented in **Fig.**12.

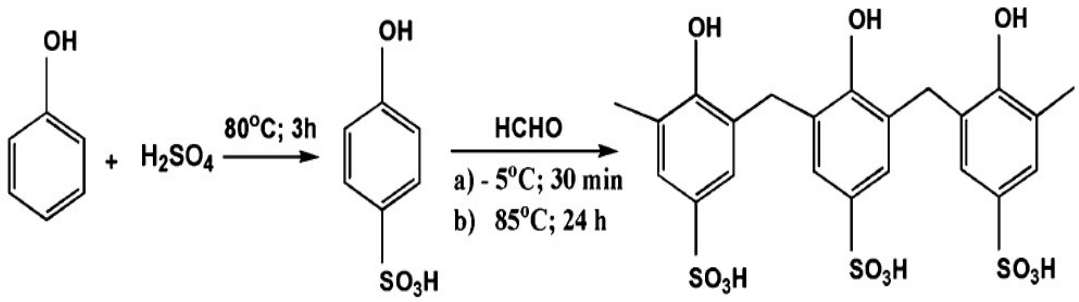

Fig. 12 Reaction of phenolsulfonic acid with formaldehyde [37]

2. Introduction of cationic characters on a preformed film using radiation grafting methods.

The synthesis of an anion-exchange membrane based on ETFE is as follows. The film of ETFE is irradiated with an electron beam and the irradiated film is immersed in vinyl benzyl chloride solution. The resulting grafted poly(vinyl benzyl chloride) copolymer film is soaked in trimethylamine solution to obtain quaternary ammonium groups. Then an alkaline exchange process is done by dipping the membrane into KOH solution.

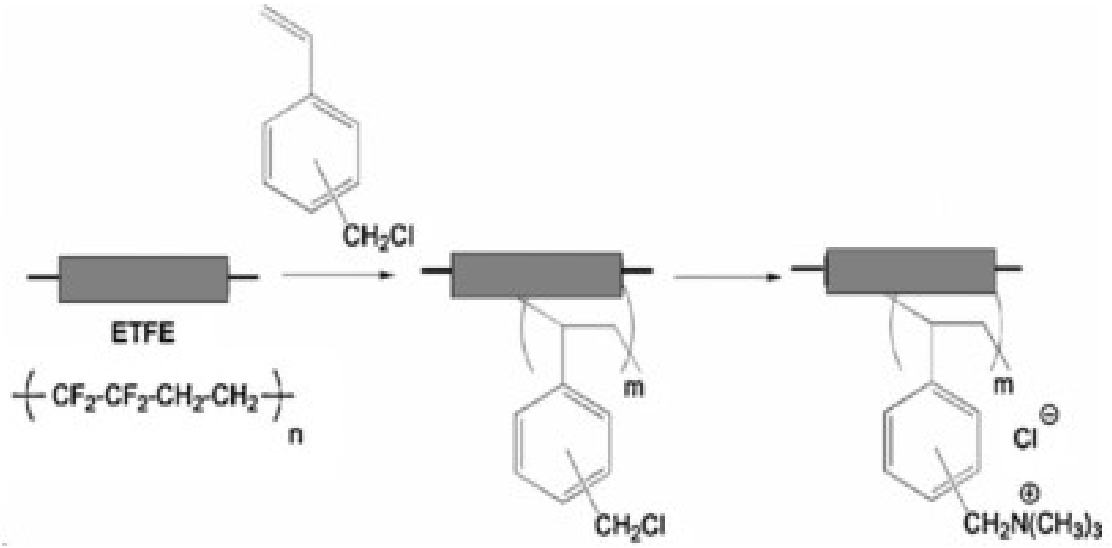

Fig. 13 The synthesis of a radiation-grafted ETFE AEM [37]

3. Chemical modification of a polymer film.

The membranes based on chloro-methyl styrene and divinyl benzene are used as starting materials. The membrane is prepared in three steps: copolymerization, chloromethylation and quaternary amination.

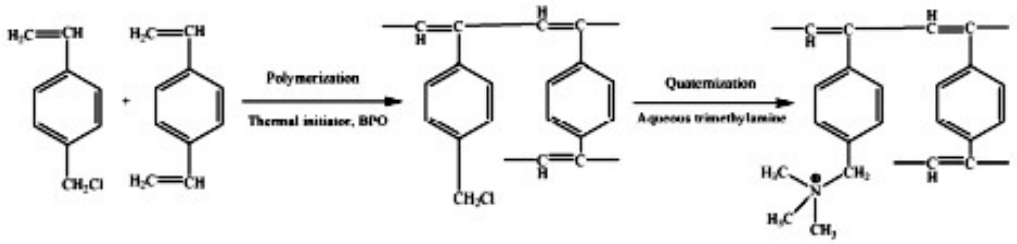

Fig. 14 Chemical structure of chloromethyl styrene-divinyl benzene anion-exchange membrane

1.5 Desired properties of the anion-exchange membranes

In recent years, much effort has been made to develop AEMs for energy storage applications. The membranes are required not only to conduct anions, but also to serve as a barrier for the fuel and electrolytes. The AEM is one of the core components which determines the performance of electrochemical devices like flow batteries and fuel cells [9]. A successful commercial AEM must possess high anion conductivity, good chemical stability, better mechanical strength and cheap. The ionic conductivity of the membranes must be high enough to support a large current. This can be improved by increasing the amount of cationic groups in the membrane; however it causes a loss of the mechanical properties by promoting excessive water uptake. Therefore, optimization of the membrane composition is required to improve the mechanical properties [9]. In summary, the primary requirements of AEMs for practical application are the following:

- Good mechanical and thermal stability
- High anionic conductivity
- High electrical resistance to the flow of electrons
- Low thickness (50–80 μm) in order to reduce the resistance to the flow of electrons
- Low cost.

1.6. Transport mechanisms in anion-exchange membranes

The mechanism of hydroxide ion transport through AEMs include Grotthuss mechanism, diffusion, convection and surface site hopping [9]. The majority of hydroxide ions are transported through AEMs by the Grotthuss mechanism in aqueous solutions [38]. According to Grotthuss mechanism, hydroxide ions diffuse through the hydrogen-bonded network of water molecules through the formation and cleavage of covalent bonds. Hydroxyl ion transport in diffusive mechanism occurs in the presence of a concentration gradient or electrical potential gradient. In convection mechanism hydroxyl ion transport takes place when it moves through the membrane, dragging water molecules with them. Surface site hopping of hydroxyl anions in the presence of quaternary ammonium groups is considered as a secondary transport across the

membrane where the water present in the system acts as a permanent dipole and interacts with the fixed charges of the membrane [9].

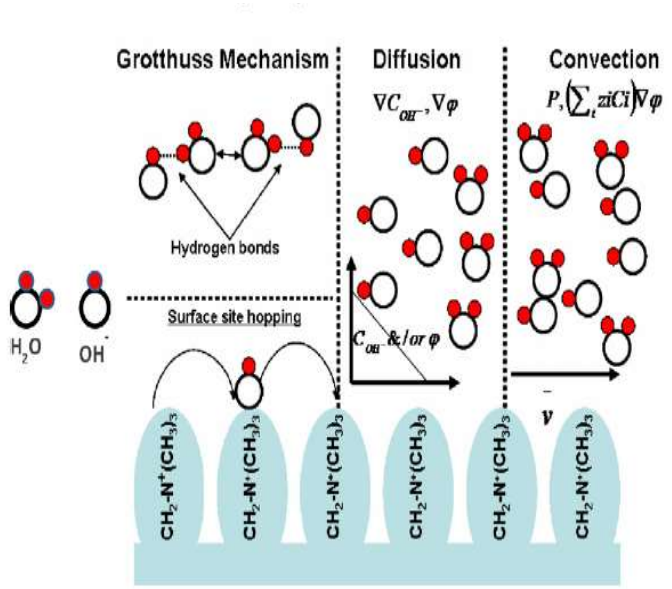

Fig. 15 Transport mechanism for hydroxide ions in the anion-exchange membrane [9]

1.7. Chemical stability of anion-exchange membranes

A major challenge in the development of AEMs is their chemical stability. The degradation of the polymer backbone and the cationic groups of the membrane occurs at high pH and highly oxidative environments [11,39,40]. Degradation of the polymer backbone is mainly due to the hydroxyl attack or by strong oxidative environments. AEMs based on polyvinylidene fluoride (PVDF) and vinylidene fluoride (VDF) copolymers undergoes degradation in high pH and oxidative environments [41]. Due to fast degradation, the membranes get darkened and exhibits poor mechanical strength during operating conditions. VDF and PVDF are therefore not recommended as starting materials for AEMs. Polysulfones [42] and fluorocarbon [33] based AEMs developed by radiation-induced grafting of cationic moieties show better chemical stability for polymer backbone.

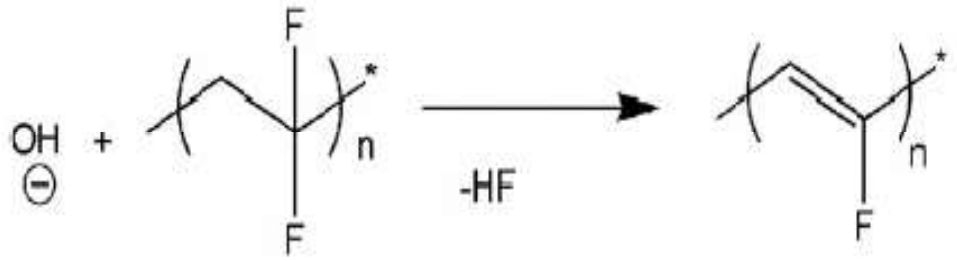

Fig. 16 Degradation of PVDF in alkaline media

1.7.1 Mechanism of degradation of cationic groups

Cationic groups such as ammonium, phosphonium, sulfonium, pyridinium, guanidinium, and imidazolium groups are used as anion-exchange sites in the AEMs [29,37,40]. The mechanism of degradation includes either elimination or substitution processes. The cleavage of the quaternary ammonium by OH^- attack followed by elimination is called Hoffmann degradation or E_2 elimination (**Fig.**18). The hydroxyl ions attack a beta-hydrogen of the ammonium leading to the formation of an alkene, an amine and a water molecule [43].

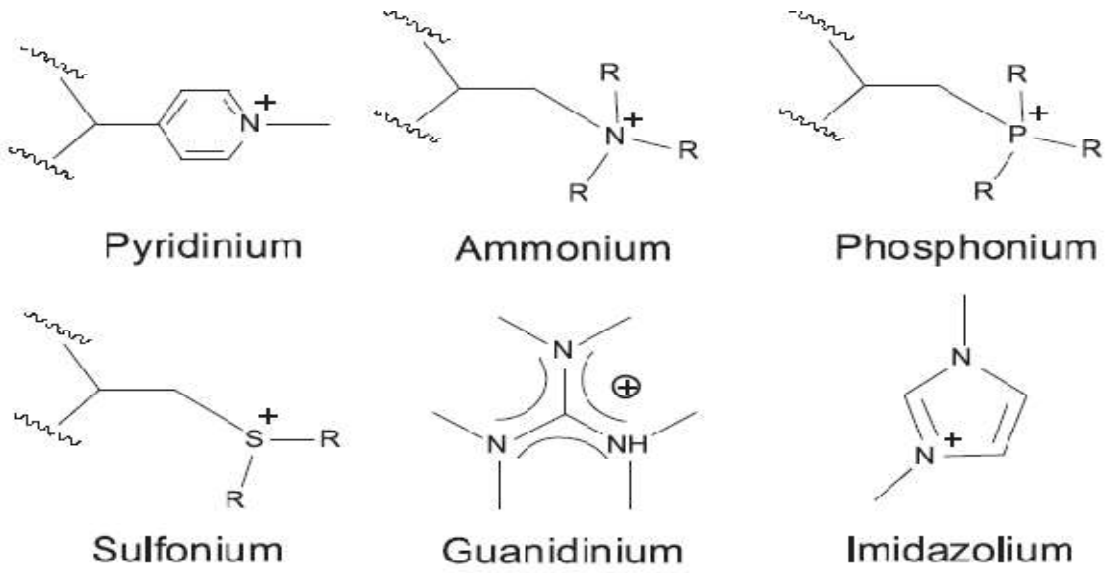

Fig. 17 Cationic groups used as anion-exchange sites

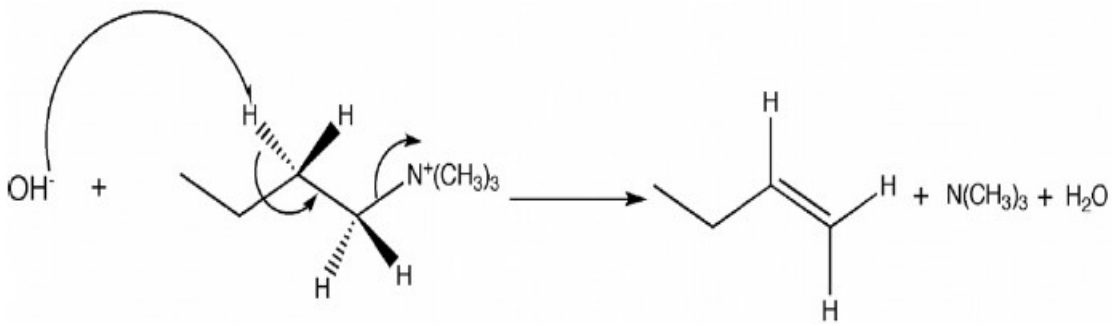

Fig. 18 Degradation of the ammonium groups in alkaline media by E_2 elimination

When bulky groups are present on the quarternary ammonium group, E_1 elimination occurs. This elimination occurs on the carbon located in the alpha or the beta position of the ammonium group [44]. Here the hydroxyl ions attack the hydrogen of the methyl group belonging to the ammonium followed by a rearrangement leading to the formation of an alkene and an amine **Fig.** 19.

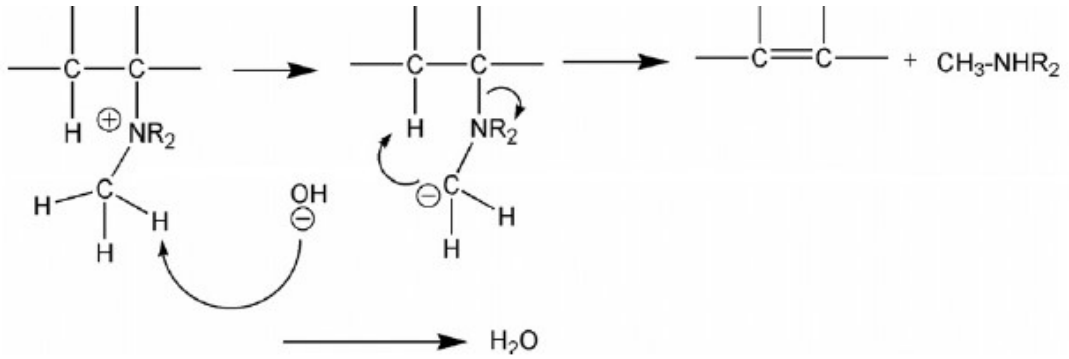

Fig. 19 Degradation of the ammonium groups in alkaline media by E_1 elimination [44]

The degradation mechanism by nucleophilic substitution (SN^2) results from the hydroxyl attack on alpha-hydrogen of the quaternary ammonium group (**Fig.** 20). Alcohol and amine are formed. The unstable cationic group causes considerable reduction of ionic conductivity, limiting the AEM's durability and hence its application in electrochemical devices [45].

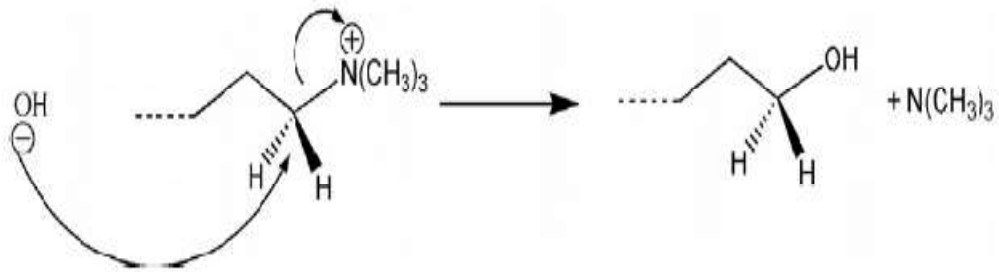

Fig. 20 Degradation of the ammonium groups in alkaline media by (SN^2) nucleophilic substitution [45]

1.7.2 Strategies for improving the chemical stability of AEMs

Quaternary ammonium is the most widely used cationic groups for AEMs despite its decomposition issue. To improve alkaline stability of the AEMs Tomoi et al. introduced a spacer chain longer than three carbon atoms between the quaternary nitrogen atom and the benzene ring of the main chain [46]. Hibbs et al. introduced hexamethylene trimethyl ammonium group in the poly(phenylene) AEMs and membranes showed better stability than the membranes containing benzyl trimethylammonium [47]. Modified membranes exhibited only a 5% conductivity loss after immersion in 4 M KOH at 90°C for 14 days instead of a 33% loss of conductivity in the benzyl trimethylammonium group containing membrane. The improved alkaline stability of membranes by the introduction of a long alkyl chain between the quaternary nitrogen atom and the benzene ring of the main chain can be explained based on computation chemistry and simulation studies besides the sterric effect produced by long alkyl group. As the spacer length is equivalent to a long side chain, it may alter the hydration state of the cations and thus influence their interaction with hydroxide [31].

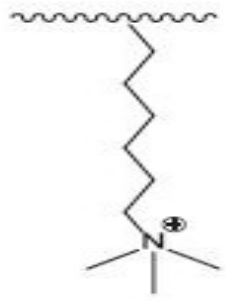

Fig. 21 AAEM materials functionalized with hexamethylene-trimethylammonium cation [30]

Imidazolium cations and their modifications

As an alternative to quaternary ammonium, imidazolium group was recently introduced and found to be stable due to its resonance structures, where the positive charge is delocalized over the ring and its interaction with hydroxide ion can be weakened [48]. For further improvement of imidazolium stability, C_2-substituted imidazolium model compounds and corresponding AEMs were synthesized and analyzed [49]. The alkali induced degradation of imidazolium cations is mainly due to the nucleophilic OH^- attack on the imidazole ring at the C_2 position. Price et al. improved the imidazolium stability by methyl substitution on the C_2 position, and the ring-opening decomposition of imidazolium was avoided [50]. These membranes exhibited good chemical stability and its conductivity degraded only 15.82 % after immersing in 4M KOH solution at 80°C for 240 h.

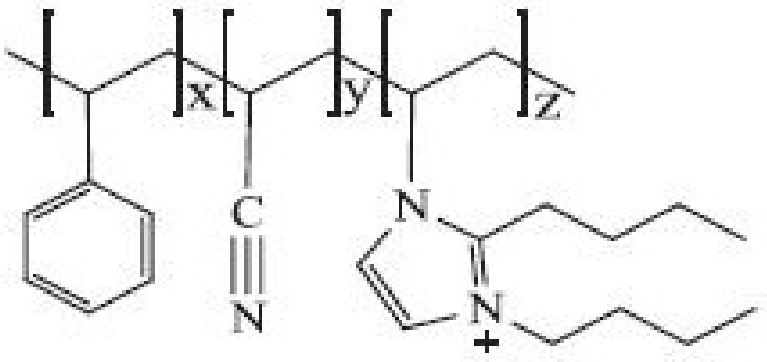

Fig. 22 Chemical structure of AEMs with N_1, C_2 and N_3 Substituted imidazolium cations [30]

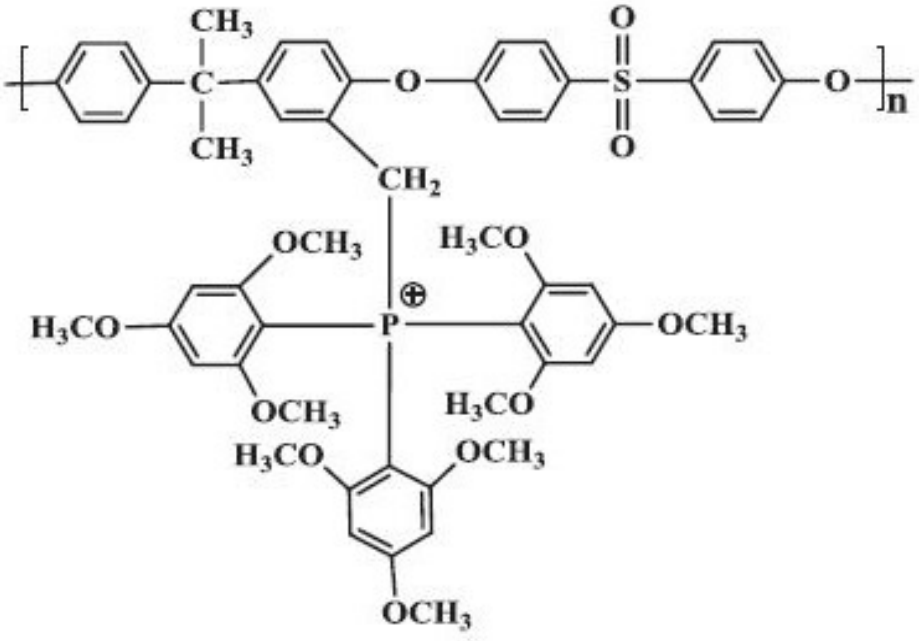

Fig. 23 Chemical structure of quaternary phosphonium functionalized polyether sulfone

AEMs with other novel cation groups

In the past few years AEMs containing novel cations like quaternary phosphonium, and guanidinium have also introduced. Among these novel cation groups, guanidinium is found to be most stable one due to resonance stabilization. The high alkalinity of guanidines yields high concentration of mobile hydroxide ions and thus makes the membrane highly conductive [51,52]. Therefore, many researchers designed and synthesized guanidinium functionalized polymers for alkaline AEM fabrication, these membranes showed a promising conductivity of 23-36 mS cm^{-1} after immersing in 0.5M NaOH for 38 h and excellent chemical stability [11,53].

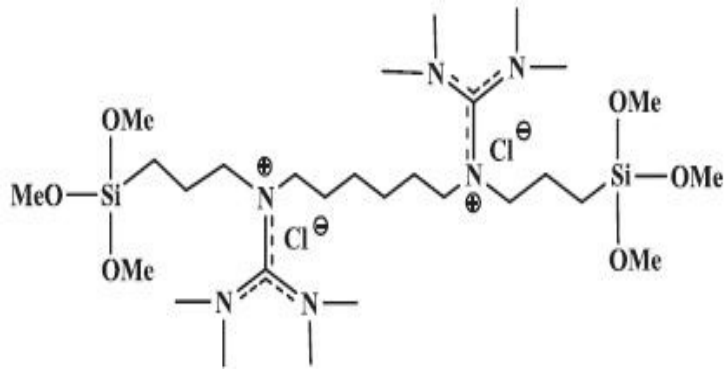

Fig. 24 Chemical structure of biguanidium-bridged silsesquioxane

One more novel cation for AEM is quaternary phosphonium. Yan et al. [38] reported a polysulfone ionomer containing this cation (**Fig.** 23). The stability is associated with the special phosphomium cation structure, consisting of three bulky trimethoxyphenyl groups surrounding the phosphorous atom protect the cation from hydroxide attack and increase the free volume of polymer chains, leading to good stability, high conductivity and alkaline stability. Yan and co-workers made a conclusion that both electron donating groups attached to the cation and steric hindrance of the substituted groups are effective in improving the AEM durability under alkaline conditions [54]. The phosphonium modified membranes showed a conductivity of 27 mS cm^{-1} at 20°C, and good alkaline stability. The membranes made of this ionomer maintained their ionic conductivity and mechanical properties even after immersion in 10M KOH solution at room temperature for 48 h and there is no decrease of ionic conductivity after immersion in 1M KOH for 30 days at 60°C.

Effect of cross-linking

Cross-linking can improve the chemical stability of AEMs [55]. Cross-linked macromolecules form a network, reducing the free volume between the main chains, and thus the attack of hydroxide ions on the cations become more difficult [56]. Na et al. synthesized novel self-cross-linked poly(ethersulfone) AEMs which showed high dimensional stability and good alkaline stability [46]. The resulting cross-linked copolymer membranes exhibited a negligible decrease in ionic-conductivity under a wide temperature range of 20-80°C after immersion in 1M NaOH for 30 days. Yan et al synthesized cross-linked AEMs based on the alkaline imidazolium type ionic liquids via in situ cross-linking of 1-vinyl-3-methylimidazolium iodide with styrene and acrylonitrile, and followed by anion-exchange with hydroxide ions [57]. The conductivity of the membrane was 83 mS cm^{-1} with an ion-exchange capacity of 2.19 m mol g^{-1}. But the mechanical properties of the membranes were insufficient for fuel cell applications.

Composite polymer membrane

Another interesting option is metal-ion intercalation method. Yang and co-workers fabricated PVA/TiO_2 composite polymer membrane by solution casting method and the composite polymer membrane exhibited enhanced chemical, thermal and mechanical stabilities. [55]. Zeng et al. synthesized cross-linked poly(vinyl alcohol) (PVA)/LDH composite membranes by intercalating PVA polymer into layered structures of Mg-Al layered double hydroxides (LDHs) uniformly, the membranes exhibited only a slight conductivity decrease from 23.9 to 22.7 mS cm^{-1} when used in a direct ethanol fuel cell for more than 80 h at 80°C [58] .

Recently, Cuiyan Tong et al. reported a new type of nano composite membrane by incorporating quaternized graphene into the matrix of chloromethylated polysulfone (CMPSU) [59]. The nanocomposite membrane exhibited excellent hydroxide conductivity 85 mS cm^{-1} at 65°C and good chemical stability in a boiling solution of 6M KOH for 21 days and a peak power density of 86.68 mW cm^{-2} when the nanocomposite membrane was used in alkaline fuel cell. This membrane is different from most of conventional anion-exchange membranes, which contain pure organic cations. Its excellent conductivity and alkaline stability makes it a very promising membrane for alkaline fuel cell applications. With these advances and further innovations in the cation structure, backbone structure, membrane architecture, it is anticipated that AEMs with further improved alkaline stability can be developed and put into practical application in fuel cells and batteries.

1.8. AEM fabrication methods

Important methods for AEMs fabrication are paste method, block polymerization, copolymerization, solution casting, sol-gel technique, grafting, plasma polymerization, pore-filling method and supported composite AEMs [60].

1.8.1 AEMs prepared by the paste method

The paste method [61] is widely used for the preparation of commercial AEMs such as Neosepta. Here, a paste consisting of mono vinyl monomers such as styrene,

chloro methyl styrenes and vinyl pyridines, divinyl monomers such as divinyl benezene, dimethacrylate, initiators of polymerization, and a plasticizer along with the reinforcing polymer (PVC) was prepared, and continuously coated on a backing fabric and covered on both sides with PVA/PTFE separating films. The composite was heated to copolymerize the monomers into a film, while the reinforcing polymer PVC was melted and fused to form a continuous film. An alternative method consists of polymerizing a mixture of vinyl monomers, peroxide, additives and linear polymers on a reinforcing fabric between two glass plates or between plastic films.

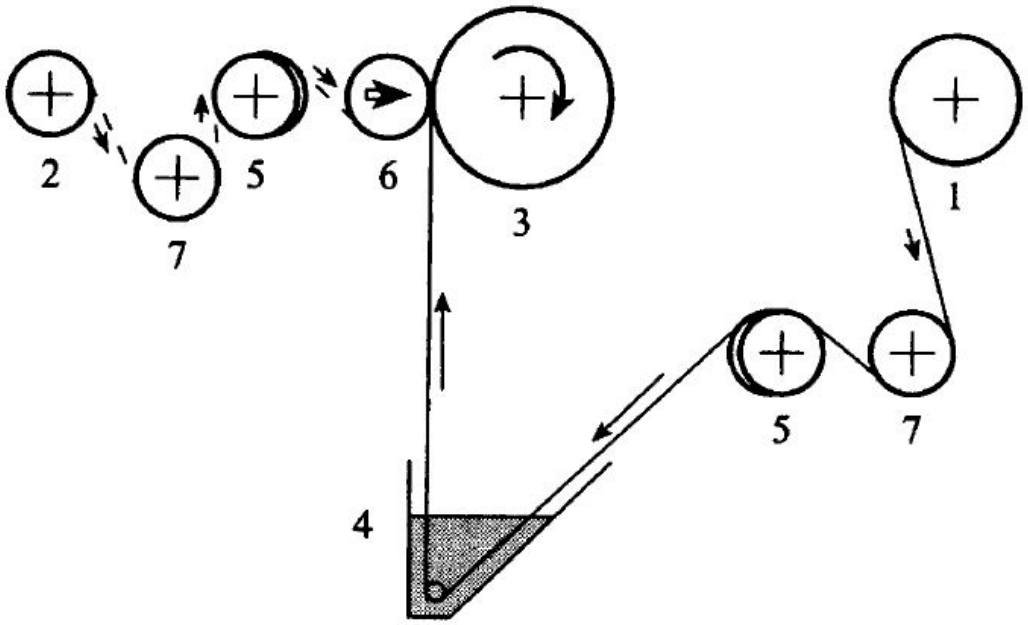

Fig.25 Schematic diagram of paste method. (I) Reserve roll of reinforcing fabric (2) reserve roll of separating film (3) receiving roll (4) paste(mixture of vinyl monomers, inert polymers, initiator, additives, etc.) reservoir (5) expand roll (6) press roll (7) guide roll.

1.8.2 AEMs prepared by the polymerization of monomers

Fabrication of AEMs by co-polymerization of monomers is feasible where at least one of the monomers contains a functional group which can be converted into cations [60]. For example a copolymer consisting of VBC or 4-vinyl pyridine and divinyl benzene, and inert polymers to improve the mechanical strength of the membrane can be casted directly on glass plates. This can be further quaternized either by a tertiary amine or an alkyl halide. These membranes exhibit high ion exchange capacity and low

electrical resistance, but poor mechanical properties and hence cannot be used as such without a proper support material. The mechanical strength of these styrene-divinlybenzene-based membranes can be improved by the addition of linear polymers like polyvinylchloride and polyethylene styrene butadiene rubber, and by using a fabric backing such as net covered on both sides with a glass plate. Recently, a solvent free method was introduced by Wu et al. The process began with the dissolution of the bromomethylated poly(2,6-dimethyl-1,4-phenylene oxide) (BPPO) polymer in the monomers followed by in situ polymerization and quaternization using trimethylamine [29] .

Polymerisation of monomers without functional groups results in a block, which can be sliced into thin films. For example, styrene with DVB was polymerized into a block in the presence of benzoyl peroxide [30]. The resultant membranes were subjected to chloromethylation and quaternization, for imparting anion-exchange functionality. Instead of styrene, the addition of vinylpyridine, yielded an AEM directly when quaternized with an alkyl halide. Homogeneous structure of membranes contributed excellent electrochemical properties for the AEMs. However, slicing a large block of polymer requires high precision instruments. Therefore, this method is not feasible for laboratory scale membrane preparation.

1.8.3 AEMs prepared by the solution casting method

The solution casting is a simple method and applicable in the case of soluble polymers, their blends, or copolymers. This method consists of dissolution of the polymer, functional group introduction by chloromethylation, film casting, and quaternization [60]. Hwang et al. prepared an AEM by synthesizing a block copolymer of polystyrene and poly phenylene sulfide sulfone, followed by chloromethylation and quaternization, using solution casting method [62]. To avoid the use of carcinogenic reagents bromination and 4-bromomethylation were adopted for the synthesis of AEMs, using N-Bromosuccinimide (NBS) in chlorinated solvents such as tetrachloroethane or dichloroethane. Bromination was considered to be a safe procedure, where the degree of bromination can be controlled by the amount of NBS and the bromomethylated polymers were casted as thin films, followed by quaternization [63].

In the case of composite membrane, polymer electrolyte films were fabricated by simple casting procedure. Following steps were involved in this method: (a) Dispersion of ceramic fillers in suitable solvents (b) Addition of a specified amount of the homogeneous polymer solution to the mixture (c) Mixing by means of stirrer or ultrasonic equipment (d) Casting the mixture homogeneously on a substrate (e) Finally the cast membrane was dried in vacuum or in an inert atmosphere [64].

1.8.4 AEMs prepared by the grafting method

The main advantage of radiation grafting method is its versatility. One can easily modify the membrane composition by adjusting the reaction conditions [33]. In graft copolymerization a branched copolymer was obtained by covalently attaching the side chain grafts to the main chain of the polymer backbone. The degree of grafting was estimated from the increase in the polymer weight. Radiation-induced graft copolymerization is simple and cost effective, and polymerization can be initiated in a wide range of polymers that are incompatible with monomers. Energy sources commonly employed in radiation grafting of monomers onto polymer skeletons are UV, plasma, γ-rays (from Co-60) and electron beams (EB). In radiation grafting process monomer is covalently attached to a preformed membrane, so the nature of the polymer backbone plays an important role [33].

To develop AEMs by the radiation grafting vinyl monomers such as VBC, vinyl pyridines, and glycidyl methacrylates were grafted onto different polymer films. Non-fluorinated polymer substrates such as polyethylene (PE) and polypropylene (PP), partially fluorinated polymers such as polyvinylidene fluoride (PVDF) and ethylene tetrafluoroethylene (ETFE), and polymers such as fluorinated ethylene propylene (FEP) and polytetrafluoro ethylene (PTFE) were used for grafting the monomers by direct irradiation methods using UV or plasma radiation [33,65]. Subsequent amination and ion-exchange yielded anion-exchange membranes [26].

1.8.5 Plasma polymerization

Plasma polymerization is a chemical vapor deposition technique which can be obtained through slow discharge, as the case of ionizing radiation [66]. Plasma grafting

consists of three steps: electron-induced excitation, ionization, and dissociation. In a plasma grafting process, exciting species such as electrons, ions, and neutral particles within the plasma, bombard the polymer surface creating active sites to form bonds with functional groups. Thus, the active species induce cleavage of the original chemical bonds in the polymer matrix to form macromolecular radicals to initiate graft copolymerization.

Huet al. introduced benzyl-trimethyl ammonium cationic groups in a polyvinyl chloride matrix by plasma polymerization technique The plasma-grafted alkaline anion-exchange membrane exhibited an ionic exchange capacity of 1.01mmol g^{-1}, good thermal stability, mechanical properties, ionic conductivity of the order of 14.5 mS cm^{-1} and methanol permeability 9.59×10^{-12} m^2 s^{-1}, showing a great potential for application in direct alcohol fuel cells. Alkaline ethanol fuel cell using plasma-grafted alkaline anion-exchange membrane shows an open circuit voltage of 0.796V with 1M EtOH solution at ambient temperature. [67].

Zhang et al. used plasma polymerization for the preparation of alkaline membranes with large amounts of functional groups. The excellent properties of the pulsed plasma-polymerized anion-exchange membranes include good adhesion to the substrate, chemical stability, and thermal stability, high ion-exchange capacity of 1.42 mmol g^{-1} and water uptake of 59.73 wt%. The membrane exhibited an ionic conductivity of 20.5 mS cm^{-1} in deionized water at 20°C and ethanol permeability of 3.37×10^{-11} m^2 s^{-1} shows the great potential of this membrane for direct alcohol fuel cell application [68].

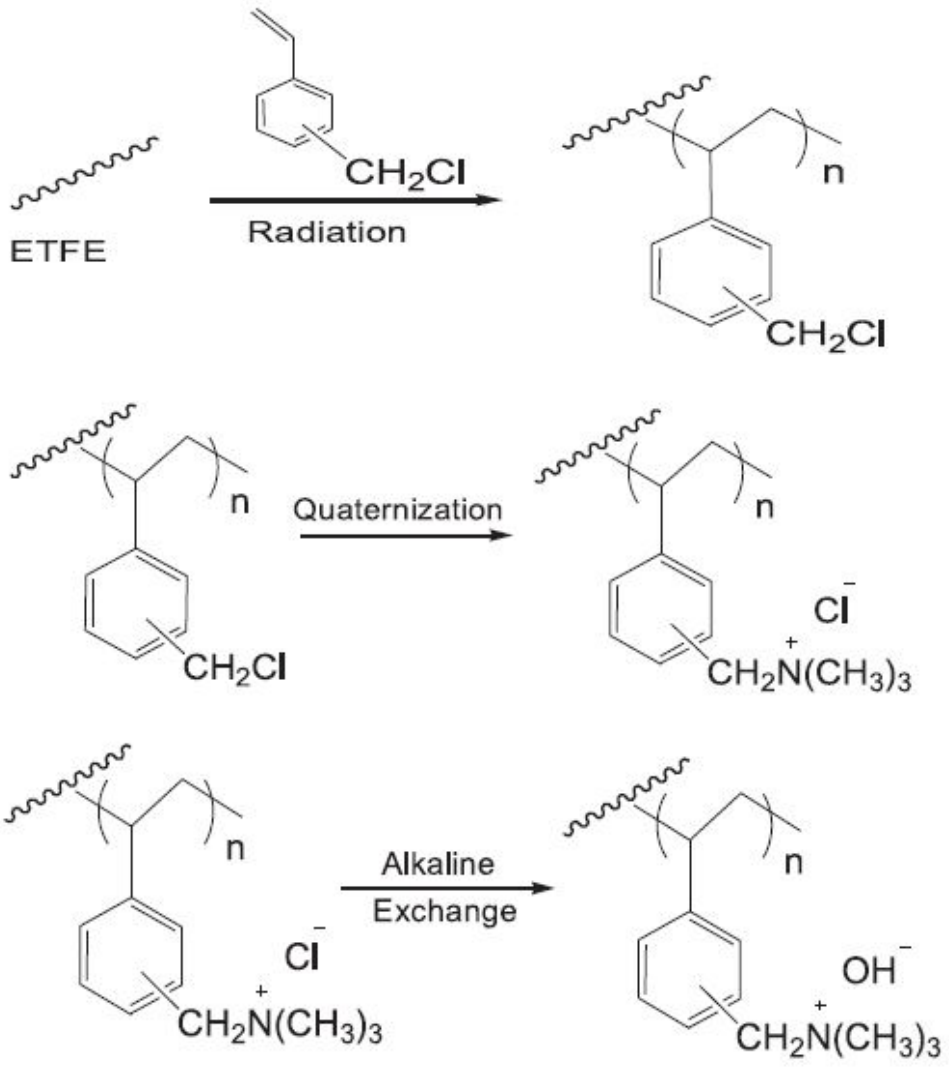

Fig. 26 ETFE-g-CMS radiation-grafted membrane

1.8.6 Pore filling

The pore-filling method was introduced by Yamaguchi in 1991 to develop IEMs with low swelling and high selectivity for liquid separation applications [69]. To prepare IEMs using pore filling method a chemically inert and mechanically stable porous substrate is required, which will restrict the expansion of soft electrolyte polymers in pores. Polyacrylonitrile (PAN), high-density polyethylene (PE), polypropylene (PP) and inorganic materials, such as porous alumina are some of the available porous substrates. For retaining the ionomers inside pores, concentrated solutions of ionomers having sufficient viscosity are retained on the surface of the porous membranes [70]. In this

method, porous PE was filled with VBC monomers, followed by polymerization and quaternization with amines. The membranes prepared by using trimethylamine showed a conductivity of 38.1 mS cm^{-1} at room temperature. These membranes exhibited improved electrochemical properties and low swelling properties. Pore-filled composite membranes have also been developed and characterized for use in alkaline fuel cells and non-aqueous vanadium redox flow batteries. The dense structure of pore-filled membranes reduces the permeability of liquid fuels and ions in fuel cells and redox flow batteries. Physical reinforcement with inert polymers and quaternization with long carbon chain amines improves the chemical stability of the membranes in alkaline solutions. But, their chemical stability in redox systems is to be improved [60,71].

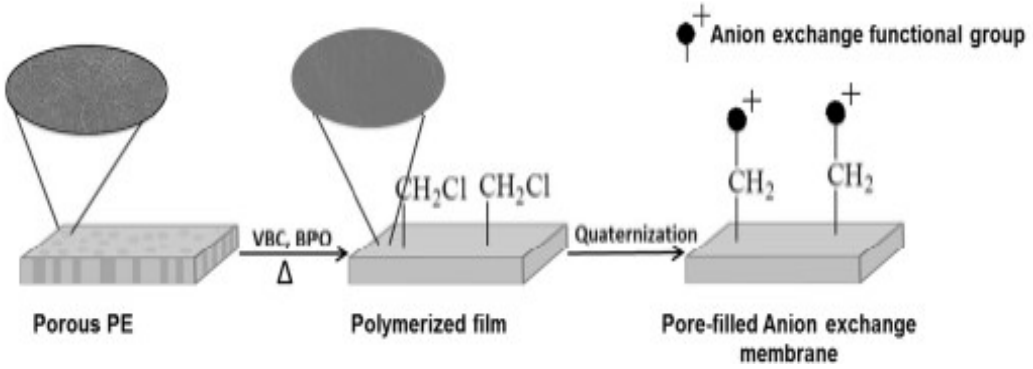

Fig. 27 Schematic diagram for the preparation of anion-exchange membrane by pore-filling method [60]

The composite organic-inorganic membranes were also developed by pore-filling method. For example, PAN (polyacrylonitrile) ultrafiltration membrane was hydrolyzed by immersing in 2M sodium hydroxide aqueous solution and the membranes were loaded in a filtration cell. PVA-GO (graphene oxide) suspension was poured into the loaded filtration cell, and filtration was carried out under a certain pressure. Then, the membranes were removed and dried in an oven to prepare a “pore filling” composite membrane. The results of the swelling experiment showed that the pore-filling structure could effectively reduce swelling of the nanohybrid membranes. Assembly of the nanohybrid membranes by molecular level dispersion of GO in PVA improved the affinity of the membrane to aromatic compounds and this increased the performance of the membrane in the pervaporation of toluene/n-heptane mixtures. The separation performance of the membrane could be easily controlled by adjusting the pressure, filtration time, polymer, and GO concentration [72].

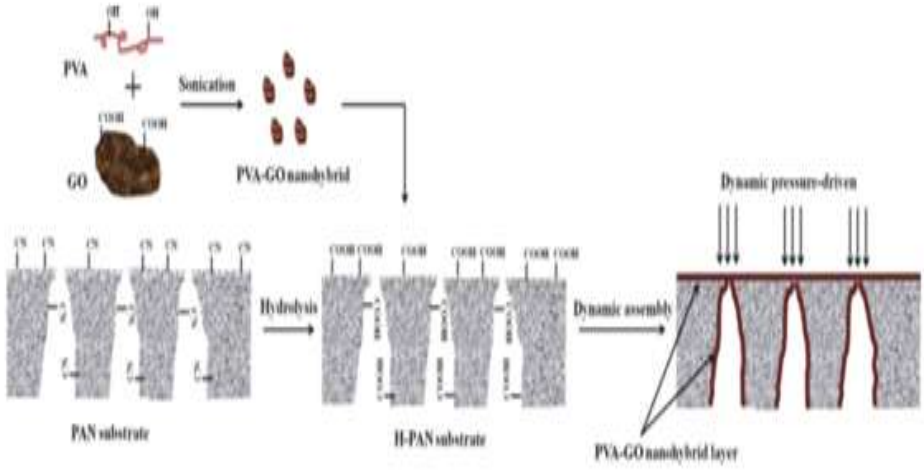

Fig. 28 Schematic diagram for the preparation of PVA-GO nanohybrid anion-exchange membrane by pore-filling method

1.8.7 AEMs prepared by the Sol-gel process

The sol-gel process is an efficient method to synthesize organic-inorganic hybrid membranes, since it allows a broad variation in compositions [60]. The incorporation of inorganic materials in the polymer matrix enhances the chemical and mechanical properties of the resulting membranes. Composite membranes fabricated by the sol-gel method consist of chemical bonds between the inorganic and organic molecules. The organic domains contribute the electrochemical properties, and the inorganic domains impart mechanical strength to the membranes. This technique offers a low temperature procedure and very good compatibility in the molecular level between the organic and inorganic phases. Dispersions of colloidal particles in the solvent are sols and polymer chains interconnected by hydrogen bonding are gels. Sol–gel reactions generally consist of two steps: 1) hydrolysis of metal alkoxides to produce hydroxyl groups and 2) polycondensation of the hydroxyl groups to form a three-dimensional network. The sol–gel process generally occurs in low molecular weight solvents with alkoxide precursors M $(OR)_n$, (M is a network-forming element: Si, Ti, Zr, Al, B, etc., and R is an alkyl group (C_xH_{2x+1}). During hydrolysis and condensation reactions, low molecular weight byproducts (alcohol or water) are eliminated. This method was used to fabricate polymer/silica hybrid membranes with the formation of an inorganic network in the presence of an organic polymer, and resulting in the formation of organic polymer and metal oxide, inter penetrating networks [73]. Some of organic-inorganic hybrid membranes synthesized from organic polymers capable of hydrogen bonding include

poly(2-methyl-2-oxazoline), poly(vinyl pyridines), poly(methylmethacrylate), poly(vinyl acetate), polyamides, and polymeric perfluoro alkylsulfonates (Nafion). In this method, alkoxysilane or quaternary amino groups are introduced as anion-exchange domains. Anion-exchange hybrid membranes based on the copolymerization of VBC and γ-methacryloxypropyl trimethoxysilane (γ-MPS) are prepared through quaternization and sol-gel reaction with monophenyl triethoxysilane. To provide mechanical strength and control the water uptake polyethylene terephthalate (PET) fabric is used. The reinforcement by polyethylene terephthalate fabric reduced the ionic-conductivity of the membrane to the range of 0.227-0.433 mS cm^{-1}. Inspite of high ion-exchange capacity values of 1.70-2.20 meq g^{-1}such membranes showed too low ionic conductivity so that such membranes cannot be used in fuel cells. Wu et al. synthesized AEMs from silica/poly (2, 6-dimethyl-1, 4-phenylene oxide) using the sol-gel method. The effect of heat treatment showed that it caused functional group degradation, whereas an increase in the silica content improved the ion-exchange capacity values and swelling resistance. Silica chains may act as a physical barrier for the penetration of vanadium ions across the membranes [74].

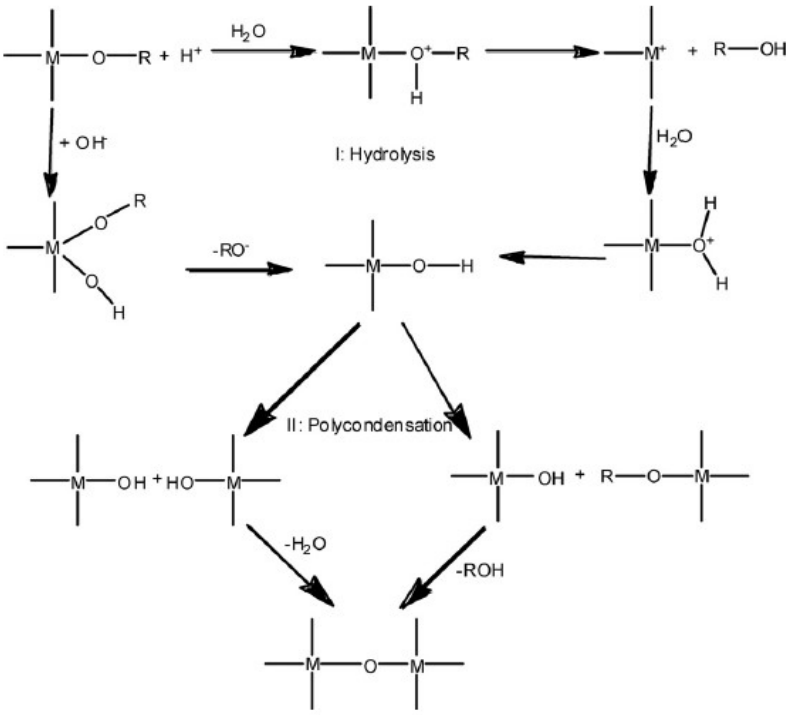

Fig. 29 Schematic presentation of sol-gel reaction route for metal alkoxide [74]

1.9. Applications

1.9.1. Fuel cells

Fuel cells are considered as highly efficient, environmentally friendly energy conversion device for the 21st century. It is capable of converting chemical energy stored in the fuel and oxidant directly into DC electricity with water and heat as the only byproducts [75]. Fuel cells are not limited by thermodynamic limitations of the Carnot efficiency, since the intermediate steps of producing heat and mechanical work of most conventional power generation methods are avoided. As combustion is avoided, fuel cells can produce power without the generation of harmful greenhouse gases like SO_x, NO_x, CO_2 and CO. Unlike batteries, the reductant and oxidant in fuel cells must be continuously replenished to allow continuous operation [76]. Sir William Robert Grove in 1839 first introduced Fuel Cells [12]. The costly component materials, problems of hydrogen storage, long-term durability and performance of the system still remain to be solved to enable large-scale commercialization [77,78]. Significant work on fuel cells began in 1930s, by Francis Bacon. In 1950s, the first practical alkaline fuel cell was developed which used molten KOH as the electrolyte. NASA used alkaline fuel cells in the 1960s to power Apollo space missions [79]. Electrochemical reactions of an alkaline fuel cell are as follows:

$$\text{Anode reaction: } 2H_2 + 4OH^- \rightarrow 4H_2O + 4\,e^-$$

$$\text{Cathode reaction: } O_2 + 4e^- + 2H_2O \rightarrow 4OH^-$$

$$\text{Overall reaction: } 2H_2\,(gas) + O_2\,(gas) \longrightarrow 2H_2O + \text{energy}$$

The basic physical structure of a fuel cell

Basically a fuel cell consists of an electrolyte in contact with an anode and a cathode. Fuel is fed to the anode and an oxidant to the cathode. As a result of electrochemical reactions, electricity is produced where the only byproduct is water. Schematic representation of a unit cell is shown in **Fig.**30.

The technology however suffers problems such as the use of liquid electrolytes, in particular the inevitable shunt currents and poisoning by carbon dioxide, which leads to the formation of carbonate precipitates in the liquid electrolyte.

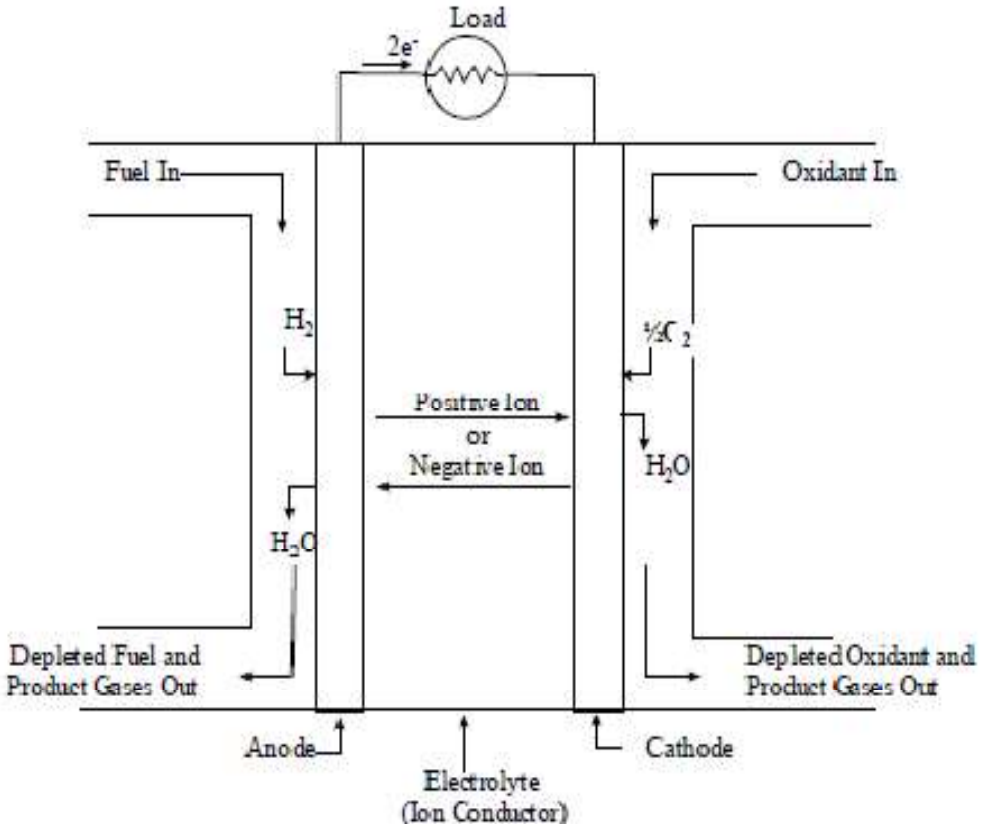

Fig. 30 Schematic representation of a fuel cell unit

The chemistry behind the carbonate precipitation problem is presented below [80].

$$CO_2 + 2OH^- \rightarrow CO_3^{2-} + H_2O$$

$$CO_2 + OH^- \rightarrow HCO_3^-$$

$$HCO_3^- \leftrightarrow CO_3^{2-} + H^+$$

$$CO_3^{2-} + 2K^+ \leftrightarrow K_2CO_3(s)$$

The strongly alkaline electrolytes absorb even the smallest amount of CO_2, which in turn reduces the conductivity of the electrolyte. Consequently, pure hydrogen and highly purified oxygen must be used as the fuel and oxidant feeds. The use of such high purity oxygen, in particular, increases significantly the cost of generating electricity with a liquid electrolyte alkaline fuel cell.

1.9.2 Fuel Cell Classifications

Fuel cells are classified based on the type of electrolyte and fuel, which determine the electrode reactions and the ions that carry the current across the electrolyte. Fuel cells are classified as (1) polymer electrolyte fuel cell (PEFC) (2) alkaline fuel cell (AFC) (3) phosphoric acid fuel cell (PAFC) (4) molten carbonate fuel cell (MCFC) and (5) solid oxide fuel cell (SOFC). The choice of electrolyte determines the operating temperature range of the fuel cell and the physicochemical and thermo-mechanical properties of materials used [9]. Aqueous electrolytes are limited to temperature of about 200°C or lower because of their high vapor pressure and rapid degradation at higher temperatures [76].

Polymer Electrolyte Membrane Fuel Cell (PEMFC)

Among the different types of fuel cell systems, proton exchange membrane fuel cells (PEMFC) are the most developed for portable and automotive applications due to their high power density, high energy-conversion efficiencies, lower starting temperature, and ease of handling.

In 1960 DuPont Company developed a cation-exchange membrane called Nafion, which has a poly tetrafluoro ethylene backbone and perfluorinated vinyl ether pendant side chains terminated by sulfonate ionic groups [81]. The widespread commercialization of PEMFCs, however, remains a challenge due to the drawbacks of Nafion membrane such as high cost, poor durability, carbon monoxide poisoning of noble-metal catalysts at low temperatures, fuel cross-over and collapse of proton conductivity at higher operating temperatures [49,57,79]. The electrochemical reactions at the anode and cathode for power generation in a PEMFC are as follows:

$$\text{Anode: } 2H_2 \rightarrow 4H^+ + 4e^-$$
$$\text{Cathode: } O_2 + 4e^- + 4H^+ \rightarrow 2H_2O$$
$$\text{Cell reaction: } 2H_2 + O_2 \rightarrow 2H_2O$$

The hydrogen ions move from anode to cathode through the polymer electrolyte membrane while restricting the flow of electrons and fuel through the membrane.

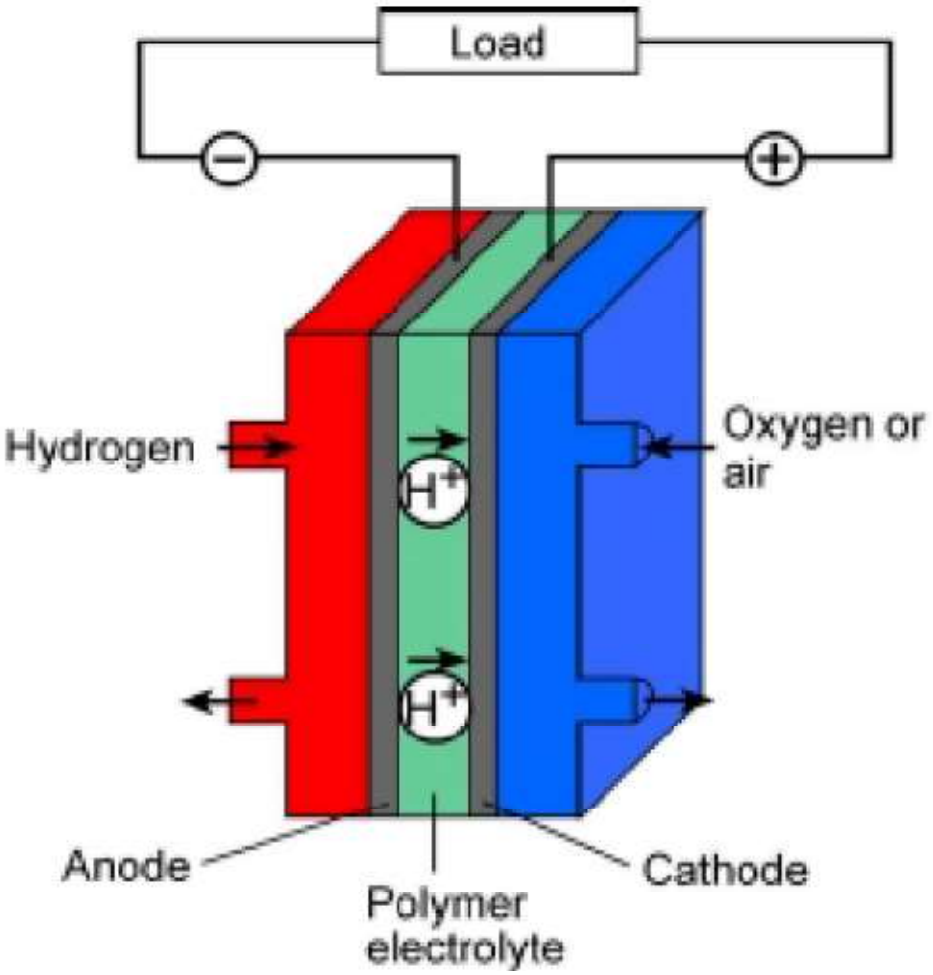

Fig. 31 Polymer electrolyte membrane fuel cells (PEMFCs)

Anion-exchange membrane fuel cells (AEMFCs) have attracted attention during the past decades which uses AEM as the polymer electrolyte, where the charge carriers are hydroxide ions (or other anions) instead of protons. Both fuel oxidation and the oxygen reduction reaction kinetics are more facile in alkaline medium than in acidic medium. Non-noble metals such as Co and Ni can be used as catalysts, making the fuel cell more cost effective and have long lifetime due to low corrosion properties under alkaline conditions. Furthermore, AEMFCs also offer fuel flexibility, reduced fuel crossover, and high fuel cell efficiencies [57,82,83]

The associated fuel cell reactions both for a traditional AFC and also for an AMFC are:

Anode: $2H_2 + 4OH^- \rightarrow 4H_2O + 4e^-$

Cathode: $O_2 + 2H_2O + 4e^- \rightarrow 4OH^-$

Overall: $2H_2 + O_2 \rightarrow 2H_2O$

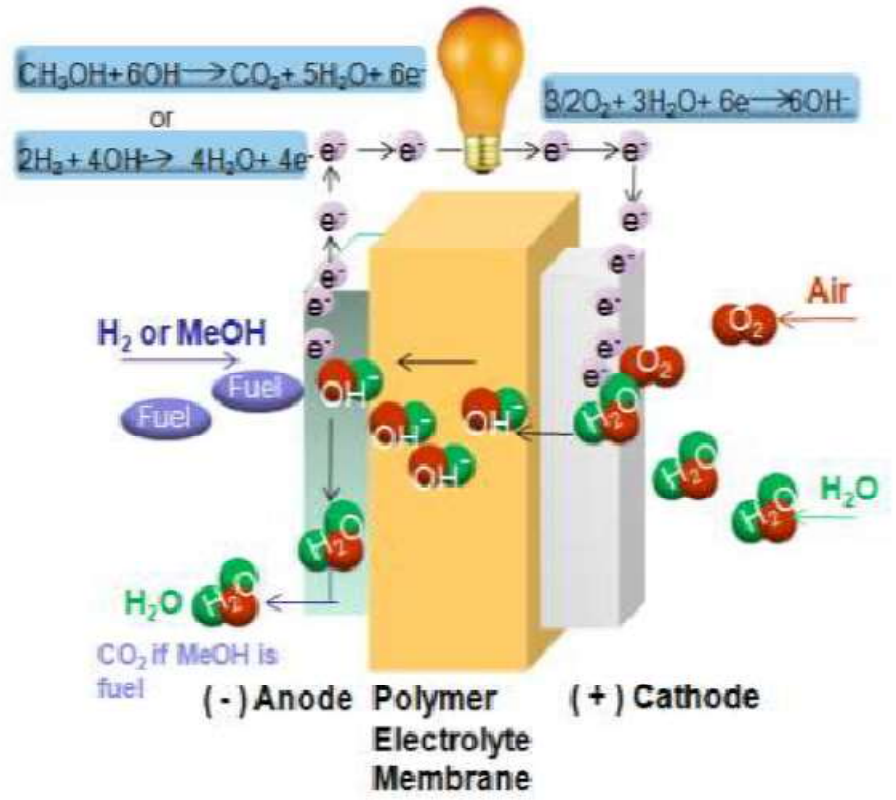

Fig. 32 Schematic diagram of AEMFC

A major issue with traditional AFCs is that of the electrolyte and electrode degradation caused by the formation of carbonate/bicarbonate (CO_3^{2-}/HCO_3^-) on the reaction of OH^- ions with CO_2 contamination in the oxidant gas stream blocking pores of the electrodes, mechanically disrupting and destroying active layers. The use of an AEM as a solid electrolyte including no metal cations prevent precipitation of carbonate/bicarbonate salts because the electrolyte containing the cationic groups is already a solid [84].

1.10 Redox flow batteries

Solar and wind power are the most widely used alternative energy sources. However, because of their intermittent nature, the potential of these two energy sources can be fully exploited only if efficient, safe, and reliable electrical energy storage (EES) systems are introduced [85]. Among energy storage technologies, battery energy storage technology is considered to be the most viable. In particular, a redox flow battery is suitable for large scale energy storage. Redox flow battery (RFB) was introduced in the 1970s [60]. Unlike other batteries, in redox flow batteries, electricity is stored as chemical energy in flowing electrolytes. The electrolytes are stored in tanks outside the active battery area and pumped through the battery system during its working. Here two electrolyte solutions undergo redox reactions in the respective half-cells of the battery during charge and discharge of the system. Electrical energy is stored during charging cycle and energy is released during discharging cycle. The concentration and volume of the liquid electrolytes determine the energy storage capacity of the battery. The power of the redox flow battery, on the other hand, is determined by the size of the electrodes and the number of individual cells. This ability to tune the storage capacity and power of redox flow batteries make these devices useful for large-scale applications such as balancing grid loads.

1.10.1 Types of redox flow cells

Currently existing flow battery systems include, All vanadium redox flow battery [13, 86], All iron flow battery [87] and All copper redox flow battery. It is also possible to operate a flow battery in a hybrid configuration. Hybrid flow batteries, such as bromine/polysulphide redox system, vanadium-bromine redox system [88], Fe–Cr redox system [89], Zinc/bromine redox system and Zinc/cerium redox system are also existing. Charging and discharging of these batteries involves plating/stripping of metal deposits at the negative electrode. The energy capacity is directly related to the amount of metal that can be plated.

The membrane is a key component of redox flow batteries as it determines the performance as well as the economic viability of the batteries. The functions of the membrane in a redox flow cell is to prevent the cross-mixing of the positive and negative

half-cell electrolytes, prevents short circuiting of the two half-cell electrodes and simultaneously allow the transport of ions to complete the circuit during the passage of current. Another important function of the membrane is to prevent the preferential transfer of water from one half-cell to the other. The preferential transfer of water is a problem in redox flow cells as one half-cell is flooded and diluted, while the other becomes more concentrated, adversely affecting the overall operation of the cell. The performance of the most membranes deteriorated with long-term exposure to the vanadium solutions. During the charge/discharge cycles, the redox couples undergo electrochemical redox reactions and the IEM allows the transport of ions to maintain electroneutrality.

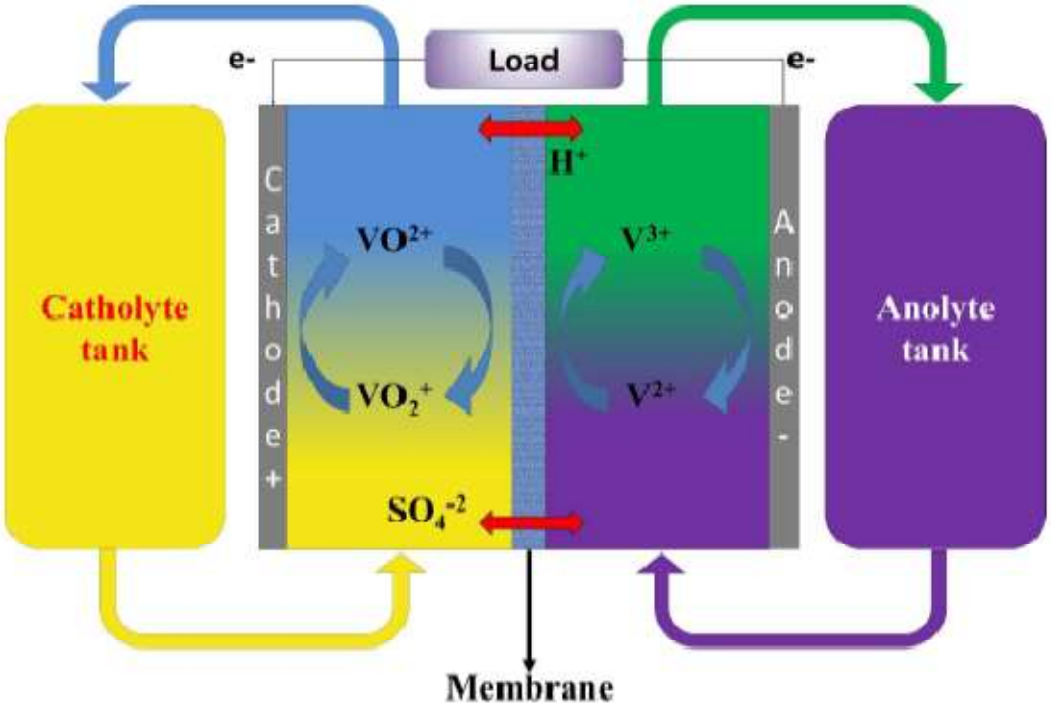

Fig. 33 Schematic representation of an All-vanadium redox flow battery

Among the various RFBs, vanadium redox flow batteries (VRFBs) have gained attention due to the presence of the same metal cation in the catholyte and the anolyte solutions [90]. The crossover of the vanadium ions through the membrane is a reversible regeneration process, which provides a long life to the electrolyte solution. VRFBs assembled with CEMs exhibit low coulombic efficiency. AEMs will degrade in strong oxidizing VO_2^+ solutions during the continuous charge/discharge cycles [90]. So the

development of chemically stable membrane in strong oxidizing environment is a great challenge.

The abundant earth resources of iron and chloride, low cost of the reactants and the use of a single species as the reactant make iron-chloride redox flow battery highly attractive for large-scale applications. The operating principle of an iron-chloride redox flow battery is based on the iron (II) chloride/iron (III) chloride couple at the cathode and the iron (II) chloride/metallic iron couple at the anode. The reactions that take place during the charging and discharging of an iron-chloride redox flow battery are shown in Fig. 33. During discharge of the battery, iron (III) chloride is reduced to iron (II) chloride at the cathode. At the anode, metallic iron dissolves into the electrolyte as iron (II) chloride; these processes are reversed during battery charging. The open-circuit voltage of the iron-chloride redox flow battery is about 1.21 V

Positive electrode: $2FeCl_3 + 2e^- \rightarrow 2FeCl_2 + 2Cl^-$ $E^o = 0.77V$

Negative electrode: $Fe + 2Cl^- \rightarrow FeCl_2 + 2e^-$ $E^o = -0.44V$

Overall cell reaction: $Fe + 2FeCl_3 \rightarrow 3FeCl_2$ E^o cell = 1.21V

Aswin K. Manohar and et al. have reported an all-iron redox flow battery with a high charging efficiency of 97% by keeping the pH of the negative electrolyte at a value of 2 and by using indium chloride as an additive in electrolyte. The high charging efficiency of the negative electrode was found to be stable during at least 50 repeated cycles. They have showed that by using a graphite felt electrode, the over-potential losses were reduced at the positive and negative electrodes and the electrodes were operated at current densities as high as 100 mA cm^{-2}. These results show that, the iron-chloride redox flow battery will be an efficient solution for large-scale energy storage [87].

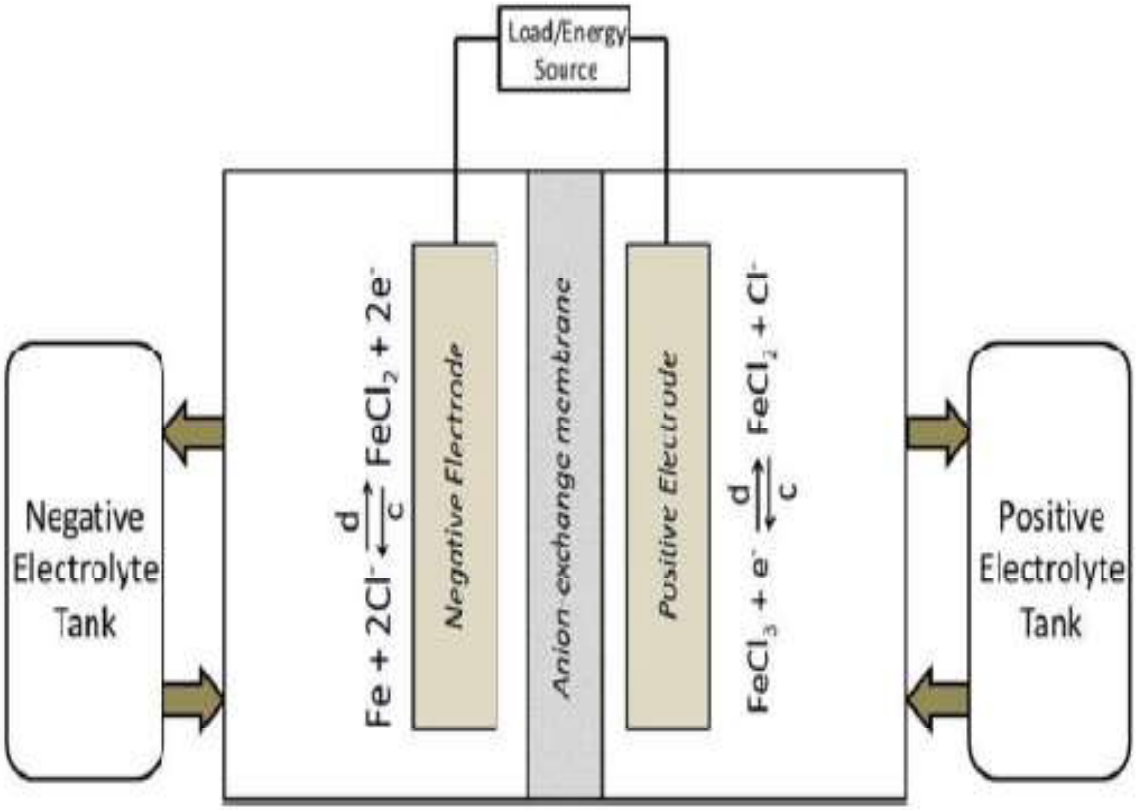

Fig. 34 Schematic representation of an All-iron flow battery

1.11. Conclusions

Development of AEM materials has been a subject of extensive research in the last decade due to its potential applications in the field of energy conversion and storage technologies. Still there are severe challenges regarding the aspects of materials. For example, ionic conductivity, chemical stability and mechanical properties of the membranes should be improved further to ensure the viability for commercialization. Much works are reported in the literature on the development of various anion-exchange membranes. The objectives of the work presented in this thesis are to develop AEMs with better performance in electrochemical devices.

Objectives of the present work

- To fabricate heterogeneous and homogeneous anion-exchange polymer membrane having high conductivity and stability.
- Characterization of membranes using FT-IR, SEM, TGA, EIS techniques and properties of membranes such as IEC, TS, ionic conductivity, water uptake, alkaline stability, oxidative stability, and methanol permeability tests.
- To study the performance of flow battery using the developed membrane as separator.

References

[1] Ban Ki-moon Secretary-General of the United Nations, Energy for a Sustainable Future, 2010. doi: 10.1016/j.enbuild.2006.04.011.

[2] E. Güler, Thesis on anion exchange membrane design for reverse electrodialysis, University of Twente, 2014. ISBN: 978-90-365-3570-0
doi: 10.3990/9789036535700

[3] UNIDO energy, development and security Energy issues in the current macroeconomic context.

[4] United Nations Department of Public Information New York, Basic Facts about the United Nations, 2011.

[5] M. El Baradei, Tackling the Global Energy Crisis, Int. At. Energy Agency. (2008) 50–51.

[6] U. Nations, Kyoto Protocol To the United Nations Framework Kyoto Protocol To the United Nations Framework, Rev. Eur. Community Int. Environ. Law. 7 (1998) 214–217. doi:10.1111/1467-9388.00150.

[7] F. H. Shu, Global Change and the Energy Crisis Frank Hsia-San Shu University of California, San Diego

[8] X. Li, H. Zhang, Z. Mai, H. Zhang, I. Vankelecom, Ion exchange membranes for vanadium redox flow battery (VRB) applications, Energy Environ. Sci. 4 (2011) 1147. doi:10.1039/c0ee00770f.

[9] G. Merle, M. Wessling, K. Nijmeijer, Anion exchange membranes for alkaline fuel cells : A review, J. Memb. Sci. 377 (2011) 1–35. doi:10.1016/j.memsci.2011.04.043.

[10] V. Pupkevich, V. Glibin, D. Karamanev, Phosphorylated polyvinyl alcohol membranes for redox Fe^{3+}/H_2 flow cells, J. Power Sources. 228 (2013) 300–307.

doi:10.1016/j.jpowsour.2012.11.080.

[11] X. Lin, L. Wu, Y. Liu, A.L. Ong, S.D. Poynton, J.R. Varcoe, T. Xu, Alkali resistant and conductive guanidinium-based anion-exchange membranes for alkaline polymer electrolyte fuel cells, J. Power Sources. 217 (2012) 373–380. doi:10.1016/j.jpowsour. 2012.05.062.

[12] Z. Zakaria, S.K. Kamarudin, S.N. Timmiati, Membranes for direct ethanol fuel cells: An overview, Appl. Energy. 163 (2016) 334–342. doi:10.1016/j.apenergy.2015.10.124.

[13] H. Prifti, A. Parasuraman, S. Winardi, T.M. Lim, M. Skyllas-Kazacos, Membranes for redox flow battery applications, Membranes (Basel). 2 (2012) 275–306. doi:10.3390/membranes 2020275.

[14] D. Aili, M. Kalmar, R. Fulgence, Q. Li, E. Christensen, J. Oluf, N.J. Bjerrum, Heterogeneous anion conducting membranes based on linear and crosslinked KOH doped polybenzimidazole for alkaline water electrolysis, J. Memb. Sci. 447 (2013) 424–432. doi:10.1016/j.memsci.2013.07.054.

[15] J. Yin, B. Deng, Polymer-matrix nanocomposite membrances for water treatment, J. Memb. Sci. (2014). doi:10.1016/j.memsci. 2014.11.019.

[16] K. P. Lee, T.C. Arnot, D. Mattia, A review of reverse osmosis membrane materials for desalination - Development to date and future potential, J. Memb. Sci. 370 (2011) 1–22. doi:10.1016/j. memsci.2010.12.036.

[17] G. Kang, Y. Cao, Application and modification of poly(vinylidene fluoride) (PVDF) membranes–A review, J. Memb. Sci. 463 (2014) 145–165. doi:10.1016/j.memsci.2014.03.055.

[18] T. Sukkar, M. Skyllas-Kazacos, Modification of membranes using polyelectrolytes to improve water transfer properties in the vanadium redox battery, J. Memb. Sci. 222 (2003) 249–264. doi:10.1016/S0376-7388(03)00316-8.

[19] Y.A. A.A. Mohamad, N.S. Mohamed, M.Z.A. Yahya, R. Othman, S. Ramesh, A.K. Arof, A.A. Mohamad, N.S. Mohamed, M.Z.A. Yahya, R. Othman, S. Ramesh, Y. Alias, A.K. Arof, Ionic conductivity studies of poly(vinyl alcohol) alkaline solid polymer electrolyte and its use in nickel–zinc cells, Solid State Ionics 156 (2003) 171–177.

[20] W. Ostwald, Elektrische Eigenschaften halbdurchlissiger Scheidewinde., Z. Phys. Chem. (Leipzig) 6, (1890) 71–82.

[21] V. A. Shaposhnik, Evolution of the membrane electrochemistry, Russ. J. Electrochem. 38 (2002) 800–805. doi:10.1023/A: 1016845208109.

[22] A. F. L. Michaelis The electric phenomen and ion permeability of membranes. II. Permeability of apple peel, Biochem. Z. 158 28. (1925).

[23] K. S¨ollner, Uber mosaikmembraen, Biochem. Z. 244 390. (1932).

[24] Hans Wassenegger, United States Patent Office 2,204,539, (1919).

[25] H.S. K.H. Meyer, La perm´eabilit´e des membranes VI, sur lepassage du courant ´electrique a travers des membranes s´elective, Helv. Chim. Acta 23 795. (1940).

[26] T. Nishiwaki, Concentration of electrolytes prior to evaporation with an electro-membrane process, in: R.F. Lacey, S. Loch (Eds.), Industrial Process with Membranes, Wiley–Interscience, New York, 1972. (1972).

[27] W.G. Grot, Laminates of support material and fluorinated polymer containing pendant side chains containing sulfonyl groups. U.S. Patent 3,770,567 (1973).

[28] T. Xu, Ion exchange membranes : State of their development and perspective, J. Memb. Sci. 263 (2005) 1–29. doi:10.1016/j.memsci.2005.05.002.

[29] J. Ran, L. Wu, Y. He, Z. Yang, Y. Wang, C. Jiang, L. Ge, E. Bakangura, T. Xu, Ion exchange membranes: New developments and applications, J. Memb. Sci. 522 (2017) 267–291. doi:10.1016/j.memsci.2016.09.033.

[30] T. Sata, Ion Exchange Membranes Preparation, Characterization, Modification and Application, The Royal Society of Chemistry, Thomas Graham House, Science Park, Milton Road, Cambridge CB4 OWF, UK 2002.

[31] M. Luqman, Ion exchenge technology I, 2013. doi:10.1007/978-94-007-1700-8.

[32] B. Smitha, S. Sridhar, A. A. Khan, Solid polymer electrolyte membranes for fuel cell applications- a review, J. Memb. Sci. 259 (2005) 10–26. doi:10.1016/j.memsci.2005.01.035.

[33] T. Zhou, R. Shao, S. Chen, X. He, J. Qiao, J. Zhang, A review of radiation-grafted polymer electrolyte membranes for alkaline polymer electrolyte membrane fuel cells, J. Power Sources. 293 (2015) 946–975. doi:10.1016/j.jpowsour.2015.06.026.

[34] J. Rozi, D.J. Jones, Non fluorinated polymer materials for proton exchange membrane fuel cells, Annu. Rev. Mater. Res. 2003. 33503–55. (2003). doi:10.1146/annurev.matsci.33.022702.154657.

[35] R. S. L. Yee, R. A. Rozendal, K. Zhang, B. P. Ladewig, Cost effective cation exchange membranes : A review, Chem. Eng. Res. Des. 90 (2011) 950–959. doi:10.1016/j.cherd.2011.10.015.

[36] R. K. Nagarale, G. S. Gohil, V. K. Shahi, Recent developments on ion-exchange membranes and electro-membrane processes, Advances in Colloid and Interface Science 119 (2006) 97–130. doi:10.1016/j.cis.2005.09.005.

[37] G. Merle, M. Wessling, K. Nijmeijer, Anion exchange membranes for alkaline fuel cells : A review, 377 (2011) 1–35. doi:10.1016/j.memsci.2011.04.043.

[38] M. E. Tuckerman, D. Marx, M. Parrinello, The nature and transport mechanism of hydrated hydroxide ions in aqueous solution, Nature. 417 (2002) 925–929. doi:10.1038/nature00794.1.

[39] O. D. Thomas, K. J. W. Y. Soo, T. J. Peckham, M. P. Kulkarni, S. Holdcroft, A Stable Hydroxide-Conducting Polymer, J. Am. Chem. Soc. (2012) 10753–10756. doi:dx.doi.org/10.1021/ja303067t.

[40] Y. Liu, B. Zhang, C.L. Kinsinger, Y. Yang, S. Seifert, Y. Yan, C. Mark Maupin, M.W. Liberatore, A.M. Herring, Anion exchange membranes composed of a poly(2,6-dimethyl-1,4-phenylene oxide) random copolymer functionalized with a bulky phosphonium cation, J. Memb. Sci. 506 (2016) 50–59. doi:10.1016/j. memsci.2016.01.042.

[41] J. R.Varcoe, T. N. Danks, R. C. T. Slade, Comparison of PVDFand FEP based radiation-grafted alkaline anion-exchange membranes for use in low temperature portable DMFCs, J. Mater. Chem. 12 (2002) 3371–3373.

[42] D. Q. P. Zschocke, Novel ion exchange membranes based on an aromatic polyethersulfone, J. Memb. Sci. 22 (1985) 325–332.

[43] B.S.P. S. Chempath, J. M. Boncella, L. R. Pratt, N. Henson, Density functional theory study of degradation of tetraalkylammonium hydroxides, J. Phys. Chem. C. 114 (2010) 425-436.

[44] A.S.M. A.C. Cope, Mechanism of the Hoffmann elimination reaction: an ylide intermediate in the pyrolysis of a highly branched quaternary hydroxide, J. Am. Chem. Soc. 85 (1963) 1949–1952.

[45] J. A. R. S. Chempath, B. R. Einsla, L. R. Pratt, C. S. Macomber, J. M. Boncella, B.S. Pivovar, Mechanism of tetraalkylammonium headgroup degradation in alkaline fuel cell membranes, J. Phys. Chem. C. 112 (2008) 3179–3182.

[46] J. Cheng, G. He, F. Zhang, A mini-review on anion exchange membranes for fuel cell applications: Stability issue and addressing strategies, Int. J. Hydrogen Energy. 40 (2015) 7348–7360. doi:10.1016/j.ijhydene.2015.04.040.

[47] Hibbs. M. R., Alkaline stability of poly(phenylene)-based anion exchange membranes with various cations, J Polym Sci Part B Polym Phys. 51 (2013) 1736–42.

[48] H. Wu, W. Jia, Y. Liu, An imidazolium-type hybrid alkaline anion exchange membrane with improved membrane stability for alkaline fuel cells applications, J. Mater. Sci. 52 (2017) 1704–1716. doi:10.1007/s10853-016-0462-y.

[49] B. Lin, F. Chu, Y. Ren, B. Jia, N. Yuan, H. Shang, T. Feng, Y. Zhu J. Ding, Alkaline stable C_2-substituted imidazolium-based crosslinked anion exchange membranes for alkaline fuel cell applications, 266 (2014) 186–193.

[50] B. F. Price S. C, Williams K. S, Relationships between structure and alkaline stability of imidazolium cations for fuel cell membrane applications., ACS Macro Lett. 3 (2014) 160–165.

[51] TSUTOMU ISHIKAWA, Superbases for Organic Synthesis: Guanidines, Amidines, Phosphazenes and Related Organocatalysts, John Wiley & Sons, Ltd 2009. doi:10.1351/pac198860111627.

[52] Q. Zhang, S. Li, S. Zhang, A novel guanidinium grafted poly(aryl ether sulfone) for high-performance hydroxide-exchange membranes, Chem. Commun. 46 (2010) 7495–7497.

[53] S. D. Sajjad, Y. Hong, F. Liu, Synthesis of guanidinium-based anion exchange membranes and their stability assessment, Polym. Adv.Technol. 25 (2014) 108–116. doi:10.1002/pat.3211.

[54] Y. Y. Liu, Y. Wang, J. Yang Y. Brenner, Anion transport in a chemically stable, sterically bulky modified imidazolium functionalized anion exchange membrane, J Phys Chem C.118 (2014) 15136–15145.

[55] C. Yang, Synthesis and characterization of the cross-linked PVA/TiO_2 composite polymer membrane for alkaline DMFC, J. Memb. Sci. (2006) 51–60. doi:10.1016/j.memsci.2006.10.048.

[56] L. Zeng, T. S. Zhao, L. Wei, Y.K. Zeng, Z.H. Zhang, Highly stable pyridinium-functionalized cross-linked anion exchange membranes for all vanadium redox flow batteries, J. Power Sources. 331 (2016) 452–461. doi:10.1016/j.jpowsour.2016.09.065.

[57] B. Lin, L. Qiu, J. Lu, F. Yan, Cross-linked alkaline ionic liquid-based polymer electrolytes for alkaline fuel cell applications, Chem. Mater. 22 (2010) 6718–6725. doi:10.1021/cm102957g.

[58] L. Zeng, T. S. Zhao, Y. S. Li, Synthesis and characterization of crosslinked poly (vinyl alcohol)/layered double hydroxide composite polymer membranes for alkaline direct ethanol fuel cells, Int. J. Hydrogen Energy. 7 (2012) 1–8.

[59] L. Liu, C. Tong, Y. He, Y. Zhao, C. Lü, Enhanced properties of quaternized graphenes reinforced polysulfone based composite anion exchange membranes for alkaline fuel cell, J. Memb. Sci. 487 (2015) 99–108. doi:10.1016/j.memsci.2015.03.077.

[60] S. Maurya, S. H. Shin, Y. Kim, S. H. Moon, A review on recent developments of anion exchange membranes for fuel cells and redox flow batteries, RSC Adv. 5 (2015) 37206–37230. doi:10.1039/C5RA04741B.

[61] J. Toshikatsu Sata, Ion Exchange Membranes Preparation, Characterization, Modification and Application, Tokuyama Research, Tokuyama Ciy, 2002.

[62] Grab-Jin, Hwang, H. Ohya, Preparation of anion-exchange membranes based on block copolymers, J. Memb. Sci. 140 (1998) 195-203. doi:10.1016/S0376-7388 (97) 00283-4.

[63] S. Sharma, M. Dinda, C.R. Sharma, P.K. Ghosh, A safer route for preparation of anion exchange membrane from inter-polymer film and performance evaluation in electrodialytic application, J. Memb. Sci. 459 (2014) 122–131. doi:10.1016/j.memsci.2014.02.011.

[64] I. G. Wenten, Khoiruddin, Recent developments in heterogeneous ion-exchange membrane : preparation, modification, characterization and performance evaluation J. of Engineering Science and Technology, 11 (2016) 916-934.

[65] H. Liu, S. Yang, S. Wang, J. Fang, L. Jiang, G. Sun, Preparation and characterization of radiation-grafted poly(tetrafluoroethylene-co-perfluoropropyl vinyl ether) membranes for alkaline anion-exchange membrane fuel cells, J. Memb. Sci. 369 (2011) 277–283. doi:10.1016/j.memsci.2010.12.002.

[66] T. Yamaguchi, S. Yamahara, S. ichi Nakao, S. Kimura, Preparation of pervaporation membranes for removal of dissolved organics from water by plasma-graft filling polymerization, J. Memb. Sci. 95 (1994) 39–49. doi:10.1016/0376-7388(94)85027-5.

[67] J. Hu, C. Zhang, J. Cong, H. Toyoda, M. Nagatsu, Y. Meng, Plasma-grafted alkaline anion-exchange membranes based on polyvinyl chloride for potential application in direct alcohol fuel cell, J. Power Sources. 196 (2011) 4483–4490. doi:10.1016/j.jpowsour.2011.01.034.

[68] C. Zhang, J. Hu, M. Nagatsu, Y. Meng, W. Shen, H. Toyoda, X. Shu, High-performance plasma-polymerized alkaline anion-exchange membranes for potential application in direct alcohol fuel cells, J. Power Source 196 (2011) 5386-5393.

[69] T. Yamaguchi, S. Nakao, S. Kimura, Plasma-graft filling polymerization: preparation of a new type of pervaporation membrane for organic liquid mixtures, Macromolecules. 24 (1991) 5522–5527. doi:10.1021/ma00020a006.

[70] D.H. Kim, J.H. Park, S.J. Seo, J.S. Park, S. Jung, Y.S. Kang, J.H. Choi, M.S. Kang, Development of thin anion-exchange pore-filled membranes for high diffusion dialysis performance, J. Memb. Sci. 447 (2013) 80–86. doi:10.1016/j.memsci.2013.07.017.

[71] T. Wang, F. Sun, H. Wang, S. Yang, L. Fan, Preparation and properties of pore-filling membranes based on sulfonated copolyimides and porous polyimide matrix, Polym. (United Kingdom). 53 (2012) 3154–3162. doi:10.1016/j.polymer. 2012.05.049.

[72] N. Wang, S. Ji, J. Li, R. Zhang, G. Zhang, Poly(vinyl alcohol)-graphene oxide nanohybrid "pore-filling" membrane for pervaporation of toluene/n-heptane mixtures, J. Memb. Sci. 455 (2014) 113–120. doi:10.1016/j.memsci.2013.12.023.

[73] B.P. Tripathi, V.K. Shahi, Organic-inorganic nanocomposite polymer electrolyte membranes for fuel cell applications, Prog. Polym. Sci. 36 (2011) 945–979. doi:10.1016/j.progpolymsci .2010.12.005.

[74] Y. Wu, C. Wu, T. Xu, F. Yu, Y. Fu, Novel anion-exchange organic-inorganic hybrid membranes: Preparation and characterizations for potential use in fuel cells, J. Memb. Sci. 321 (2008) 299–308. doi:10.1016/j.memsci.2008.05.003.

[75] H. Lade, V. Kumar, G. Arthanareeswaran, A.F. Ismail, Sulfonated poly(arylene ether sulfone) nanocomposite electrolyte membrane for fuel cell applications : A review, Int. J. Hydrogen Energy. (2016). doi:10.1016/j.ijhydene. 2016.10.038.

[76] I. EG&G Technical Services, Fuel Cell Handbook, Fuel Cell. 7 Edition (2004) 1–352. doi:10.1002/zaac.200300050.

[77] C. Musse, S. Sharma, M. Madalena, D.C. Forte, R. Steinberger-wilckens, New approaches towards novel composite and multilayer membranes for intermediate temperature-polymer electrolyte fuel cells and direct methanol fuel cells, J. Power Sources. 316 (2016) 139–159. doi:10.1016/j.jpowsour.2016.03.052.

[78] Brain Cook, An introduction to fuel cells and hydrogen technology Heliocentris 3652 West 5th Avenue Canada, (2001).

[79] C.G. Arges, V. Ramani, P.N. Pintauro, Anion Exchange Membrane Fuel Cells, Elctrochemical Soc. Interface. (2010) 31–35. doi:10.3384/ecp110571227.

[80] R. C. T. Slade, J. P. Kizewski, S. D. Poynton, R. Zeng, J. R. Varcoe, Alkaline Membrane Fuel Cells, (2013). doi:10.1007/978-1-4419-0851-3.

[81] A. Amel, S. B. Smedley, D. R. Dekel, M. A. Hickner, Characterization and Chemical Stability of Anion Exchange Membranes Cross-Linked with Polar Electron-Donating Linkers, J. Electrochem. Soc. 162 (2015) F1047–F1055. doi:10.1149/2.0891509jes.

[82] C. Qu, H. Zhang, F. Zhang, B. Liu, A high-performance anion exchange membrane based on bi-guanidinium bridged polysilsesquioxane for alkaline fuel cell application, J. Mater. Mater. Chem. 22 (2012) 8203–8207. doi:10.1039/c2jm16211c.

[83] T. Hibino, K. Kobayashi, An intermediate-temperature alkaline fuel cell using an $Sn_{0.92}Sb_{0.08}P_2O_7$ -based hydroxide-ion-conducting electrolyte and electrodes, J. Mater. Chem. A. 1 (2013) 1134–1140. doi:10.1039/C2TA00368F.

[84] E. Gülzow, Alkaline Fuel Cells, Fuel Cells. 4 (2004) 251–255.

[85] T. Shigematsu, Redox Flow Battery for Energy Storage, SEI technical review 73 october 2011.

[86] C. Ponce de Len, A. Frias-Ferrer, J. Gonzlez-Garcia, D.A. Sznto, F. C. Walsh, Redox flow cells for energy conversion, J. Power sources. 160 (2006) 716–732. doi:10.1016/j.jpowsour. 2006.02.095.

[87] A. K. Manohar, K. M. Kim, E. Plichta, M. Hendrickson, S. Rawlings S. R. Narayanan, A High Efficiency Iron-Chloride Redox Flow Battery for Large-Scale Energy Storage, J. Electrochem. Soc. 163 (2016) 5118–5125. doi:10.1149/2.0161601jes.

[88] M. Skyllas-Kazacos, Novel vanadium chloride/polyhalide redox flow battery, J. Power Sources. 124 (2003) 299–302. doi:10.1016/S0378-7753(03)00621-9.

[89] G. Codina, A. Aldaz, Scale-up studies of an Fe/Cr redox flow battery based on shunt current analysis, J. Appl. Electrochem. 22 (1992) 668–674. doi:10.1007/BF01092617.

[90] C. N. Sun, Z. Tang, C. Belcher, T.A. Zawodzinski, C. Fujimoto, Evaluation of Diels-Alder poly(phenylene) anion exchange membranes in all-vanadium redox flow batteries, Electrochem. Commun. 43 (2014) 63–66. doi:10.1016/j.elecom.2014.03.010.

CHAPTER 2

EXPERIMENTAL TECHNIQUES

2.1. FT-IR

The chemical structures of the anion-exchange materials and anion-exchange membranes were characterized by Fourier transform infrared spectroscopy (FT-IR) using Perkin Elmer spectrum Two instrument (Model L160000A) in the range of 4000-400 cm^{-1}. The measurements were performed using an attenuated total reflectance (ATR) attachment. Dry and clean samples were pressed onto the crystal, without any further sample preparation.

2.2. X-ray powder diffraction

The synthesized powders were characterized by X-ray powder diffraction (XRD). XRD patterns were recorded with a SHIMADZU, XRD 700 powder diffractometer operated at 35 kV voltage and 30 mA current using CoKα radiation. Data were scanned in the angular range 20-80° (2θ), with a step size of 0.0196°/s. Diffraction patterns of the samples were correlated with standard JCPDS data for its identification.

2.3. TEM

The microstructure of the particles was investigated by means of Transmission electron microscopy (TEM). The TEM images of the nanoparticles were recorded using a JEOL 4000EX High Resolution Transmission Electron Microscope (HRTEM) operated at 400 kV. The TEM images reveal the particle morphology and size of the nanopowder.

2.4. SEM

Scanning electron microscopy was used to investigate the surface morphology of the samples. SEM images of the samples were acquired with a scanning electron microscope (JSM-5600, JEOL Co., Japan). Samples were kept in a vacuum oven at

30°C overnight and were coated with a thin layer of gold by ion sputtering prior to microscopic examination. The energy dispersive analyzer was used for the elemental detection of the samples.

2.5. Ion exchange capacity

The ion exchange capacity (IEC) of the membranes, which is the amount of charged groups in the membrane, was measured using a titration method [1]. The ion exchange capacities (IECs) of the composite membranes were determined by double titration method. Samples were accurately weighed and were immersed in 25 ml of 0.05M HCl solution for 48 h and the HCl solution was back titrated by 0.05M NaOH solution using phenolphthalein as indicator. IECs of the samples were calculated using the equation:

$$\text{IEC} = \frac{n_1 - n_2}{M_{dry}}$$

Where n_1 and n_2 are the concentrations of (m mol) hydrochloric acid required before and after equilibrium respectively, and M_{dry} is the mass in g of the dried sample. The average value of the three samples calculated from the above equation is the IEC value of the membrane.

2.6. Thermo Gravimetric Analysis (TGA)

TGA thermograms of the membranes were recorded on a Shimadzu TGA-50H analyzer by heating the samples from room temperature to 850°C under nitrogen atmosphere at a heating rate of 10°C/min. This technique gives an indication of the short-term thermal properties and stabilities of the polymers.

2.7. Water uptake

Water uptake of the composite membranes was determined by weighing the membranes under wet conditions after being equilibrated in distilled water for 24 h at room temperature. The surfaces of the membranes were then carefully wiped with filter

paper and the membranes were weighed immediately. The samples were vacuum dried for two days and weighed again. The water uptake was calculated as follows [2].

$$Water\ uptake\ (\%) = \frac{W_{wet} - W_{dry}}{W_{dry}} \times 100\,\%$$

Where W_{wet} is the mass of the water swollen membrane, and W_{dry} is the mass of the dry membrane.

2.8. Alkaline stability

The stability of the membranes in alkaline solution was examined by immersing the membrane samples in N_2 saturated 2M aq. NaOH at room temperature [3]. For this purpose, the membrane sample with a size of 3cm x 3cm was immersed in 2M aq. NaOH at room temperature for 2 weeks. They were taken out, washed with D.I. water, wiped with tissue paper, and then studied using FT-IR technique to detect any degradation or changes in chemical structures. Weight loss of the membrane is also recorded to detect their stability.

2.9. Oxidative stability

The oxidative stability of the membranes was tested by immersing the membranes in Fenton's reagent (4 ppm $FeSO_4$ in 3% H_2O_2) for period of 24 h at room temperature. The membranes were intermittently taken out of the solution and weighed after wiping off the excess surface water. During this test membranes are subjected to free radical attack by $OH^{\cdot}$ and $OOH^{\cdot}$ formed by H_2O_2 in the presence of Fe^{2+} and this may cause membrane degradation. Weight loss of the membranes was recorded to detect their stability [4,5].

2.10. Measurements of methanol permeability through membranes

The methanol permeability of the membranes was measured by Gasa's method [6]. 20ml glass vials were filled with 10ml pure methanol. The membranes were clamped between the mouth of the vial and the cap. The cap had a 2cm x 2cm size hole so that the

methanol could escape only through the hole. The mass of the methanol inside the cell was measured as a function of time at room temperature. The methanol permeability (P) was calculated using the equation

$$P = \frac{N \times l}{V.P. \times A \times t}$$

where N is the number of moles of methanol lost (moles), l is the thickness of the membrane (cm), P is the saturated vapor pressure of methanol, A is the area of the small hole on the cap (cm^2), and t is the time (days).

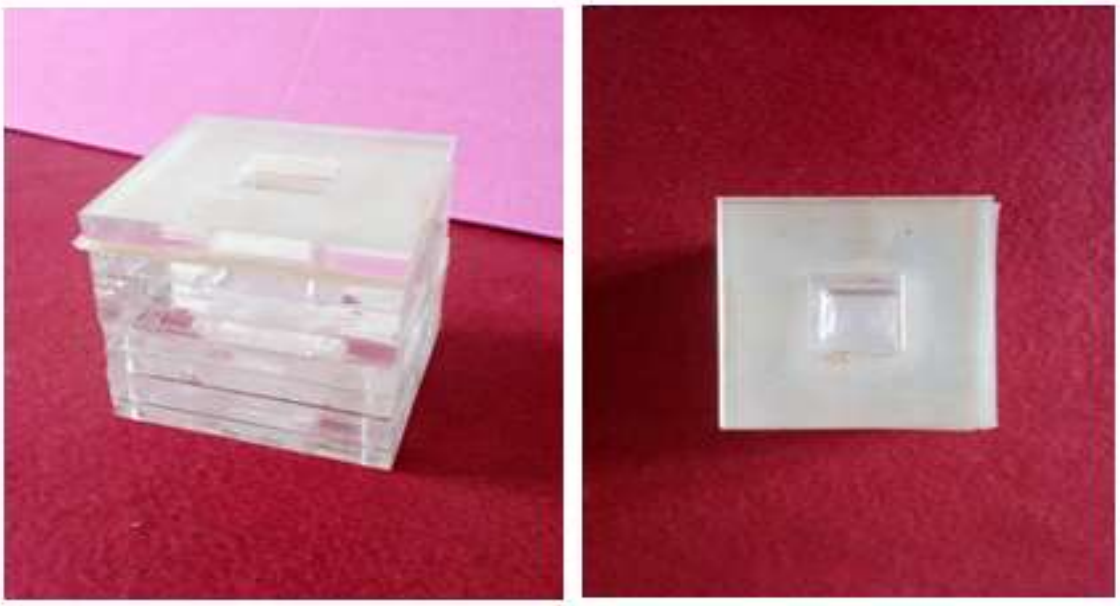

Fig. 35 Cell for methanol permeability measurements

2.11 Electrochemical impedance spectroscopy (EIS) techniques

Electrochemical impedance describes the response of a circuit to an alternating current or voltage as a function of frequency [7]. In DC circuit, only resistors resist the flow of current which is defined by Ohm's Law: E = I R. where E, I and R are potential, current and ohmic resistance respectively. While in an AC circuit, two other circuit elements, capacitors and inductors, impede the flow of electrons given by the analogous equation E = I Z, where E, I and Z are potential, current and impedance respectively. Impedance values are also measured in ohms. Impedance can be expressed as a complex

number, where the resistance is the real component and the combined capacitance and inductance is the imaginary component.

Modeling of equivalent circuit

An electrochemical cell has electrical double layers in the phase boundaries between interfaces of electrodes and electrolytes. This double layer has two opposite electric charges in the phase boundaries, which can be considered as a capacitor when we apply a low AC voltage [8].

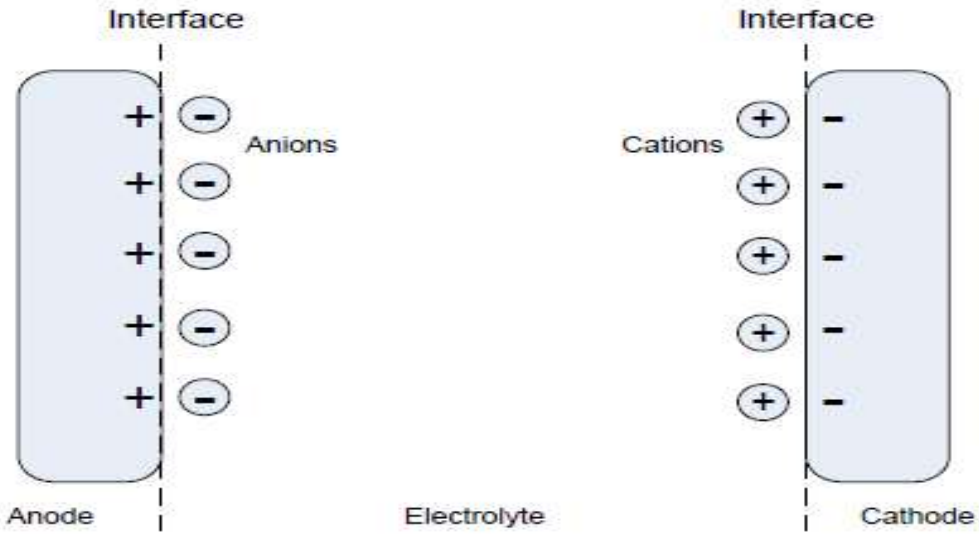

Fig. 36 The interface concept between the electrodes and the electrolyte [8]

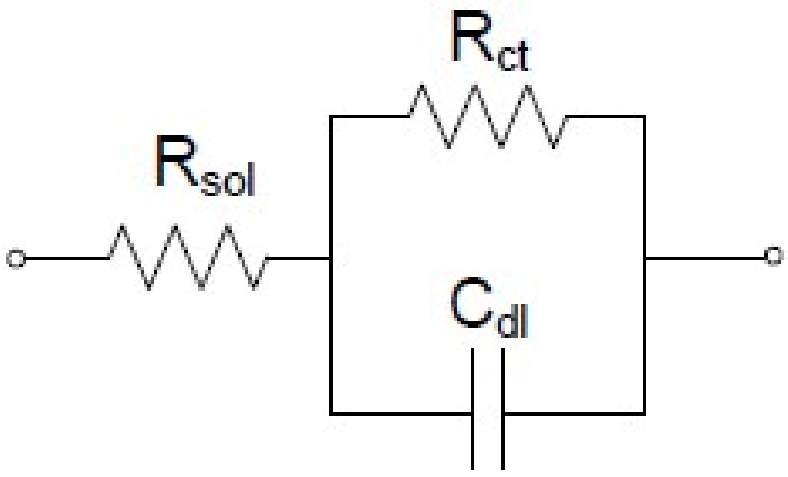

Fig. 37 The equivalent circuit for measuring the membrane resistance [8]

An electrical circuit equivalent to this electrochemical system can be represented as above, where R_{sol}, R_{ct}, and C_{dl} are the resistance of the solution, the charge transfer resistance, and the double layer capacitance. The charge transfer resistance is due to the difficulty of charge transfer on the surface of electrode. The double layer capacitance is the capacitance at the electrode surface. On applying an AC voltage V, to the capacitor

$$V = V_0 \, exp \, (j2\pi ft)$$

Where j is an imaginary unit, f is frequency of the applied voltage, and t time by second. The current *i*, can be written as

$$I = \frac{dQ}{dt} = C_{dl} \frac{dV}{dt} = (j2\pi \, f \, C_{dl}) \, E_0 \exp(j \, 2\pi \, f \, t) = (j \, 2\pi \, f \, C_{dl}) \, V$$

Where Q stands for the total electrical charge passed. The impedance of the double layer Z is

$$Z = \frac{V}{I} = \frac{1}{j \, (2\pi \, f \, Cdl)}$$

The above equation shows that the impedance of an electrochemical system varies with applied frequency. For a circuit as in Fig. 37 the impedance is

$$Z = R_{sol.} + \frac{Rct}{1+j \, (2\pi \, f \, Rct \, Cdl)} = (R_{sol} + \frac{Rct}{1+ \, (2\pi \, f \, Rct \, Cdl)^2}) \text{ -- } j\frac{2\pi \, f \, R_{ct}^2 Cdl}{1+ \, (2\pi \, f \, Rct \, Cdl)^2}$$

Above equation shows that imaginary part of impedance varies with the applied frequency. When the frequency increases toward infinity ($f \rightarrow \infty$), the impedance approximates the solution resistance (Rsol). When the frequency increases toward zero ($f \rightarrow 0$), the impedance approximates the sum of the solution resistant and the charge transfer resistance [8].

The Nyquist Plot

The EIS experiment involves applying a small sinusoidal voltage of about 10 mV and measuring the resulting current along with the phase angle [7]. Using this data, the real impedance component (Z') and imaginary impedance components (Z") are calculated and plotted against each other for varying frequencies in the Nyquist spectra [9]. The real impedance value (Z') at the highest frequency measurement in the Nyquist plot was taken as the resistance of the membrane.

Ionic conductivity of the membranes was evaluated using AUTOLAB 50519 PGSTAT instrument. Impedance measurements of the membranes were performed in a two electrode setup where the membranes were clamped between two platinum electrodes and the cell was thermostated at 25±0.1°C for at least 20 minutes to ensure thermal equilibrium [10]. Impedance measurements were performed in the frequency range 100 Hz-1000 kHz using an alternating potential of amplitude 10 mV. Fully hydrated membranes were placed in the conductivity cell and it was filled with 1M NaOH. The real impedance value at the highest frequency measurement in the Nyquist plot was taken as the resistance of the membrane. This was then used to calculate the membrane conductivity. The resistance of the membrane and solution was measured (R_{total}) [8]. The resistance of the solution was measured without the membrane ($R_{solution}$). Membrane resistance (R_{mem}) was obtained from the difference of the measured resistances ($R_{mem} = R_{total} - R_{solution}$) [11]. The thickness of the membrane was measured with a digital micrometer by placing the membrane between two glass slides to ensure both a planar surface and limited compression. The conductivity of the membrane was calculated as follows $\sigma = L/RA$ mS cm^{-1}, Where σ is the hydroxide conductivity in mS cm^{-1}, R is the ohmic resistance of the membrane (**Ω**), L is the thickness of the membrane (in cm), A is the cross sectional area of membrane samples (cm^2).

Fig. 38 AUTOLAB 50519 PGSTAT instrument used for impedance measurements

Fig. 39 Conductivity cell used for the impedance measurements

2.12 Tensile strength measurements

Tensile testing is the most common methodology for the measurement of the tensile/mechanical strength of a material. The membrane samples were evaluated under a controlled strain rate until failure. The mechanical properties of the composite membranes were measured with universal testing machine (UTM) (Zwick, Model 1446-60, Germany). For this test the samples were prepared according to ASTM-D882 standard. The films were then placed between the grips of the testing machine. The grip length was 5cm and speed of testing was set at the rate of 10 mm min^{-1}.

2.13 Performance of membranes as separator in all-iron flow battery

All-iron flow battery experiments were performed in the 36 cm^2 flow cell hardware with electrolyte flowing across two electrodes, separated by the membrane prepared [12]. All experiments were performed with electrolyte flow rates of 25 ml min^{-1}. Electrolyte for both positive and negative electrodes consisted of 1M $FeCl_2$ and 1.5 M NH_4Cl. The electrodes were made from densified graphite with a cross-sectional area of 16 cm^2. The charging efficiency of the all-iron redox flow cell was determined by Charging the cell at 100 mA cm^{-2} for 100 s followed by discharging at 50 mA cm^{-2} using AUTOLAB 50519 PGSTAT instrument. The cell performance is normally determined by its coulombic efficiency (CE). CE is the ratio of a cell's discharge capacity (Q dis) to its charge capacity (Q ch).

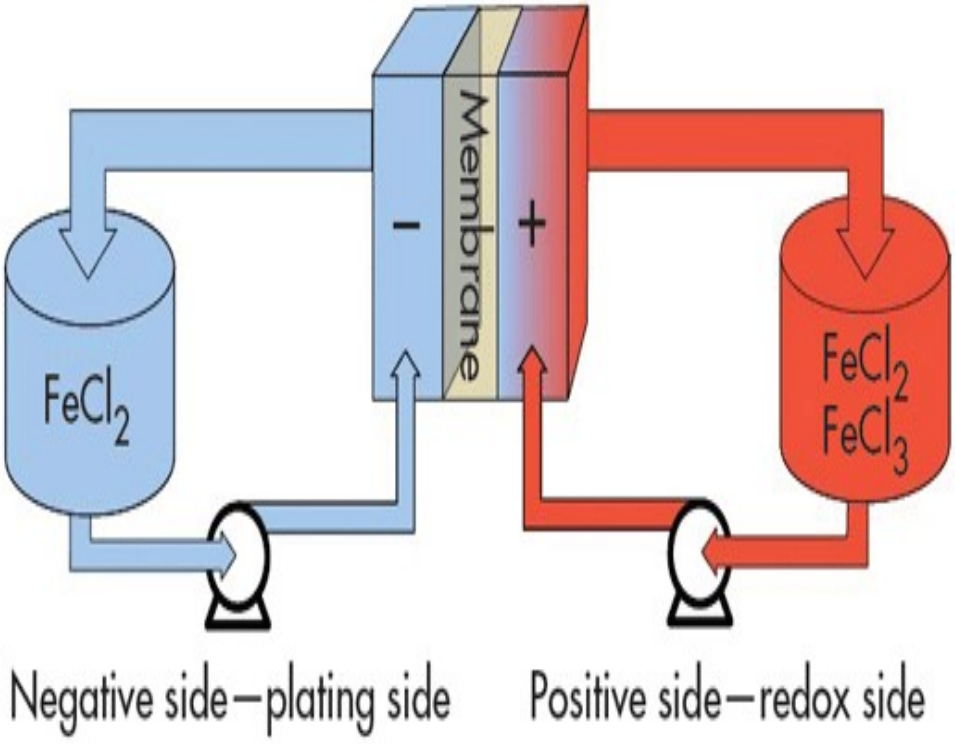

Fig. 40 All-iron flow battery Schematic diagram

2.14 References

[1] H. Wang, Y. Liu, M. Li, H. Huang, H. M. Xu, R. J. Hong, H. Shen, Multifunctional TiO_2 nanowires-modified nanoparticles bilayer film for 3D dye-sensitized solar cells, Optoelectron. Adv. Mater. Rapid Commun. 4 (2010) 1166–1169. doi:10.1039/b000000x.

[2] M. Heydari, A. Moheb, M. Ghiaci, M. Masoomi, Effect of cross-linking time on the thermal and mechanical properties and pervaporation performance of poly(vinyl alcohol) membrane cross-linked with fumaric acid used for dehydration of isopropanol, J. Appl. Polym. Sci. 128 (2013) 1640–1651. doi:10.1002/app.38264.

[3] B. Lin, F. Chu, Y. Ren, B. Jia, N. Yuan, H. Shang, T. Feng, Y. Zhu, J. Ding, Alkaline stable C_2-substituted imidazolium-based cross-linked anion exchange membranes for alkaline fuel cell applications, J. of Power Sources. 266 (2014) 186-192 .

[4] X. Li, H. Zhang, Z. Mai, H. Zhang, I. Vankelecom, Ion exchange membranes for vanadium redox flow battery (VRB) applications, Energy Environ. Sci. 4 (2011) 1147. doi:10.1039/c0ee00770f.

[5] P. Y. Xu, T. Y. Guo, C. H. Zhao, I. Broadwell, Q. G. Zhang, Q. L. Liu, Anion exchange membranes based on poly(vinyl alcohol) and quaternized polyethyleneimine for direct methanol fuel cells, J. Appl. Polym. Sci. 128 (2013) 3853–3860. doi:10.1002/app.38592.

[6] S. D. Sajjad, D. Liu, Z. Wei, S. Sakri, Y. Shen, Y. Hong, F. Liu, Guanidinium based blend anion exchange membranes for direct methanol alkaline fuel cells (DMAFCs), J. Power Sources. 300 (2015) 95–103. doi:10.1016/j.jpowsour.2015.08.002.

[7] Application Note AC-1 Subject : Basics of Electrochemical Impedance Spectroscopy Overview.

[8] T. Naya, Conductivity of ion exchange materials, Thesis in Energy and Mineral Engineering, The Pennsylvania State University, The Graduate School Department of Energy and Mineral Engineering (2010).

[9] P. M. Gomadam, J. W. Weidner, Analysis of electrochemical impedance spectroscopy in proton exchange membrane fuel cells, Int. J. Energy Res. 29 (2005)1133–1151. doi:10.1002/er.1144.

[10] W. E. Mustain, J. A. Vega, C. Chartier, W. E. Mustain, Effect of hydroxide and carbonate alkaline media on anion exchange membranes Effect of hydroxide and carbonate alkaline media on anion exchange membranes, Journal of Power Sources 195 (2010) 7176–7180. doi:10.1016/j.jpowsour.2010.05.030.

[11] J. S. Koo, N. Kwak, T. Sung, Synthesis and properties of an anion-exchange membrane based on vinylbenzyl chloride–styrene–ethyl methacrylate copolymers, J. Memb. Sci. 423-424 (2012) 293–301. doi:10.1016/j.memsci.2012.08.024.

[12] A. K. Manohar, K. M. Kim and et al., A High Efficiency Iron-Chloride Redox Flow Battery for Large-Scale Energy Storage, J. Electrochem. Soc. 163 (2016) 5118–5125. doi:10.1149/2.0161601jes.

CHAPTER 3

SYNTHESIS AND CHARACTERIZATION OF CALCIUM TITANATE (PEROVSKITE) NANOPOWDER AS ANION-EXCHANGE MATERIAL BY CO-PRECIPITATION FROM SIMPLE PRECURSORS

3.1. Introduction

Currently, researchers in the field of material science are interested in the synthesis of variety of nanosized ceramic materials. Among different types of ceramics, perovskite belongs to a novel class of material with a variety of potential technological applications [1,2]. The general chemical formula of perovskite is ABX_3, where A represents large divalent and B is a small tetravalent cation. X can be anions like O^{-2} which is bonded to both cations. Calcium titanate can exist in three polymorphic phases, including cubic, tetragonal and orthorhombic [3]. $CaTiO_3$ based perovskites show exceptionally high dielectric properties, which makes them potentially useful resonator materials in wireless communication systems [4,5]. Wang et al. reported that $CaTiO_3$ coated Ti electrodes modified with a thin hydrophobic layer are having better corrosion resistance. Platinum doped $CaTiO_3$, Zr^{4+} doped $CaTiO_3$ and CoO doped $CaTiO_3$ powders exhibit high catalytic efficiency in water splitting, for hydrogen production [1,6]. Since calcium titanate based ceramics form a number of solid solutions with lanthanides and actinides, they find applications in the storage and treatment of nuclear wastes [7,8]. In medicine, calcium titanate is highly useful due to its bio-compatibility and finds applications in fabricating materials for bone and joint repair [1,9].

Titanium alloys are widely used as metallic implantable materials and calcium titanate coating is an effective method to enhance biocompatibility of titanium surfaces [10].

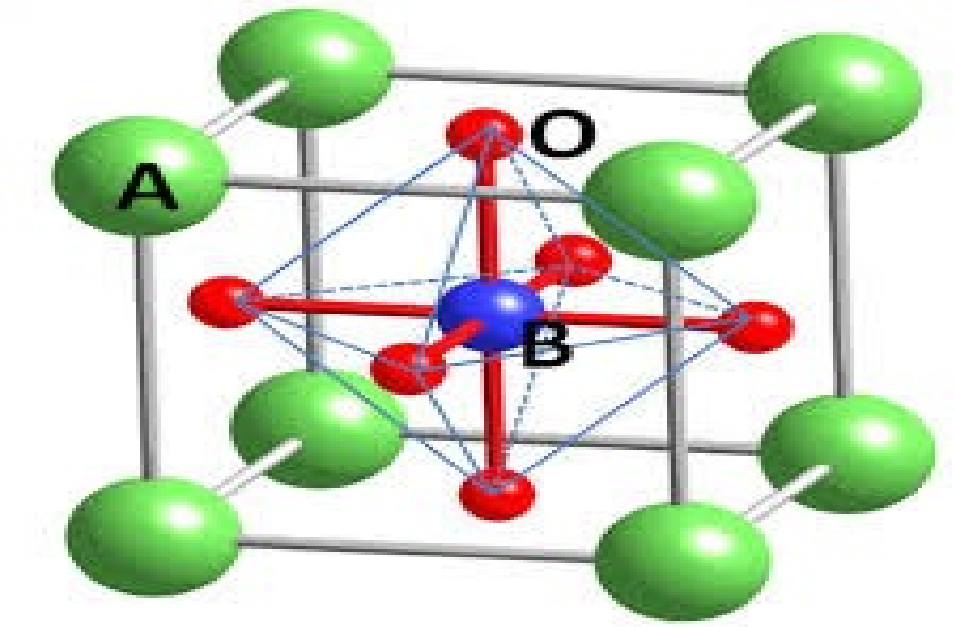

Fig. 41 Chemical structure of perovskite

Calcium titanate, when treated with bases in wet condition is converted to calcium titanate hydroxide (eqn.1) and it is reported to be an efficient anion-exchange material containing exchangeable hydroxyl groups [11].

$$CaTiO_3 + NaOH \rightarrow HCaTiO_3OH \quad \text{---------- (1)}$$

Various methods have been reported for the synthesis of nano sized calcium titanate particles, including solid state synthesis [12,13], sol-gel methods [14,15], hydrothermal methods [13], co-precipitation methods [16], mechanical alloying methods [17], solvo-thermal methods [18,19] etc. The co-precipitation method is widely used to synthesize ceramic materials since this method is simple and the mixing of the reagents occurs on an atomic level rather than a particulate level. Y.K. Sharma et al. attempted to synthesize transition metal titanates ($MTiO_3$), (M = Mn, Fe, Co, Ni and Cd) using co-precipitation of mixed metal oxalates by adding transition metal chlorides to potassium titanyl oxalate solution followed by calcination [20]. The XRD pattern showed that the $MTiO_3$ was not phase pure and contained significant amounts of transition metal oxides and other impurities [19].

Here we report the synthesis of calcium titanate nanopowder by a novel co-

precipitation method in ammoniacal medium using a simple precursor potassium titanyl oxalate followed by calcination. The structure and morphology of the synthesized nanopowder were studied by XRD, FT- IR, HRTEM, SEM and EDX techniques.

3.2. Experimental

3.2.1. Synthesis of calcium titanate nanopowder

20 g potassium titanyl oxalate (Sigma Aldrich) and 6 g calcium chloride (Sigma Aldrich) were separately dissolved in 250 ml D. I. water. The above two solutions were mixed, and slowly treated with 250 ml 0.2M ammonium oxalate solution. The solution was maintained at a pH of 9 by adding 25% ammonia solution and stirred for 2 h on a magnetic stirrer. The resulting white slurry was kept overnight for ageing at room temperature. It was then filtered, washed with D. I. water and dried at 80°C for two days. The dried precipitate was ground to fine powder and was calcined at 900°C for 2 h to obtain pure calcium titanate.

The synthesis procedure is shown in equation (1).

$$K_2[TiO(C_2O_4)_2].2H_2O \xrightarrow{(NH_4)_2C_2O_4,\ NH_4OH} CaTi(OH)_x(C_2O_4)_y \xrightarrow{900\ ^oC,\ 2h} CaTiO_3 \quad (1)$$

3.2.2. Characterization Techniques

X-ray powder diffraction data of the synthesized nanopowder was collected at room temperature with a SHIMADZU, XRD700 powder diffractometer using Co-K_α radiation. Data were scanned over the angular range 20-80° (2θ) with a step size of 0.0196° (2θ). FT-IR spectrum of the sample was recorded in the range of 400-4000 cm^{-1} using Perkin Elmer instrument (Model L160000A). Calcium titanate was treated with 2M NaOH for 24 h at room temperature for hydroxylation reaction. It was washed with water and then dried. FT-IR spectrum of the sample was recorded. Transmission electron microscopy (TEM) images of the obtained nanoparticles have been recorded using a JEOL 4000EX High Resolution Transmission Electron Microscope (HRTEM) operated at 400 kV. SEM images of the samples were acquired with a scanning electron microscope (JSM-5600, JEOL Co., Japan). The samples were coated with a thin layer of

gold by ion sputtering prior to microscopic examination. The energy dispersive analyzer was used for the elemental detection of the samples.

3.3. Results and discussion

3.3.1. X-ray diffraction analysis

The XRD pattern of $CaTiO_3$ obtained after calcination at 900°C is shown in **Fig.** 42. Diffraction patterns of calcium titanate powder well correlates with standard (JCPDS No. 22-153) [21] and dominant peaks are obtained at 2θ = 32.7, 47.1, 58.9, and 69, which corresponds to diffraction from (121), (202), (123), (242) planes [15,19]. In our study the XRD pattern clearly shows that the powder obtained by the thermal decomposition of ($CaTi(OH)_x(C_2O_4)_y$) at 900°C consists of pure orthorhombic perovskite nanopowder ($CaTiO_3$) without oxides or any other impurities. The crystallite size of the material was calculated using Debye-Scherrer formula [22] as given in equation (2).

$$d = \frac{0.9\lambda}{\beta \cos\theta} \quad \cdots\cdots \qquad (2)$$

Where d is the crystallite size, λ is the X-ray wavelength, β is the full width at half maxima and θ is the Bragg's angle. From this equation, the average crystallite size of the synthesized material was found to be approximately 200 nm.

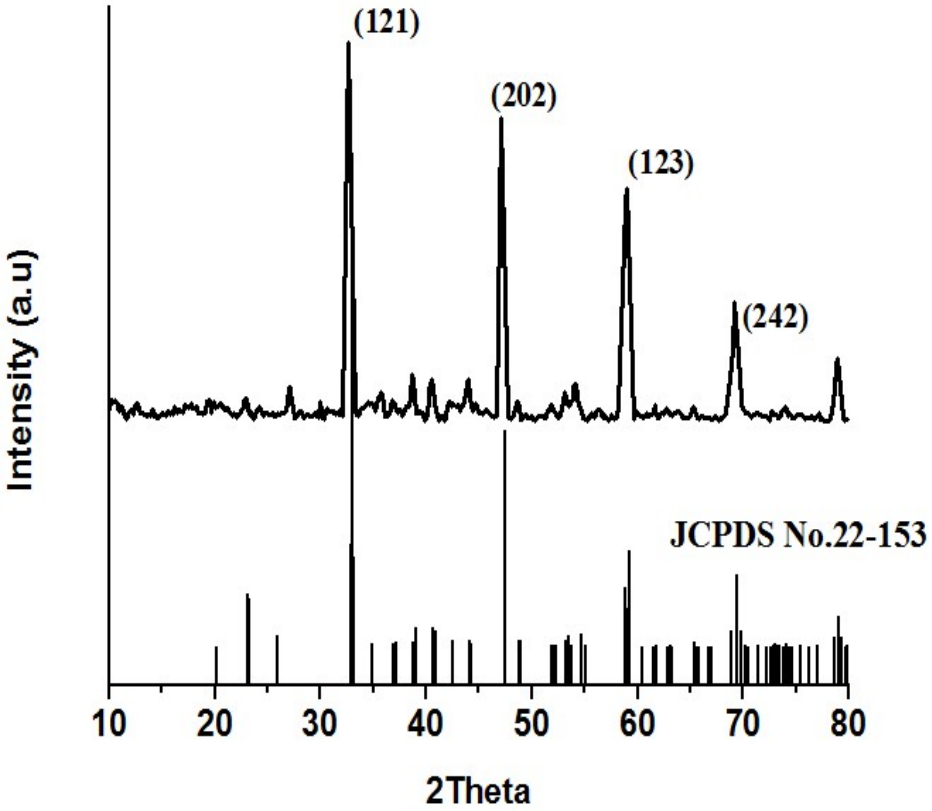

Fig. 42 XRD pattern of $CaTiO_3$ powder

3.3.2 Structural analysis

FT-IR spectra of the sample before and after calcination are presented in **Fig.** 43 (a-b). **Fig.** 43 (a) shows a characteristic peak at 1615 cm^{-1} which is assigned to the antisymmetric O-C-O stretching vibrations of the oxalate group in the sample. The absorption band at 1315 cm^{-1} is attributed to symmetric O-C-O stretching vibrations and the band at 780 cm^{-1} is assigned to the in plane O-C-O deformation vibrations, indicating the presence of oxalate group in the sample [23]. The spectrum 43(b) shows the absence of characteristic bands of oxalate group, indicating the complete elimination of oxalate after calcination at 900°C for 2 h. The absorption band at 540 cm^{-1} corresponds to specific stretching vibrations of Ti-O bonds [22,24] and the band at 450 cm^{-1} is a characteristic feature of Ca-Ti-O bending vibrations of calcium titanate [18]. The absence of characteristic vibrations of oxalate after calcination at 900°C reveals the formation of pure $CaTiO_3$.

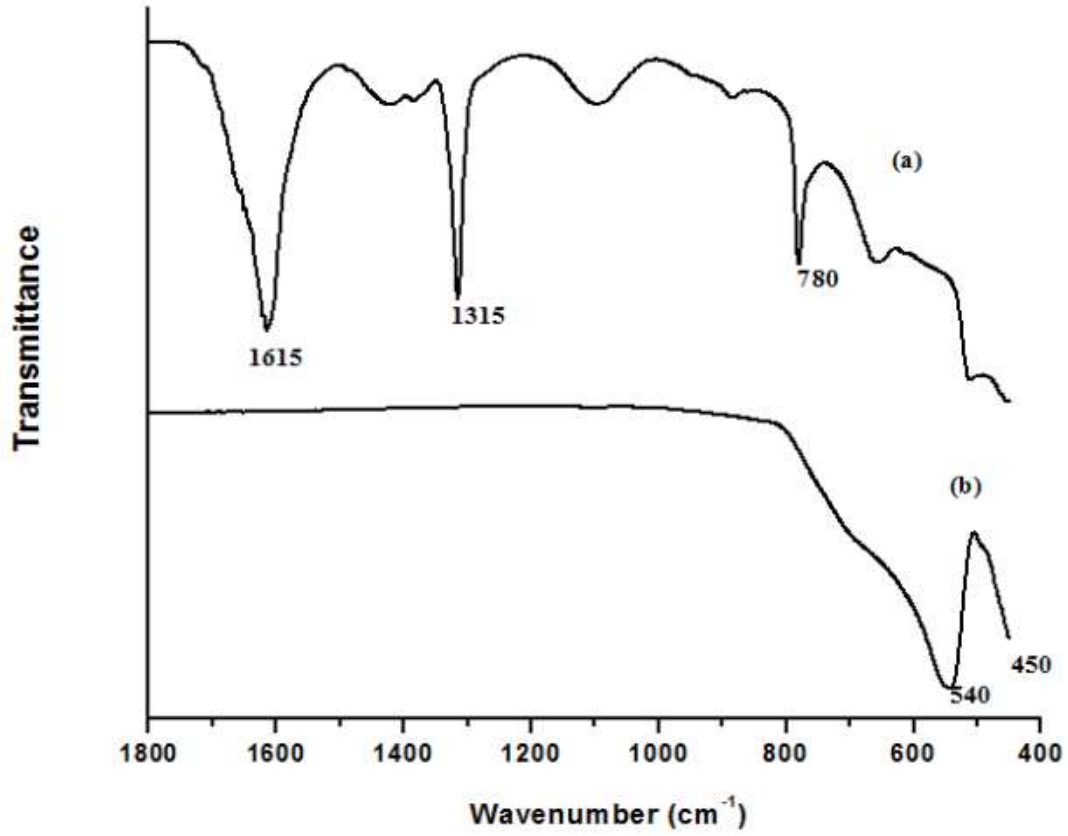

Fig. 43 FT-IR spectrum of mixed oxalate and hydroxide of calcium and Titanium (a) before calcination (b) after calcination

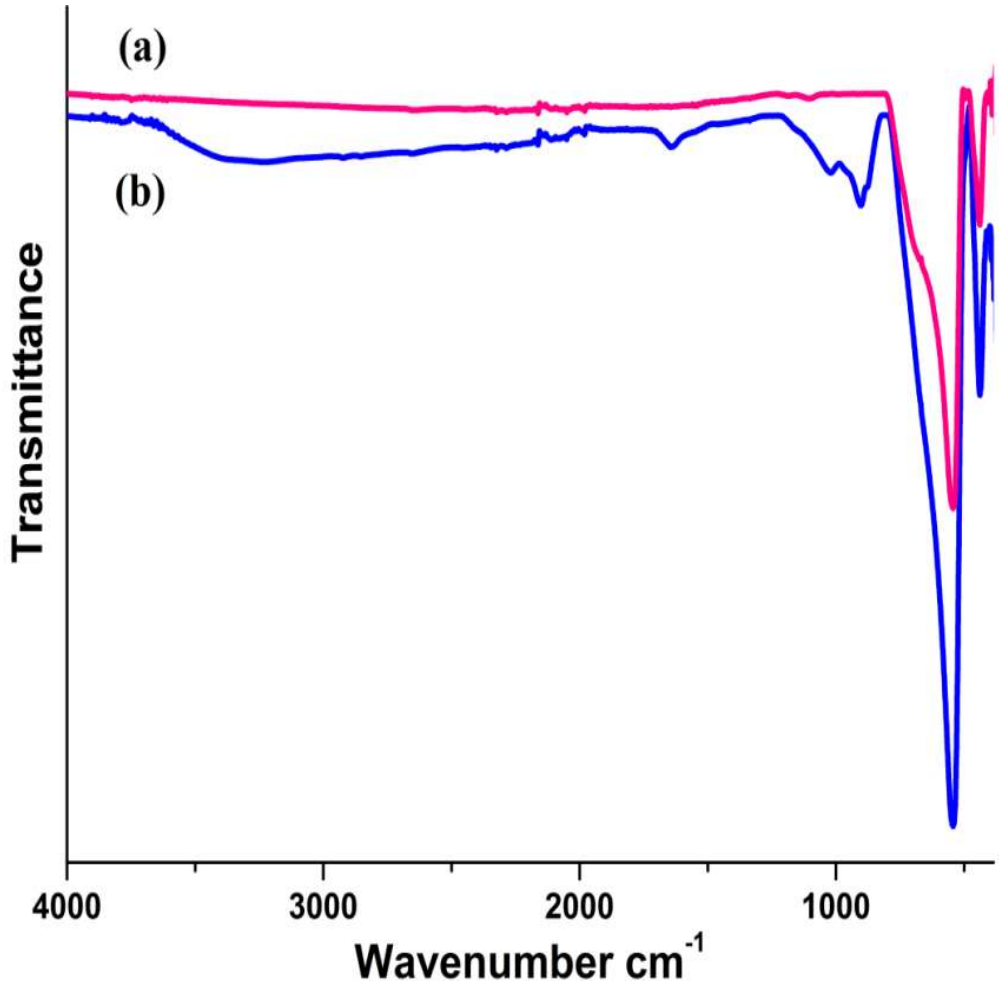

Fig. 44 FT-IR spectrum of calcium titanate (a) before hydroxylation (b) after hydroxylation

FT-IR spectrum of calcium titanate before and after hydroxylation is presented in **Fig.** 44 (a-b). **Fig.** 44(a) shows two characteristic peaks at 540 cm^{-1}, 450 cm^{-1} in the spectrum of $CaTiO_3$ which correspond to the stretching vibrations of Ti-O bonds [22] and Ca-Ti-O bending vibrations [18] respectively. As seen in **Fig.** 44(b) the band in the region 3400-3200 cm^{-1}, is attributed to stretching vibrations of –OH groups of calcium titanate hydroxide ($HCaTiO_3OH$) due to the hydroxylation of calcium titanate in alkaline environment.

3.3.3 TEM analysis

The microstructure of the particles was investigated by means of TEM. **Fig.** 45 (a, b) shows the TEM image of $CaTiO_3$ and reveals the particle morphology and size of the nanopowder. It is seen from TEM images that $CaTiO_3$ powders consist of clusters of nanoparticles. The nanoparticles are found to be spherical in shape with an average size of 200 nm.

HRTEM images **Fig.** 45(c) reveals the formation of nano-crystals with d spacing of 0.32 nm. The corresponding selected area electron diffraction (SAED) pattern is given in **Fig.** 45(d) which reveals the crystalline nature and the rings in the SAED pattern corresponds to crystal planes of calcium titanate.

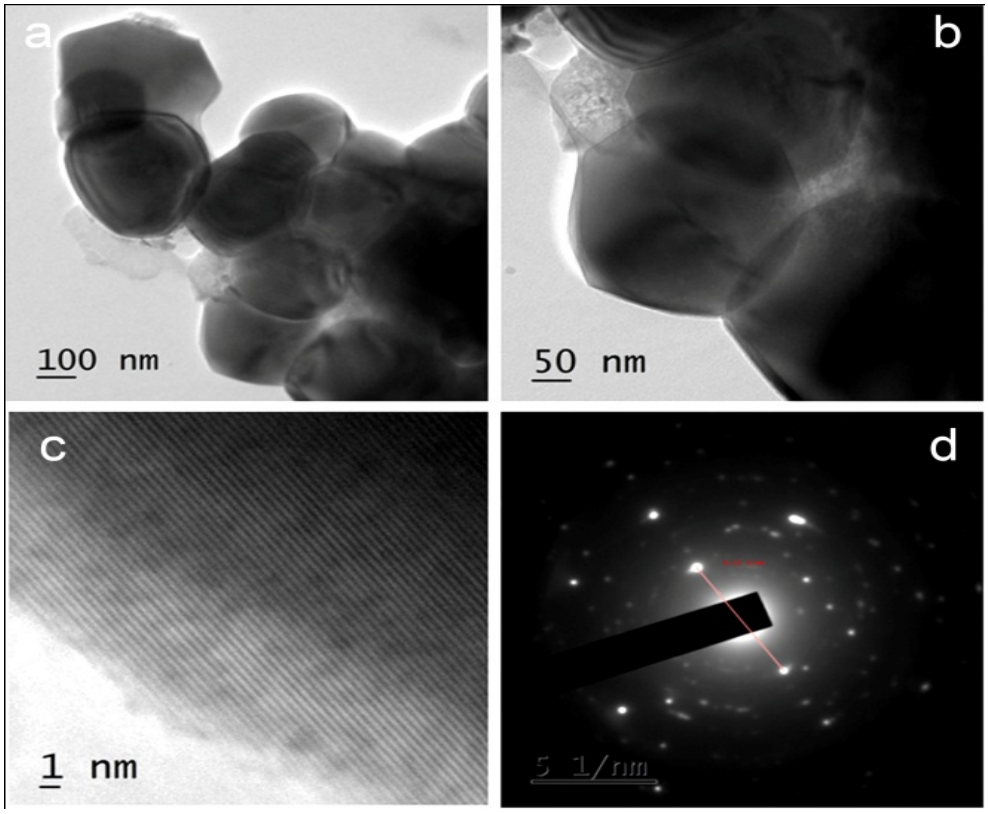

Fig. 45 (a, b) TEM images of calcium titanate at different magnifications
(c)HRTEM image of calcium titanate nanocrystals
(d) SAED pattern of calcium titanate

3.3.4. SEM analysis

The SEM images of calcium titanate are shown in Fig 46. The SEM image shows the microstructure of the particles. The images revealed the information about grain size, shape and powder agglomeration. The particles are found to be spherical in shape and are highly agglomerated. The average size of the particles was in 200 nm range.

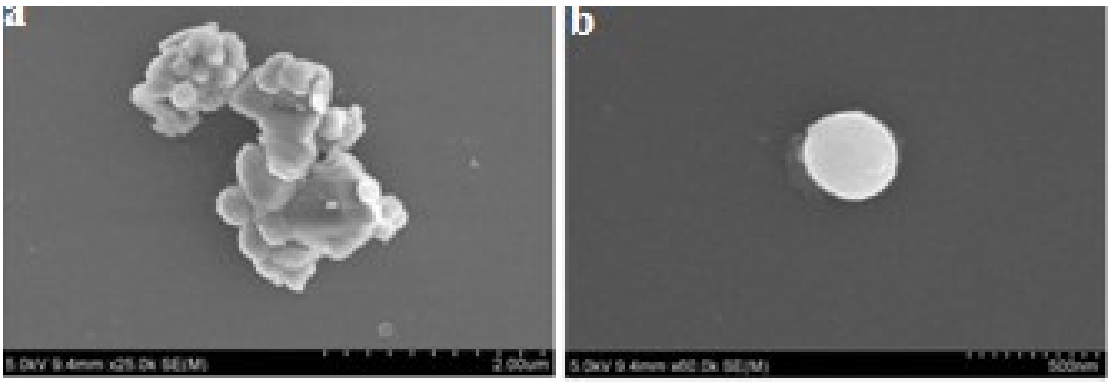

Fig. 46 (a, b) SEM images of calcium titanate with different magnifications

3.3.5 EDX analysis

EDX spectrum of calcium titanate shown in **Fig.** 47 indicates the presence of Ca, Ti and O atoms in accurate proportion in the prepared material. This further confirmed the formation of pure calcium titanate.

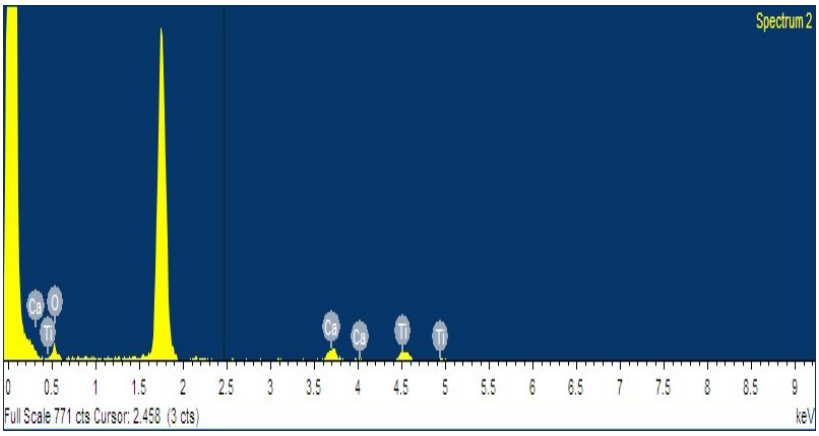

Fig. 47 The EDX spectrum of calcium titanate

3.4. Conclusions

A novel co-precipitation method has been developed to synthesize phase pure calcium titanate (perovskite) nanopowder by precipitating mixed oxalate hydroxide of calcium and titanium [CaTi $(OH)_x(C_2O_4)_y$] from a solution of potassium titanyl oxalate and calcium chloride in ammoniacal medium followed by calcination. The XRD pattern revealed the formation of phase pure orthorhombic calcium titanate. FT-IR spectrum indicated the characteristic vibrations of calcium titanate. The TEM image reveals the spherical shape of particles. The crystalline nature of the particles was also revealed by HRTEM image, and particles are found to be spherical shape, with an average size of 200 nm. Selected area electron diffraction (SAED) pattern reveals the crystalline nature of the material and the rings in the SAED pattern corresponds to the crystal planes of calcium titanate. Morphological features investigated with SEM, reveals that the $CaTiO_3$ particles are having a spherical shape with a diameter of approximately 200 nm.

3.5 References

[1] V. S. Marques, L. S. Cavalcante, J. C. Sczancoski, E.C. Paris, J. M. C. Teixeira, J. A. Varela, F. S. De Vicente, M. R. Joya, P. S. Pizani, M. Siu Li, E. Longo, Synthesis of (Ca,Nd)TiO_3 powders by complex polymerization, Rietveld refinement and optical properties, Spectrochim. Acta-Part A Mol. Biomol. Spectrosc. 74 (2009) 1050–1059. doi:10.1016/j.saa.2009.08.049.

[2] P. N. Nirmala, G. Suresh, Synthesis and Characterization of Barium Titanate, Calcium Titanate and Strontium Titanate Thin Films, IJSER 5 (2014) 587–594.

[3] S. Manafi, M. Jafarian, Determining the Optimal Conditions for Calcium Titanate Nanostructures Synthesized by Mechanical Alloying Method, Adv. Ceram. Prog. 1 (2015) 11–16

[4] H. Zheng, I. M. Reaney, C.D.C. Csete de Gyorgyfalva, Raman spe troscopy of $CaTiO_3$ based perovskite, J. Mater. Res. 19 (2004) 488–495.

[5] H. Zheng, H. Bagshaw, G.D.C. Csete de Gyrgyfalva, I.M. Reaney, R. Ubic, J. Yarwood, Raman spectroscopy and microwave properties of $CaTiO_3$-based ceramics, J. Appl. Phys. 94 (2003) 2948–56. doi:http://dx.doi.org/10.1063/1.1598271.

[6] K. Shimura, H. Miyanaga, H. Yoshida, Preparation of calcium titanate photocatalyststst for hydrogen production, Studies in Surface Science and Catalysis, 175 (2010) 85-92. doi:10.1016/S0167-2991(10)75011-4.

[7] L. T. Yazid, K. Tahar, K. Karim, New Green Dielectrics Related to Calcium Titanate: Synthesis and Characterizations, 40 (2015) 2873–2879. doi:10.1007/s13369-015-1795-6.

[8] R. Mucillo, J. R.Carmo, Synthesis and characterization of strontium and calcium titanate polycrystalline powders by a modified polymeric precursor technique, 728 (2012) 904–908. doi:10.4028/www.scientific.net/MSF.727-728.904.

[9] A. K. Dubey, B. Basu, K. Balani, R. Guo, A. S. Bhalla, Multifunctionality of Perovskites $BaTiO_3$ and $CaTiO_3$ in a Composite with Hydroxyapatite as Orthopedic Implant Materials, Integr. Ferroelectr. 131 (2011) 119–126

[10] J. P. Wiff, V. M. Fuenzalida, J. L. Arias, M. S. Fernandez, Hydro thermal, electrochemical $CaTiO_3$ coatings as precursor of a biomimetic calcium phosphate layer, Mater. Lett. 61 (2007) 2739–2743. doi:10.1016/j.matlet.2006.06.092.

[11] O.M. Urbain, W.R. Stemeri, H. Charles, United states "patent office 7", Us Patent. 2208173. (1940).

[12] A. Tripathy, S. Pramanik, A. Manna, N. Farhana, A. Shah, Ca-Mg-Ti-Fe-Oxides Based Ceramic Nanocrystals and Flexible Film of Polydimethylsiloxane Composite with Improved Mechanical and Dielectric Properties for Sensors, Sensors 16 (2016) 22. doi:10.3390/s16030292.

[13] Rai US, Singh L, Mandal KD, Singh NB (2014) An Overview on Recent Developments in the Synthesis, Characterization and Properties of High Dielectric Constant Calcium Copper Titanate Nano-Particles. Nanosci Technol 1 (2014) 1-17.

[14] S. Pilban, A. K. Zak, W. H. A. Majid, M. R. Muhamad, Synthesis and Characterization of Lead Calcium Titanate Nanocomposite, AIP Conf. Proc. 1328 (2011) 183–185. doi:10.1063/1.3573723.

[15] P. K. Mallik, G. Biswal, S. C. Patnaik, Characterisation of Sol-Gel Synthesis of Phase Pure $CaTiO_3$ Nano Powders after Drying, IOP Conf. Ser. Mater. Sci. Eng. 75 (2015) 012005 doi:10.1088/1757-899X/75/1/012005

[16] B. A. Hernandez-sanchez, B. A. Tuttle, J. A. Voigt, D. L. Moore, T. J. Garino, P. Mahoney, M. A. Rodriguez, Oxalate Co-precipitation Synthesis of Calcium Zirconate and Calcium Titanate Powders, SAND 2009-4743

[17] S. Manafi, M. Jafarian, Synthesis of perovskite $CaTiO_3$ nanopowders with different morphologies by mechanical alloying without heat treatment, ACERP. 1 (2015) 11-16. doi:10.5897/IJPS2013.0014.

[18] W. Dong, G. Zhao, Q. Bao, X. Gu, Solvothermal Preparation of $CaTiO_3$ Prism and $CaTi_2O_4(OH)_2$ Nanosheet by a Facile Surfactant-Free Method, Mater. Sci. (MEDŽIAGOTYRA). 21 (2015) 583–585. doi.org/10.5755/j01.ms.21.4.9697.

[19] Synthesis and characterization of $CaTiO_3$ particles with controlled shape and size, Integrated Ferroelectrics. 131 (2013) 119–126. doi:10.1039/c3nj40974k.

[20] Y.K. Sharma, M. Kharkwal, S. Uma, R. Nagarajan, Synthesis and characterization of titanates of the formula $MTiO_3$ (M= Mn, Fe, Co, Ni and Cd) by co-precipitation of mixed metal oxalates, Polyhedron. 28 (2009) 579–585. doi:10.1016/j.poly.2008.11.056.

[21] A.F. Demirors, A. Imhof, $BaTiO_3$, $SrTiO_3$, $CaTiO_3$, and $Ba_xSr_{1-x}TiO_3$ particles: A general approach for monodisperse colloidal perovskites, Chem. Mater. 21 (2009) 3002–3007. doi:10.1021/cm900693r.

[22] A. K. Rai, K. N. Rao, L.V. Kumar, K. D. Mandal, Synthesis and characterization of ultra fine barium calcium titanate, barium strontium titanate and $Ba_{1-2\,x}Ca_xSr_xTiO_3$ (x = 0.05, 0 .10), J. Alloys Compd. 475 (2009) 316–320. doi:10.1016/j.jallcom.2008.07.038.

[23] N. berit F. pedersen Blindern, Oslo, Interpretation of Infrared Spectra of Solid Alkali Metal Oxalates, their Hydrates and Perhydrates, Acta Chem. Scand. 21 (1967) 801-811.

[24] M. Parinitha, A. Venkateshulu, Synthesis, characterization and transport property of pani–calcium titanate composites, International Journal of Latest Research in Science and Technology. 2 (2013) 495- 498.

CHAPTER 4

CALCIUM TITANATE INCORPORATED POLYVINYL ALCOHOL NANOCOMPOSITE ANION-EXCHANGE MEMBRANES FOR RECHARGEABLE BATTERIES

4.1 Introduction

The ion-exchange membrane is a critical component of many electrochemical devices such as fuel cells [1], rechargeable batteries [2], electrodialysis devices [3], water electrolysers and desalination of sea water [4] as it determines the performance as well as the economic viability of these devices. The membrane allows selective transport of either cation or anion to complete the circuit during the passage of current [5, 6–10]. Recently, in fuel cell technology anion-exchange membranes (AEMs) are gaining more attention as they promise to overcome the disadvantages such as low CO tolerance, high electrokinetic over potentials for oxygen reduction and high catalyst cost of Proton Exchange Membrane Fuel Cells (PEMFCs) [11–13]. The cost of popular proton exchange membrane Nafion is roughly \$400 per m^2 [13]. However the currently used commercial AEMs suffers from severe draw backs, which includes low ionic conductivity, electrolyte crossover, poor chemical and mechanical stability besides high cost of the membranes [14–18]. Various kinds of AEMs have been developed in the past few decades and most of them employed quaternary ammonium group as anion exchange cites [19, 20]. These quaternary ammonium group based membranes degrade rapidly in highly alkaline solutions and hence limits the performance of these membranes in alkaline environment [13, 17]. So the developments of low cost AEMs with superior chemical stability and good ionic conductivity have been focus of research of many groups worldwide.

Organic–inorganic hybrid membranes found to be promising materials for potential applications due to their better electrochemical properties, improved mechanical, chemical and thermal properties [21]. Yang synthesized PVA/TiO_2 composite polymer membrane [18] and quaternized poly(vinyl alcohol)/alumina

composite polymer membranes [22] for alkaline direct methanol fuel cells, which exhibited excellent electrochemical performances. The incorporation of ceramic fillers such as Al_2O_3 [22], SiO_2 [23] and bentonite [24] into the polymer matrix has significantly enhanced the ionic conductivity and thermal stability of the ion-exchange membranes.

The AEMs based on PVA have received considerable attention in the recent years due to its non toxicity, good film forming ability, low cost, good mechanical strength and chemical stability, high hydrophilic behavior and low methanol permeability [18, 25, 26]. The incorporation of nanofiller into the polymer matrix of cross linked PVA have been shown to reduce the crystalline nature of the matrix and improve their performance in solid alkaline fuel cells and other electrochemical devices [18, 25–27].

A perovskite is any material with the same type of crystal structure as calcium titanate ($CaTiO_3$). The general chemical formula of perovskite is ABX_3, where A represents large divalent and B is small tetravalent cation. X can be anions like O^{2-} which is bonded to both cations. Synthesis of calcium titanate nanocrystals have gained great interest in recent years due to their exceptionally high dielectric properties which makes them potentially useful resonator materials in wireless communication systems [28,29]. Calcium titanate can exist in three polymorphic phases including cubic, tetragonal and orthorhombic [30]. Zr^{4+} doped $CaTiO_3$ and CoO doped $CaTiO_3$ powders exhibit high catalytic efficiency in water splitting for hydrogen production [31]. Due to inherent biocompatibility, calcium titanate is highly beneficial for biomedical applications, especially for bone and joint repair [32].

Several methods have been reported for the synthesis of calcium titanate nanoparticles such as solid state synthesis, sol-gel methods, hydrothermal methods, co-precipitation methods, mechanical alloying methods, solvo-thermal methods [31–33]. The limitations associated with these processes are heterogeneous products, contamination of impurities, performing the process at high temperature (above 1300°C) and existence of coarse particles with different size [33]. Calcium titanate, when treated with bases in wet condition is converted to calcium titanate hydroxide (eqn.1) and it is

reported to be an efficient anion-exchange material containing exchangeable hydroxyl groups [34].

$$CaTiO_3 + NaOH \rightarrow HCaTiO_3OH \quad \text{---------- (1)}$$

In this work calcium titanate nanoparticles were synthesized by a new method from a solution containing two simple precursors, viz potassium titanyl oxalate and calcium chloride using ammonium oxalate as precipitating agent. The powder was calcined at 900°C and characterized by XRD, TEM, SEM, and EDX analysis.

The AEMs were fabricated by incorporating calcium titanate nanocrystals to PVA matrix followed by cross-linking with glutaraldehyde. The membranes were characterized by FT-IR, TGA, SEM, and AC impedance analysis. The membrane properties such as the alkaline stability, water uptake, ion-exchange capacity and mechanical strength were also measured.

4.2. Experimental

4.2.1 Materials

PVA used in this study was analytical grade and was purchased from Merck (M_w 89,000-98,000, 99 + % hydrolysed PVA), glutaraldehyde (25 wt% solution in water of analytical grade), calcium chloride, potassium titanyl oxalate, and ammonia solution were also purchased from Merck.

4.2.2 Preparation of calcium titanate nanopowder

The method of preparation of calcium titanate nanopowder is described in chapter 3

4.2.3 Fabrication of PVA/calcium titanate nanocomposite membranes

5 wt% PVA solution was prepared by dissolving 5 g PVA in 100 ml D. I. water at 80°C and it was stirred continuously till a homogeneous solution was obtained. Then a weighed amount of calcium titanate was ultrasonicated for 6 h and stirred with PVA

solution for another 6 h. Then glutaraldehyde solution (5 wt%) as the crosslinker was added drop wise (2.5 wt% of PVA) into the mixture [8] followed by several drops of 1 M HCl as catalyst. After stirring for 3 h the mixture was degassed in vacuum for 15 min. The viscous solution was cast onto a clean glass plate using a film applicator. The composite membranes were peeled from the glass plate after drying in vacuum oven at 50°C for 48 h. PVA/x$CaTiO_3$ composite membranes (x stands for the wt% of $CaTiO_3$) were prepared at PVA/$CaTiO_3$ weight ratios (95: 5, 90: 10, 85: 15, 80: 20, and 70: 30) and the corresponding membranes are denoted as PVA5, PVA10, PVA15, PVA20 and PVA30. The thickness of the resulting membranes was 120±10μm. All the membranes were immersed in 2M NaOH solution for 24 h for converting calcium titanate to calcium titanate hydroxide which is an efficient anion exchange material containing exchangeable hydroxyl groups [34].

4.2.4. Characterization

X-ray powder diffraction data of the synthesized nanopowder were collected at room temperature with a SHIMADZU, XRD700 powder diffractometer using CoK_α radiation. Data were scanned over the angular range 20-80° (2θ) with a step size of 0.0196° (2θ). Transmission electron microscopy (TEM) images of the obtained nanoparticles have been recorded using a JEOL 4000EX High Resolution Transmission Electron Microscope (HRTEM) operated at 400 kV. FT-IR spectra were recorded on a Perkin Elmer instrument (Model L160000A) over a range of 4000-400 cm^{-1}. SEM images of the samples were acquired with a scanning electron microscope (JSM-5600, JEOL Co., Japan). The samples were coated with a thin layer of gold by ion sputtering prior to microscopic examination. The energy dispersive analyzer was used for the elemental detection of the samples. All the characterization techniques used are as described in chapter 3.

TGA thermograms of the composite membranes were recorded on a Shimadzu TGA-50H analyzer by heating the samples from room temperature to 850°C under nitrogen atmosphere at a heating rate of 10 °C/min.

Water uptake of the composite membranes was determined by weighing the membranes under wet conditions after being equilibrated in distilled water for 24 h at

room temperature. The surfaces of the membranes were then carefully wiped with filter paper and the membranes were weighed immediately. The samples were vacuum dried for two days and weighed again. The water uptake was calculated as follows.

$$Water\ uptake\ (\%) = \frac{W_{wet} - W_{dry}}{W_{dry}} \times 100\ \% \qquad (3)$$

Where W_{wet} is the mass of the water swollen membrane, and W_{dry} is the mass of the dry membrane.

The ion exchange capacities (IECs) of the composite membranes were determined by double titration method. Samples were accurately weighed and immersed in 25 ml of 0.05M HCl solution for 48 h and the HCl solution was back titrated by 0.05M NaOH .IECs of the samples were calculated using the equation:

$$\text{IEC} = \frac{n_1 - n_2}{M_{dry}}$$

Where n_1 and n_2 are the concentrations of (mmol) hydrochloric acid required before and after equilibrium respectively, and M_{dry} is the mass in g of the dried sample. The average value of the three samples calculated from the above equation is the IEC value of the membrane.

Electrochemical impedance spectroscopy (EIS) was used to evaluate ionic conductivity of the membranes, using AUTOLAB 50519 PGSTAT instrument. Impedance of the membranes were performed in a two electrode setup where the membranes were clamped between two platinum electrodes and the cell was thermostated at 25 ± 0.1°C for at least 20 minutes to ensure thermal equilibrium. Impedance measurements were performed in the frequency range 100 Hz-1000 kHz using an alternating potential of amplitude 10 mV. Fully hydrated membrane was placed in the conductivity cell and it was filled with 2M NaOH. The resistance of the membrane and solution (R_{total}) was measured. The resistance of the solution ($R_{solution}$) was measured without the membrane. Membrane resistance (R_{mem}) was obtained from the difference of the measured resistances ($R_{mem} = R_{total} - R_{solution}$). The thickness of the membrane was measured with a digital micrometer by placing the membrane between two glass slides to

ensure both a planar surface and limited compression. The conductivity of the membrane was calculated as follows σ = L/RA mS cm^{-1}, Where σ is the hydroxide conductivity in mS cm^{-1}, *R* is the ohmic resistance of the membrane (Ω), L is the thickness of the membrane (in cm), *A* is the cross sectional area of membrane samples (cm^2).

The tensile strength of the composite membranes was measured with universal testing machine (UTM) (Zwick, Model 1446-60, Germany). For this test the samples were prepared according to ASTM-D882 standard. The films were then placed between the grips of the testing machine. The grip length was 5 cm and speed of testing was set at the rate of 10 mm min^{-1}. The alkaline stability of the membrane was measured by immersing the composite membrane sample with a size of 3cm x 3cm in 2M NaOH at room temperature for 2 weeks. It was taken out, washed with D. I. water, wiped with tissue paper, and then studied using FT-IR technique to detect any degradation or changes in chemical structures. Loss of weight of the membrane was also measured. The oxidative stability of membrane was determined by immersing the samples 3cm x 3cm into Fenton's reagent (30 ppm $FeSO_4$ in 30 % H_2O_2) at 25°C, for 24 h and measured the weight of the membrane with time.

Performance of $CaTiO_3$ / PVA membrane as separator in all-iron flow battery

All-iron flow battery experiments were performed in the 36 cm^2 flow cell hardware with electrolyte flowing across two electrodes, separated by the membrane prepared [35]. All experiments were performed with electrolyte flow rates of 25 ml min^{-1}. Electrolyte for both positive and negative electrodes consisted of 1M $FeCl_2$ and 1.5 M NH_4Cl. The electrodes were made from densified graphite with a cross-sectional area of 16 cm^2. The charging efficiency of the all-iron redox flow cell was determined by charging the cell at 100 mA cm^{-2} for 100 s followed by discharging at 50 mA cm^{-2} using AUTOLAB 50519 PGSTAT instrument. The cell performance is normally determined by its coulombic efficiency (CE). CE is the ratio of discharge capacity (Q_{dis}) to charge capacity (Q_{ch}) of a cell.

4.3. Results and discussion

Fig.42 shows the XRD pattern of $CaTiO_3$ obtained after calcination at 900°C. The XRD pattern clearly shows that the powder obtained by the thermal decomposition of ($CaTi(OH)_x(C_2O_4)_y$) at 900°C consists of pure perovskite nanopowder ($CaTiO_3$) without the presence of oxides or any other impurity [30]. The microstructure of the particles was also investigated by means of TEM. **Fig.** 45 shows the TEM image of $CaTiO_3$ and reveals the particle morphology and size of the nanopowder. It is seen from TEM images that $CaTiO_3$ powders consist of clusters of nanoparticles and they are found to be spherical in shape with an average size of 200 nm. HRTEM image of calcium titanate **Fig.** 45 (c) reveals the formation of nano-crystals with d spacing of 0.32 nm. The selected area electron diffraction (SAED) pattern given in **Fig.** 45 (d) reveals the crystalline nature and the rings in the SAED pattern corresponds to crystal planes of calcium titanate.

4.3.1. Structural analysis

FT-IR spectra of $CaTiO_3$, PVA, PVA10, PVA20 and PVA30 nanocomposite membranes are presented in Fig 48 (a-e). **Fig.** 48 (a) shows two characteristic peaks at 540 cm^{-1}, 450 cm^{-1} in the spectrum of $CaTiO_3$ which correspond to the stretching vibrations of Ti-O bonds [36] and Ca-Ti-O bending vibrations [37] respectively. **Fig.** 48 (b) shows the characteristic peaks of pure PVA in the region 3400-3100 cm^{-1} due to –OH stretching, band at 2920 cm^{-1} due to -CH stretching vibrations of polymer back bone and band at 1420 cm^{-1} is attributed to bending vibrations of $-CH_2$ group as reported in literature [38,39]. **Fig.** 48 (c-e) of PVA10, PVA20 and PVA30 nanocomposite membranes show broad peak at 3400–3100 cm^{-1} indicates stretching vibrations of the hydroxyl groups of polyvinyl alcohol. The band at 2924 cm^{-1} is assigned to the stretching vibrations of -CH groups of polymer back bone and bands at 1420 cm^{-1} is attributed to bending vibrations of $-CH_2$ group [40]. The bands at 1250-1200 cm^{-1} were attributed to the ether bonds (C-O-C), formed during cross-linking with glutaraldehyde [39]. In the composite membrane, the peaks at 540 cm^{-1} and 450 cm^{-1} is attributed to the characteristic vibrations of Ti-O bonds and Ca-Ti-O bonds of calcium titanate [37]. The results show that successful incorporation of calcium titanate nanoparticles into the PVA matrix has been achieved.

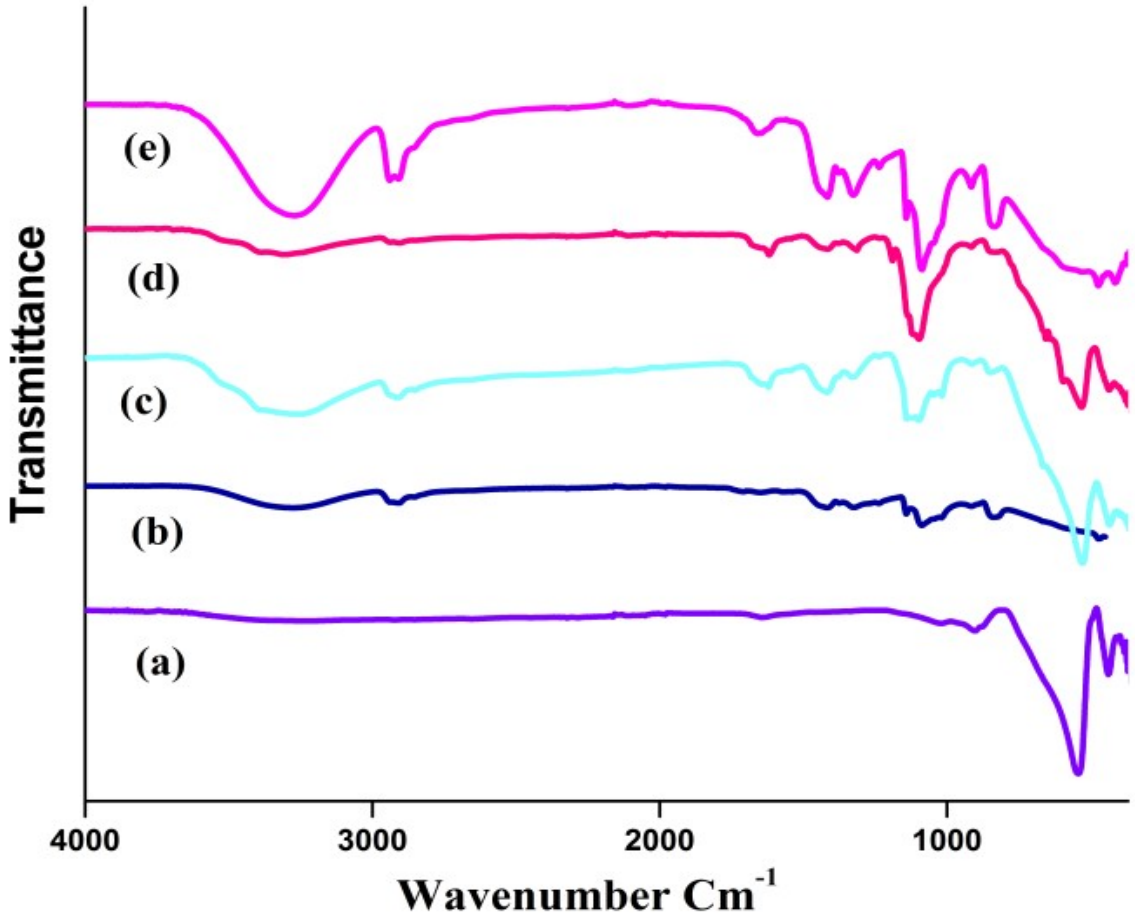

Fig. 48 FT- IR spectra of (a) $CaTiO_3$, (b) PVA, (c) PVA10, (d) PVA20 and (e) PVA30 nanocomposite membranes

4.3.2. SEM analysis

The SEM images of calcium titanate powder are shown in **Fig.** 46. The SEM image shows the microstructure of the particles. The particles were found to be spherical in shape. The average size of the particles was in 200 nm range. The EDX spectrum of calcium titanate in **Fig.** 47 indicates the presence of Ca, Ti and O atoms in accurate proportion in the prepared material, further confirmed the formation of pure calcium titanate. **Fig.** 49 (a-d) present the SEM images of surface and cross-section of PVA/$CaTiO_3$ nanocomposite membranes. There is no evidence of phase separation; crack or holes on membrane surface indicated its dense nature, which was further confirmed by cross-section image of the membrane. The surface of the membrane found to be smooth and uniform. Filler particles are found to be well embedded in the polymer

matrix, establishing strong connectivity of the particles. Size of the filler particles embedded in the PVA matrix is found to be less than 1μm and some degree of aggregation of particles are observed. The particle distribution and particle-polymer matrix reinforcement play vital roles in the improvement of the mechanical properties of the composite membranes. The distribution of particles is uniform and homogenous when the weight percent of nano $CaTiO_3$ filler is less than 20 wt%. When the filler content is beyond a limit, aggregates of filler particles makes the membrane more brittle [5]. Cross-sectional SEM image of PVA30 membrane shows that the thickness of the membrane is about 120 ±10 μm.

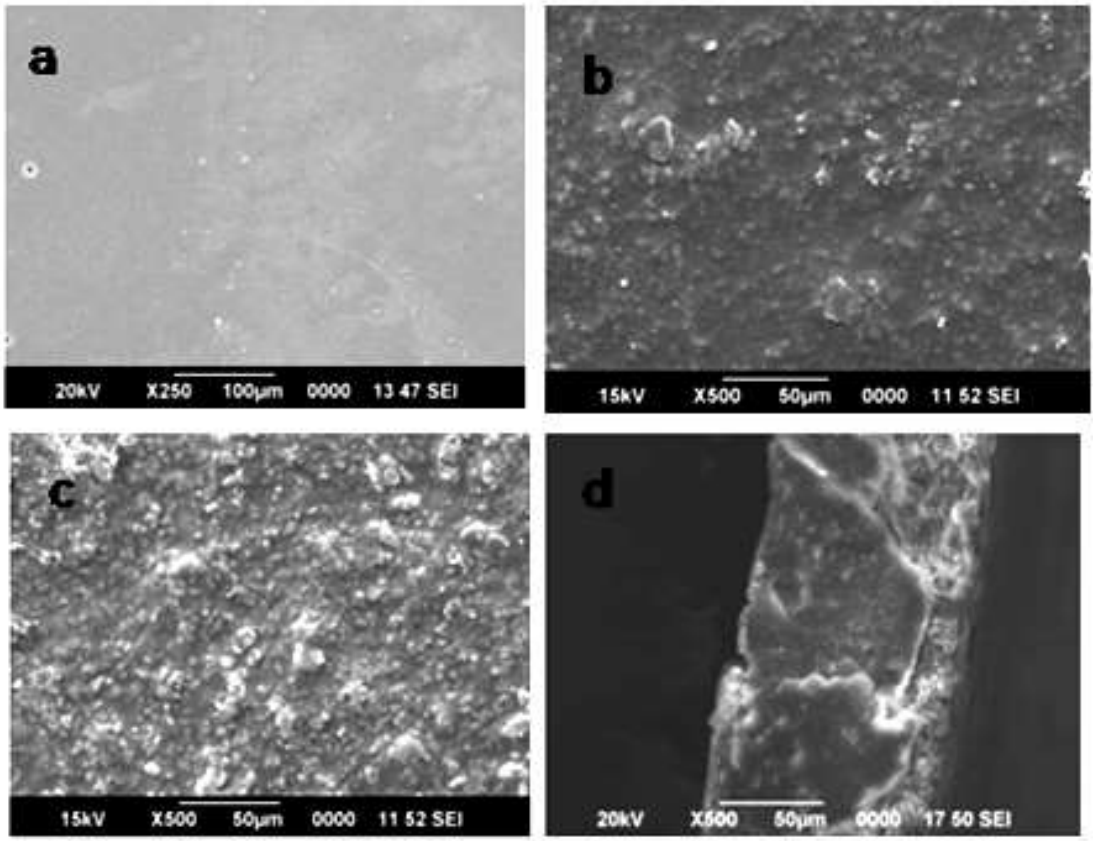

Fig. 49 SEM surface images of membranes; (a) PVA (b) PVA10 (c) PVA30 (d) SEM cross-sectional image of PVA30 membrane

4.3.3. Water uptake

Water uptake is considered as one of the essential properties of anion-exchange membranes for practical applications which depend on several parameters such as the nature of the polymer and the ion exchange groups, the counter ions, the charge density

and the cross-linking density of the membrane. The presence of water is necessary to obtain an efficient conductivity by enhancing the mobility of the ions. It is found that water uptake decrease with increase in calcium titanate content as shown in **Fig.**50. This can be explained in terms of the changes in the membrane structure. Cross-linking effects due to the inorganic network reduce polymer chain mobility thereby reducing the free volume where absorbed water could be accommodated. Here, the cross-linking effect due to the inorganic network is more prominent than the hygroscopic effect of $CaTiO_3$, and hence the total water content decreases with increasing $CaTiO_3$ content [18, 40, 41]. The decrease in water uptake with increase in calcium titanate content also indicates the dimensional stability of composite membranes.

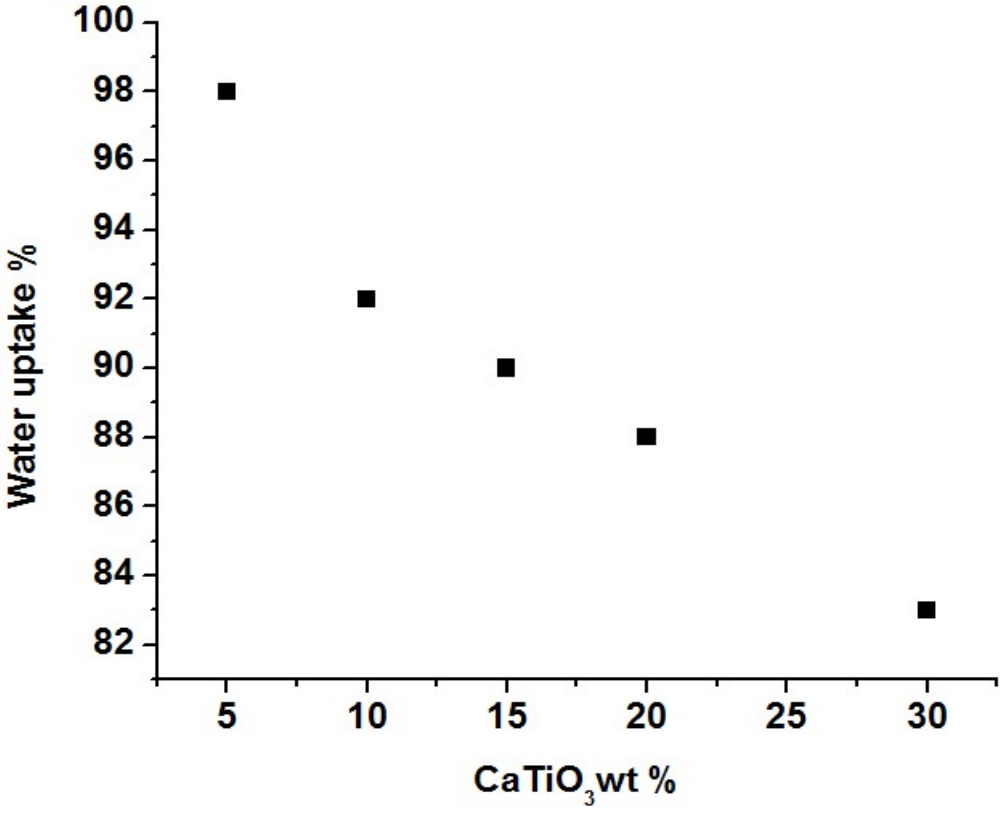

Fig. 50 Water uptake of membranes with varying $CaTiO_3$ content

Table.1 The physical properties of PVA/$CaTiO_3$ nanocomposite polymer membranes at 25°C

Types of membranes	Water Uptake (%)	IEC meq g^{-1}	Tensile strength (M Pa)	Ionic conductivity mS cm^{-1}
PVA0	116	0.38	13.6	8.2
PVA5	98	0.42	20	14
PVA10	92	0.56	25	25
PVA15	90	0.58	40	32
PVA20	88	0.64	46	39
PVA30	83	0.78	25	66

4.3.4. Ion exchange capacity (IEC)

The IEC is a key parameter for the haracterization of ion exchange membrane and it has an intensive effect on the water uptake as well as ionic conductivity of the membranes [21, 42]. IEC provides an indication of amount of exchangeable groups in the membrane [3]. **Fig.** 51 shows ion exchange capacity of membranes with varying $CaTiO_3$ content. It is found that ion exchange capacities increased gradually with increasing $CaTiO_3$ content in the composite membrane. The Ion exchange capacity values of the membranes were in the range of 0.4-0.7 meq g^{-1}. With the increasing amount of hydrophilic groups in the membrane, that regions become more inter-connected, leading to more ionic transport channels [43]. Compounds like calcium titanate when treated with bases results in the formation of calcium titanate hydroxide which is an efficient anion exchange material containing exchangeable hydroxyl groups [34]. Calcium titanate can provide a positive surface charge in the membrane which will increase affinity for anions and improve IEC values [44].

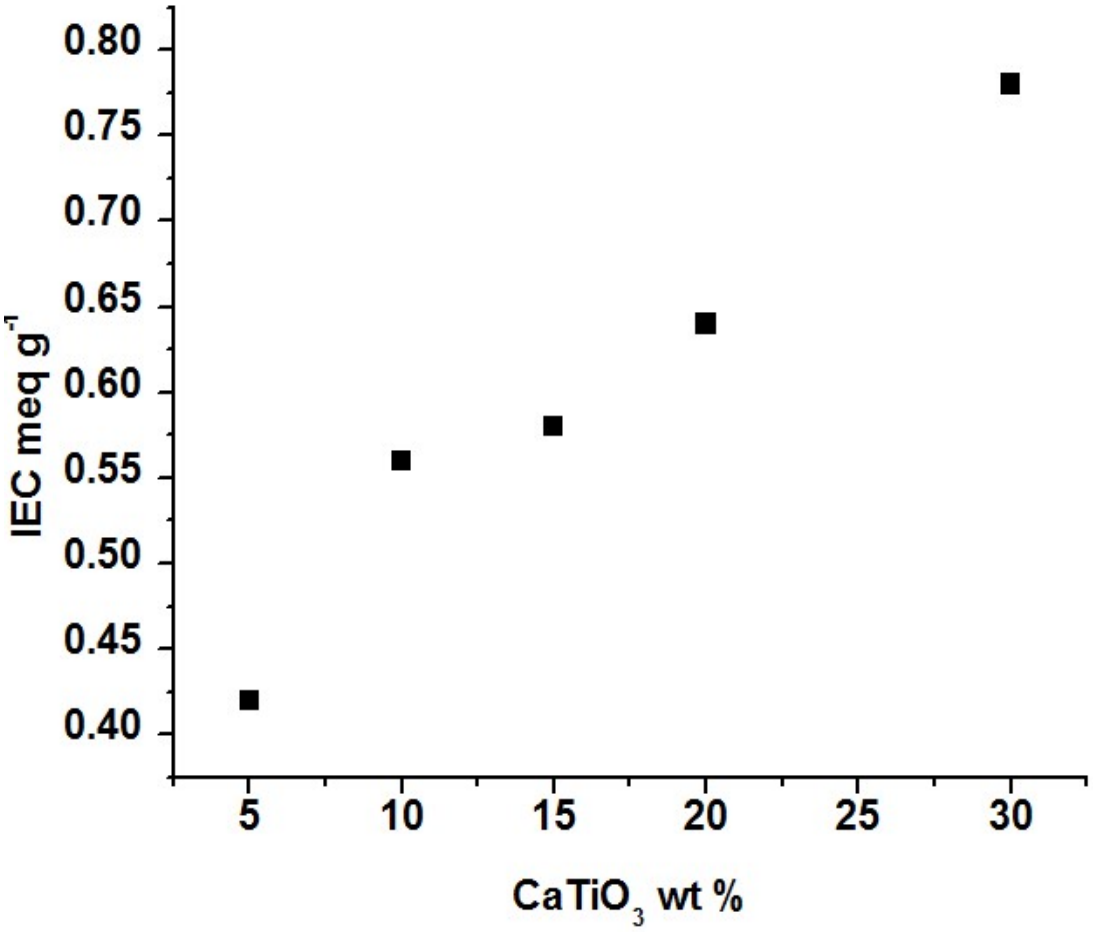

Fig. 51 Ion exchange capacity of membranes with varying $CaTiO_3$ content

4.3.5. Electrical properties

The high ionic conductivity of the anion exchange membrane is an essential property for applications in electrochemical devices. The ionic conductivities were examined by electrochemical impedance spectra (EIS) recorded in the frequency range of 100 Hz-1000 kHz and with signal amplitude of 10 mV. Typical Nyquist plots for the composite membranes are presented in **Fig.** 52 (a-e). The membrane resistance was obtained from the intercept on the Z' axis in the high frequency region. The ionic conductivities of the hydrated PVA/$CaTiO_3$ nanocomposite membranes calculated using the resistance values obtained from the Nyquist plots are shown in **Fig.** 52. The ionic conductivity is increased from 10.6 mS cm^{-1} for PVA0 to 66 mS cm^{-1} for PVA30 membranes as shown in **Fig.**53. The ionic conductivity of the membranes largely depends on the nature of inorganic fillers and hydrophilicity of the polymer matrix. High

ionic conductivity of PVA/$CaTiO_3$ nanocomposite anion-exchange membranes can be attributed to positive surface charges on $CaTiO_3$ nanoparticles which act as anion exchange sites and enable the exchange of hydroxide ions [44]. The mechanism of anion transport is schematically represented in **Fig.**54 The increase in ionic conductivity of the membrane with increasing $CaTiO_3$ content can be attributed to the increase in the positive surface charge of the membrane [34].

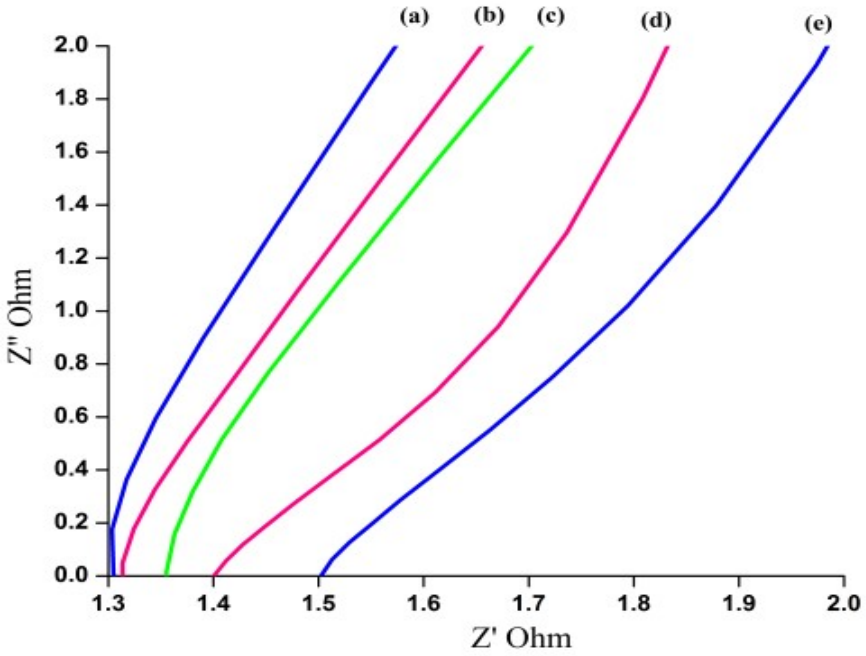

Fig. 52 Nyquist plots from AC impedance spectroscopy measurements of (a) 2 M NaOH (b) PVA30 (c) PVA20 (d) PVA10 composite membranes (e) PVA membrane

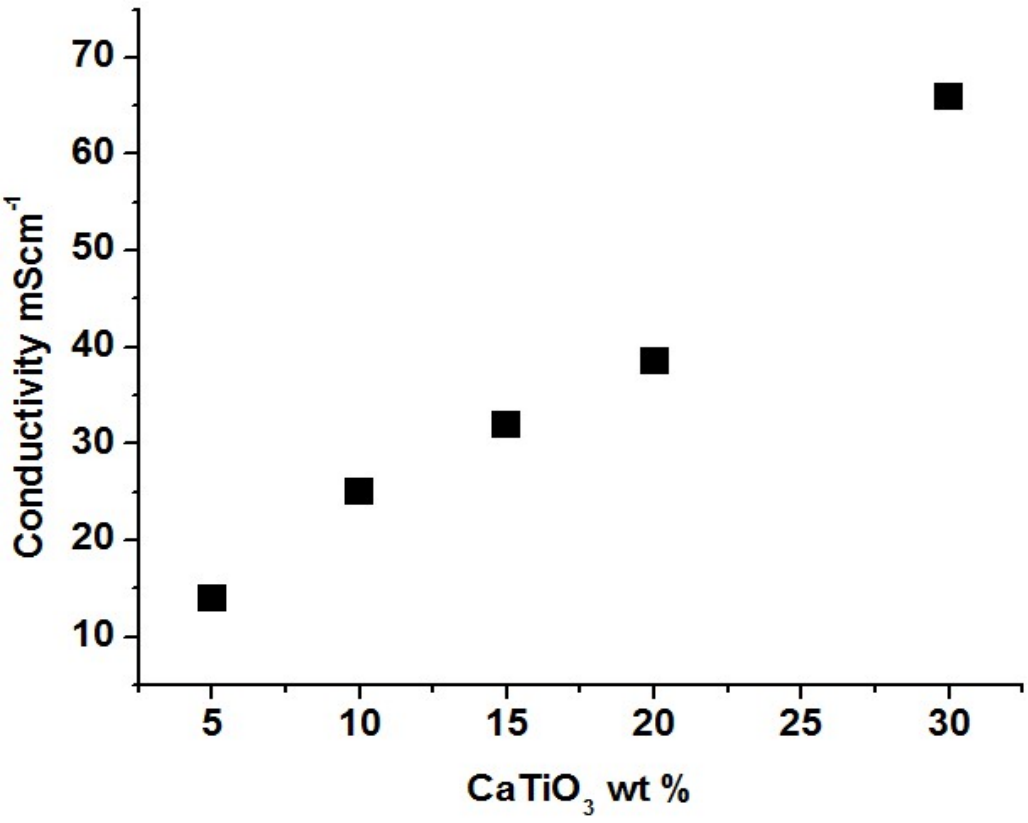

Fig. 53 Ionic conductivity of membranes with varying $CaTiO_3$ content

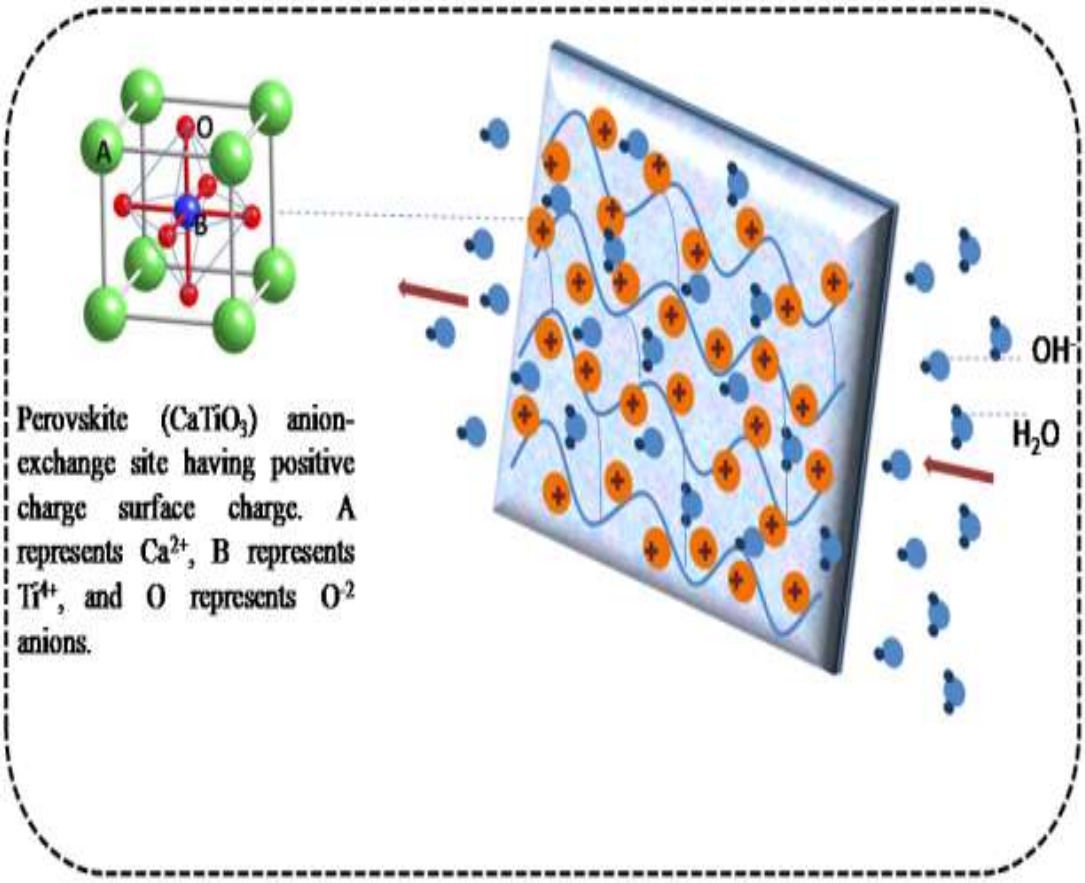

Fig. 54 Schematic representation of PVA/$CaTiO_3$ nanocomposite anion-exchange membrane with $CaTiO_3$ anion-exchange sites that enable high ionic conductivity by providing positive surface charge

4.3.6. Thermo-gravimetric analysis

Thermal stability is an important parameter for the use of membranes in high temperature electrochemical applications. The samples were heated in the temperature range from 30°C to 750°C at a constant rate of 10°C min^{-1} under nitrogen atmosphere. **Fig.**55 shows TGA curves for pure PVA film, PVA10 and PVA30 nanocomposite membranes, respectively. The TGA curve of pure PVA film shows three major weight loss regions. The first region at a temperature of 80-160°C was due to the evaporation of weakly adsorbed water and the weight loss of the membrane is about 12.9 %.

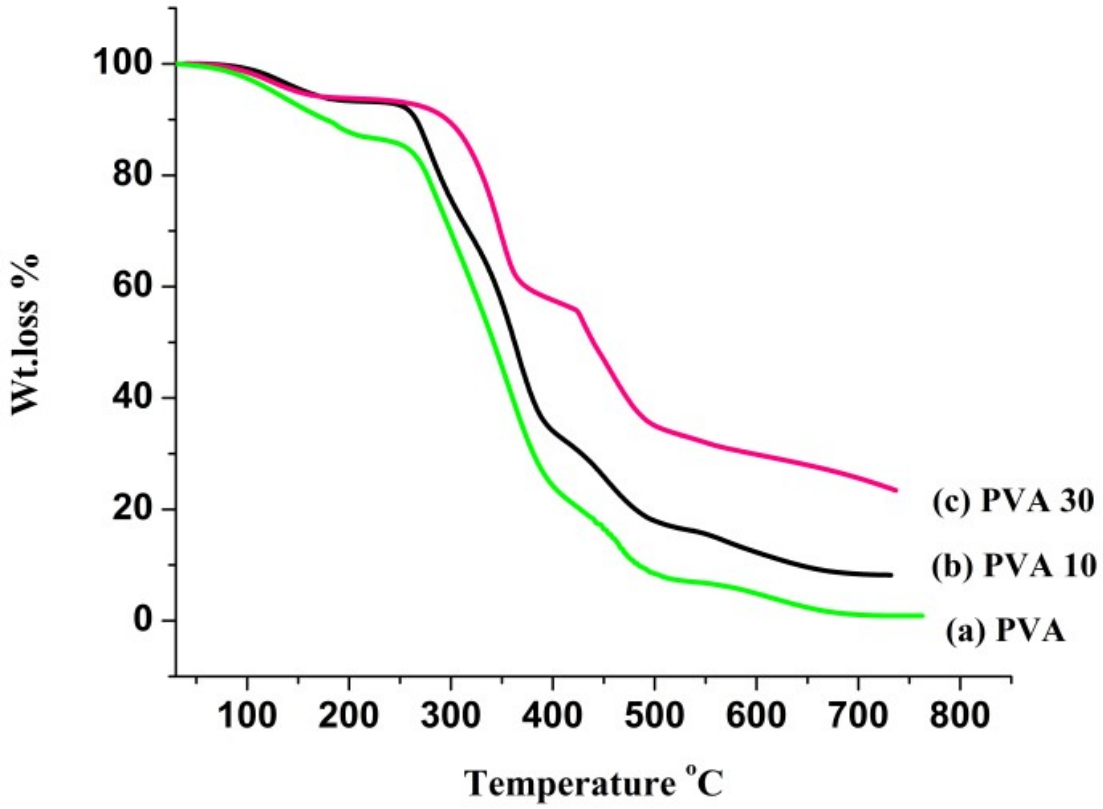

Fig. 55 TGA curves of membranes with varying $CaTiO_3$ content

The second region at about 250-350°C is associated with the degradation of PVA polymer membrane and the weight loss of the membrane at this stage is about 61%. The peak of third stage at 450°C is due to the splitting of PVA chains into small segments, associated with 87.7 % weight loss of the membrane. The total weight loss at 600°C is about 99.1% [18, 25] as listed in table 2.

TGA curves of PVA10 and PVA30 nanocomposite polymer membranes also exhibit three major weight loss regions. The first region at a temperature of 80-160°C is also due to the evaporation of weakly adsorbed water and the weight loss of the membranes is about 9.5%. The second region at 260-350°C is due to the decomposition of side chain of PVA and glutaraldehyde in the composite membranes, the weight loss of the membrane is only about 48.4% for PVA10 and 36.7% for PVA30. The second main weight loss for the cross-linked PVA/$CaTiO_3$ composite membranes was reduced when compared with that of pure PVA. The peak of third stage at 450°C is due to the degradation backbone of cross-linked PVA/ $CaTiO_3$ polymer membrane. The weight loss

of PVA10 was 78% and 58.6% for PVA30. At 600°C total weight loss for PVA10 is 91.5% and 73.8 % for PVA30.

Table. 2 Weight loss% of polymer membranes at different temperatures by TGA analysis

Temperature °C	Wt. loss % of membranes		
	PVA	**PVA10**	**PVA30**
160	12.9	9.5	9
350	61	48.4	36.7
450	87.7	78	58.6
600	99.1	91.5	73.8

TGA results as shown in **Fig.** 55 indicate that at each stage the weight loss of PVA membrane is more than that of composite membranes. This suggests that the incorporation of $CaTiO_3$ into PVA matrix and its cross-linking with glutaraldehyde improved thermal stability of the composite membranes [22, 40].

4.3.7. Mechanical properties

AEMs must have good mechanical strength for applications in electrochemical devices. The mechanical strength of composite membranes depends on the filler content [45]. **Fig.** 56 shows the tensile strength (TS) of membranes with varying $CaTiO_3$ content and has the range of 20-46 MPa. Compared to TS of Nafion-117 (34 MPa), the prepared composite membranes exhibited better values [42]. As shown in **Fig.** 56, the TS values increase with filler content up to 20 wt% $CaTiO_3$ and then decrease with increasing filler content.

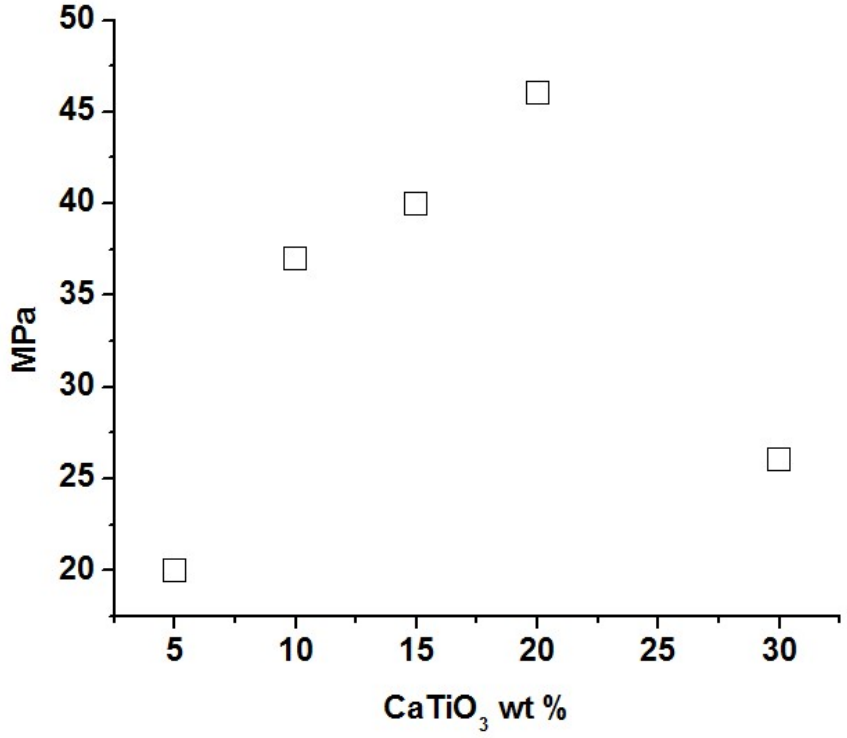

Fig. 56 Tensile strength of membranes with varying $CaTiO_3$ content

This shows that appropriate amount of filler content enhances the mechanical properties of PVA composite membrane. It may be attributed to the reduction in degree of crystallinity of the membrane and strengthened filler–matrix interactions [6]. However, an excessive amount of filler content will decrease the mechanical strength of the membranes due to the aggregation of filler particles that act as points of crack propagations [11].

4.3.8. Chemical stability

The chemical stability of anion exchange membranes is an important parameter that affects the performance of electrochemical devices, especially at high pH and strong chemical environments. FT-IR spectrum of the membrane before and after alkaline stability test is presented in **Fig.** 57 (a-b). To meet the requirements of the practical applications in strong chemical environments, the prepared AEMs must have good chemical stability, especially in the high pH environments. The results exhibit no significant change in peak positions even after an exposure of membrane in alkaline medium for 2 weeks. The peak in the region 3400-3200 cm^{-1} is intensified due to enhanced hydroxylation of calcium titanate in alkaline environment. In the composite

membrane, after alkaline stability test the characteristic vibrations of calcium titanate exhibit no significant change in peak positions. During the alkaline stability test, the membranes did not show any loss of weight. Fenton's reagent is used to simulate and accelerate the harsh operation environment for 24 h in which the $OH^{\cdot}$ and $OOH^{\cdot}$ radicals formed from H_2O_2 can cause the degradation of the AEMs. All the membranes did not show any physical deformation or colour change and the membrane exhibited a weight loss less than (~3%) after 24 h of Fenton's test as shown in **Fig.**58. This indicates the adequate oxidative stability of the synthesized membranes under oxidizing conditions.

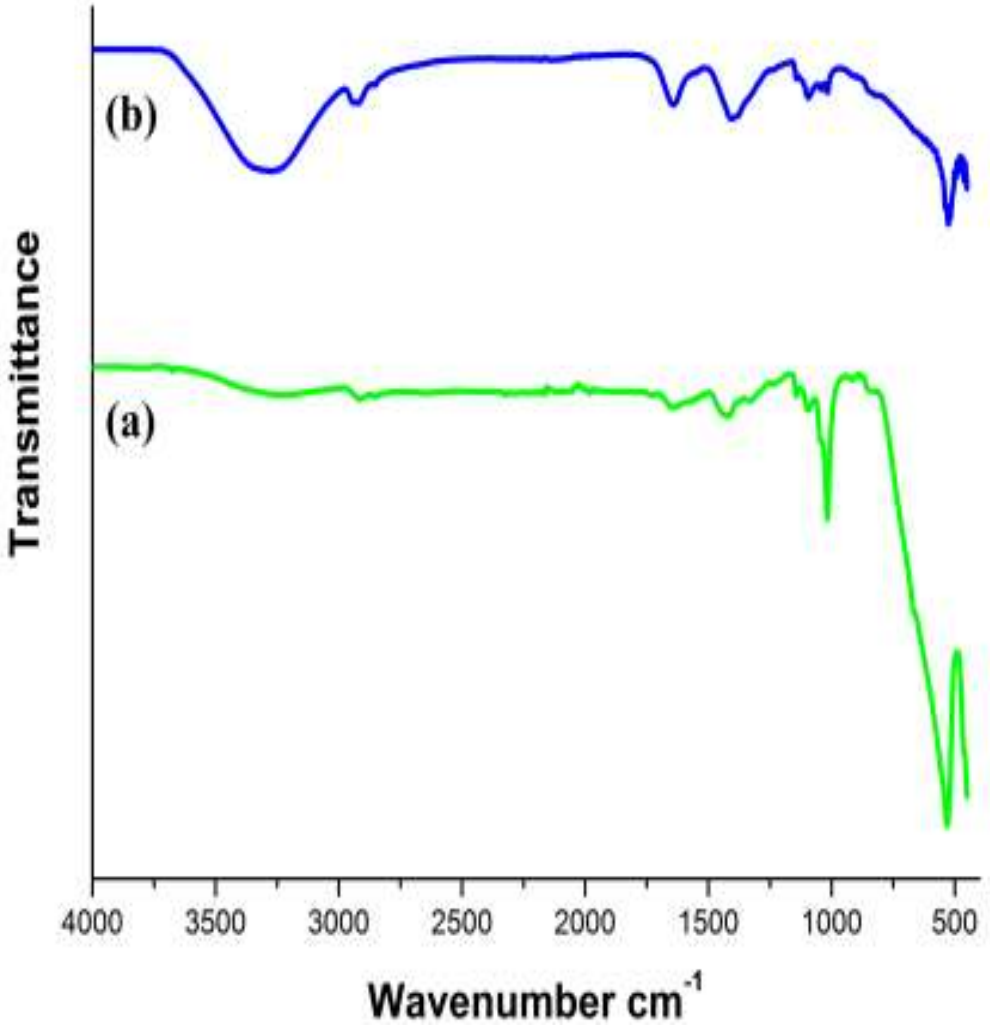

Fig. 57 FT-IR spectrum of the membrane (a) before alkaline stability test (b) after alkaline stability test

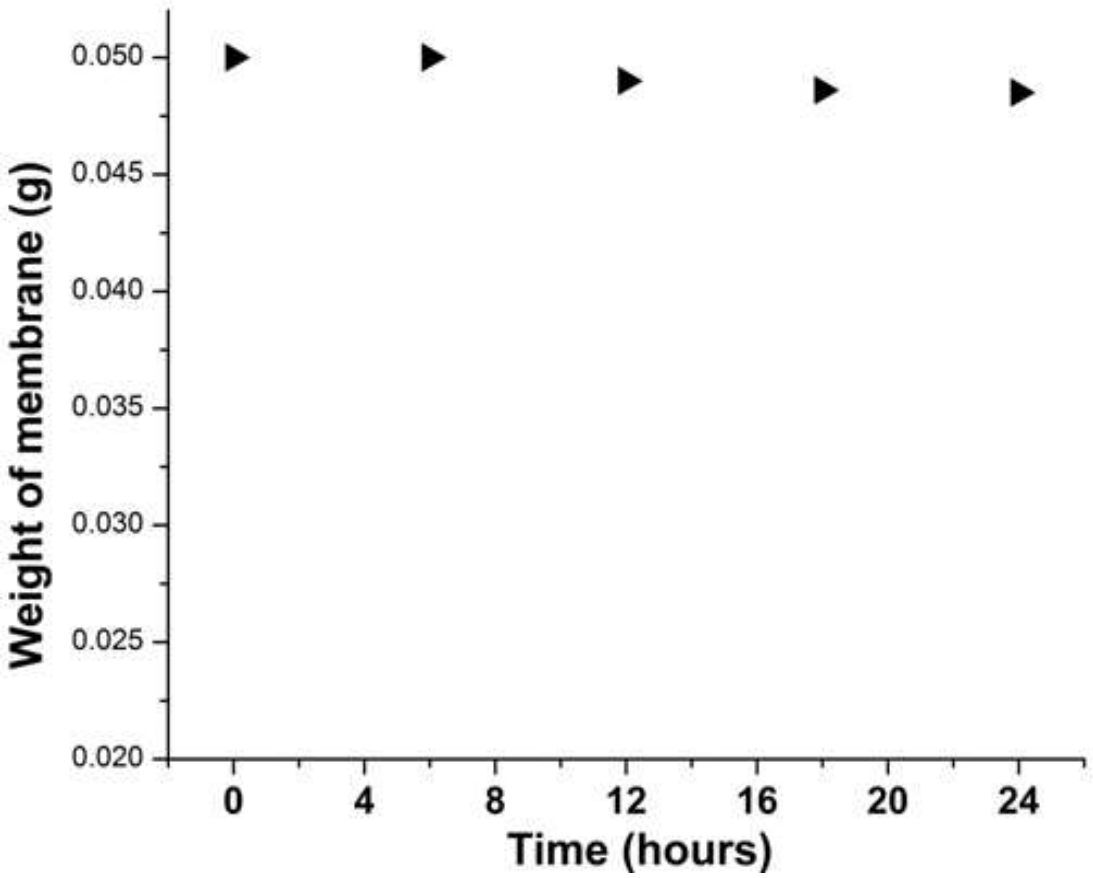

Fig. 58 Weight of membrane with time during Fenton's test

4.3.9. Performance of $CaTiO_3$ / PVA membrane as separator in all-iron flow battery

The cell voltage-time curve measured during the charging and discharging of an all-iron redox flow cell using the prepared membrane as separator is shown in **Fig.** 59. A constant current density of 100 mA cm^{-2} for charging and 50 mA cm^{-2} for discharging was used. Repeated charge-discharge measurement of the cell with high-efficiency electrolyte at 100 mA cm^{-2} demonstrated that high coulombic efficiency (> 75%) could be maintained over repeated cycles. Higher coulombic efficiency indicates low cross-mixing of ions [46]. These results confirm the viability of the new composite membrane as a separator in all-iron redox flow battery.

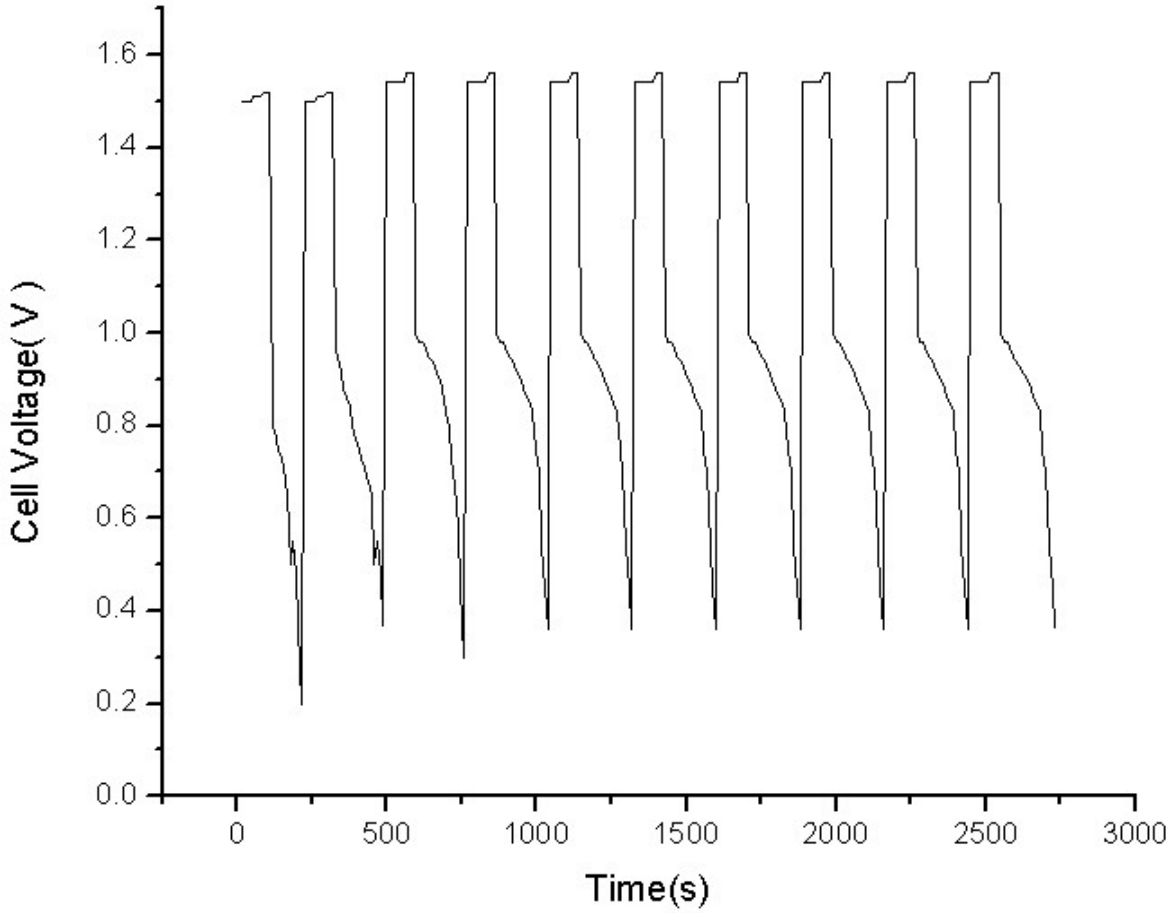

Fig. 59 The cell voltage-time curve of all- iron redox flow cell during galvanostatic charge-discharge experiment

4.4. Conclusions

We have reported a novel method to synthesize phase pure calcium titanate nanopowder by co-precipitating mixed oxalate hydroxide of calcium and titanium ($CaTi(OH)_x(C_2O_4)_y$) from a solution of potassium titanyl oxalate and calcium chloride followed by calcination. The XRD pattern revealed the formation of phase pure orthorhombic calcium titanate. The crystalline nature of the particles was also revealed by HRTEM image, and particles are found to be spherical shape, with an average size of 200 nm. The nanocomposite membrane was fabricated by incorporating calcium titanate into PVA matrix and exhibited improved thermal stability and excellent mechanical properties without compromising ionic conductivity and chemical durability. The results showed that the membrane possessed water uptake and ion exchange properties suitable for AEMs in various electrochemical devices. The composite membrane with 30 wt% of $CaTiO_3$ exhibited maximum conductivity of 66 mS cm^{-1} at room temperature. The galvanostatic charge–discharge tests of all-iron redox flow cell using the PVA/calcium titanate composite membrane as separator exhibited a coulombic efficiency of 75% during repeated charge-discharge cycles.

4. 5 References

1. Liu Y, Zhang B, Kinsinger C. L, et al (2016) Anion exchange membranes composed of a poly(2,6-dimethyl-1,4-phenylene oxide) random copolymer functionalized with a bulky phosphonium cation. J Memb Sci 506:50–59 doi: 10.1016/j.memsci.2016.01.042

2. Pupkevich V, Glibin V, Karamanev D (2013) Phosphorylated polyvinyl alcohol membranes for redox Fe^{3+}/H_2 flow cells. J Power Sources 228:300–307. doi: 10.1016/j.jpowsour.2012.11.080

3. Kariduraganavar M. Y, Nagarale R. K, Kittur A. A, Kulkarni S. S (2006) Ion-exchange membranes: preparative methods for electrodialysis and fuel cell applications. Desalination 197:225–246. doi: 10.1016/j.desal.2006.01.019

4. Lee K. P, Arnot T. C, Mattia D (2011) A review of reverse osmosis membrane materials for desalination—Development to date and future potential. J Memb Sci 370:1–22. doi: 10.1016/j.memsci.2010.12.036

5. Zeng L, Zhao T. S, Li Y. S (2012) Synthesis and characterization of crosslinked poly(vinyl alcohol)/layered double hydroxide composite polymer membranes for alkaline direct ethanol fuel cells. Int J Hydrogen Energy 7:1–8. doi: 10.1016/j.ijhydene.2012.09.089

6. Nishimura M, Higa M, Akamine K, Masudaya S (2008) Preparation and characterization of anion-exchange membranes with a semi-interpenetrating network structure of poly(vinyl alcohol) and poly(allyl amine). Desalination 233:157–165. doi: 10.1016/j.desal.2007.09.038

7. Qiu J, Li M, Ni J, et al (2007) Preparation of ETFE-based anion exchange membrane to reduce permeability of vanadium ions in vanadium redox battery. J Memb Sci 297:174–180. doi: 10.1016/j.memsci.2007.03.042

8. Vona ML Di, Narducci R, Pasquini L, et al (2014) Anion-conducting ionomers : Study of type of functionalizing amine and macromolecular. Int J Hydrogen Energy 39:14039–14049. doi: 10.1016/j.ijhydene.2014.06.166

9. Koo J. S, Kwak N, Sung T (2012) Synthesis and properties of an anion-exchange membrane based on vinylbenzyl chloride–styrene–ethyl methacrylate copolymers. J Memb Sci 423-424:293–301. doi: 10.1016/j.memsci.2012.08.024

10. Zeng R, Varcoe J (2011) Alkaline anion exchange membranes for fuel cells-a patent review. Recent Patents Chem Eng 44:1–50

11. Merle G, Wessling M, Nijmeijer K (2011) Anion exchange membranes for alkaline fuel cells: A review. J Memb Sci 377:1-35. doi: 10.1016/j.memsci.2011.04.043

12. Lin X, Wu L, Liu Y, et al. (2012) Alkali resistant and conductive guanidinium - based anion-exchange membranes for alkaline polymer electrolyte fuel cells. J Power Sources 217:373–380. doi: 10.1016/j.jpowsour.2012.05.062

13. Sajjad S. D, Liu D, Wei Z, et al. (2015) Guanidinium based blend anion exchange membranes for direct methanol alkaline fuel cells (DMAFCs). J Power Sources 300:95–103. doi: 10.1016/j.jpowsour. 2015.08.002

14. Smitha B, Sridhar S, Khan A. A (2005) Solid polymer electrolyte membranes for fuel cell applications-a review. J Memb Sci 259:10-26. doi:10.1016/j.memsci.2005.01.035

15. Sharma S, Dinda M, Sharma C. R, Ghosh P.K (2014) A safer route for preparation of anion exchange membrane from inter-polymer film and performance evaluation in electrodialytic application.J Memb Sci 459:122–131. doi: 10.1016/j.memsci.2014.02.011

16. Mizutani Y (1990) Structure of ion exchange membranes. J Memb Sci 49:121–144. doi: 10.1016/S0376-7388(00)80784-X

17. Thomas O. D, J. W. Y. SOO, Peckham T. J, et al. (2012) A Stable Hydroxide - Conducting Polymer. J Am Chem Soc 134:10753–10756. doi: dx.doi.org/10.1021/ja303067t

18. Yang C (2006) Synthesis and characterization of the cross-linked PVA/TiO_2 composite polymer membrane for alkaline DMFC. J Memb Sci 288:51–60. doi: 10.1016/j.memsci.2006.10.048

19. Faraj M, Elia E, Boccia M, et al. (2011) New Anion Conducting Membranes Based on Functionalized Styrene–Butadiene–Styrene Triblock Copolymer for Fuel Cells Applications. J Polym Sci Part A Polym Chem 49:3437–3447. doi: DOI: 10.1002/pola. 24781

20. Wang X (2011) Preparation of alkaline anion exchange polymer membrane from methylated melamine grafted poly(vinylbenzyl chloride) and its fuel cell performance Preparation of alkaline anion exchange polymer membrane from methylated. J Mater Chem· 12910–12916. doi: DOI: 10.1039/c1jm12068a

21. Wu H, Jia W, Liu Y (2017) An imidazolium-type hybrid alkaline anion-exchange membrane with improved membrane stability for alkaline fuel cells applications. J Mater Sci 52:1704–1716. 10.1007/s10853-016-0462-y

22. Yang C. C, Chiu S. J, Chien W. C, Chiu S. S (2009) Quaternized poly(vinyl alcohol)/alumina composite polymer membranes for alkaline direct methanol fuel cells. J Power Sources 195:2212–2219. doi: 10.1016/j.jpowsour.2009.10.091

23. Chang H. Y, Lin C. W (2003) Proton conducting membranes based on PEG/SiO_2 nanocomposites for direct methanol fuel cells. J Memb Sci 218:295–306. doi: 10.1016/S0376-7388(03)00187-X

24. Sang S, Zhang J, Wu Q, Liao Y (2007) Influences of Bentonite on conductivity of composite solid alkaline polymer electrolyte PVA-Bentonite-KOH-H_2O. Electrochim Acta 52:7315–7321.

25. Heydari M, Moheb A, Ghiaci M, Masoomi M (2013) Effect of cross-linking time on the thermal and mechanical properties and pervaporation performance of poly(vinyl alcohol) membrane cross-linked with fumaric acid used for dehydration of isopropanol. J Appl Polym Sci 128:1640–1651. doi: 10.1002/app.38264

26. Oliveira AHP De, Nascimento MLF, Oliveira HP De (2016) Preparation of KOH-doped PVA/PSSA Solid Polymer Electrolyte for DMFC : The Influence of TiO_2 and PVP on Performance of Membranes. Fuel Cells 1–6. doi: 10.1002/fuce.201500199.

27. Ran J, Wu L, He Y, et al. (2017) Ion exchange membranes: New developments and applications. J Memb Sci 522:267–291. doi: 10.1016/j.memsci.2016.09.033

28. Zheng H, Reaney I. M, Csete de Gyorgyfalva CDC (2004) Raman spectroscopy of $CaTiO_3$ -based perovskite. J Mater Res 19:488–95

29. Zheng H, Bagshaw H, Csete de Gyrgyfalva GDC, et al. (2003) Raman spectroscopy and microwave properties of $CaTiO_3$-based ceramics. J Appl Phys 94:2948–2956. doi.org/10.1063/1.1598271

30. Demirors A.F, Imhof A (2009) $BaTiO_3$, $SrTiO_3$, $CaTiO_3$, and $Ba_xSr_{1-x}TiO_3$ particles: A general approach for monodisperse colloidal perovskites. Chem Mater 21:3002–3007. doi: 10.1021/cm900693r

31. Marques V. S, Cavalcante L. S, Sczancoski J. C, et al. (2009) Synthesis of (Ca, Nd)TiO_3 powders by complex polymerization, Rietveld refinement and optical properties. Spectrochim Acta - Part A Mol Biomol Spectrosc 74:1050–1059. doi: 10.1016/j.saa.2009. 08.049

32. Dubey A. K, Basu B, Balani K, et al. (2011) Multifunctionality of Perovskites $BaTiO_3$ and $CaTiO_3$ in a Composite with Hydroxyapatite as Orthopedic Implant Materials. Integr Ferroelectr. 131:119–126. doi.org/10.1080/ 10584587.2011. 616425.

33. Sharma Y. K, Kharkwal M, Uma S, Nagarajan R (2009) Synthesis and characterization of titanates of the formula $MTiO_3$ (M =Mn, Fe, Co, Ni and Cd) by co-precipitation of mixed metal oxalates. Polyhedron 28:579–585. doi: 10.1016/j.poly.2008.11.056

34. Urbain OM, Stemeri WR, Charles H (1940) United states "patent office 7" us Pat. 2208173

35. Manohar A. K, Kim K. M, Plichta E, et al. (2016). A High Efficiency Iron-Chloride Redox Flow Battery for Large-Scale Energy Storage. J Electrochem Soc 163:5118–5125. doi: 10.1149/2.0161601jes

36. Rai A. K, Rao K. N, Kumar L. V, Mandal K. D (2009) Synthesis and characterization of ultra fine barium calcium titanate, barium strontium titanate and $Ba_{1-2x}Ca_x$ Sr_xTiO_3(x = 0.05, 0.10). J Alloys Compd 475:316–320. doi: 10.1016/j.jallcom.2008.07.038

37. Dong W, Zhao G, Bao Q, Gu X (2015) Solvothermal Preparation of $CaTiO_3$ Prism and $CaTi_2O_4(OH)_2$ Nanosheet by a Facile Surfactant-free Method. Mater Sci(MEDŽIAGOTYRA)21:583–585.
doi: http://dx.doi.org/10.5755/j01.ms.21.4.9697

38. Wang ED, Zhao TS, Yang WW (2010) Poly(vinyl alcohol)/3-(trimethylammonium) propyl-functionalized silica hybrid membranes for alkaline direct ethanol fuel cells. Int J Hydrogen Energy 35:2183–2189. doi: 10.1016/j.ijhydene.2009.12.179

39. AL-Sabagh A. M, Abdeen Z (2010) Preparation and Characterization of Hydrogel Based on Poly(vinyl alcohol) Cross- linked by Different Cross-Linkers

Used to Dry Organic Solvents. J Polym Environ 18:576–583. doi: 10.1007/s10924-010-0200-5

40. Xiong Y, Liu Q. L, Zhu A. M, et al. (2009) Performance of organic –inorganic hybrid anion-exchange membranes for alkaline direct methanol fuel cells. J Power Sources 186:328–333. doi: 10.1016/j.jpowsour.2008.10.070

41. Fu R, Woo J, Seo S, et al (2008) Covalent organic/inorganic hybrid proton-conductive membrane with semi-interpenetrating polymer network : Preparation and characterizations. J Power Sources 179: 458–466. doi: 10.1016/j.jpowsour.2007.12.118

42. Pandey J, Mir FQ, Shukla A (2014) Synthesis of silica immobilized phosphotungstic acid (Si-PWA)-poly (vinyl alcohol) (PVA) composite ion-exchange membrane for direct methanol fuel cell. Int. J. Hydrogen Energy 1–9. doi: 10.1016/j.ijhydene.2014.03.237

43. Ran J, Wu L, Varcoe J. R, (2012) Development of imidazolium-type alkaline anion exchange membranes for fuel cell application. J. Memb Sci 415-416:242–249. doi: 10.1016/j.memsci. 2012.05.006

44. Fuenzalida V. M, Arias J. L, Fernandez M. S (2007) Hydrothermal-electrochemical $CaTiO_3$ coatings as a precursor of bio-mimetic calcium phosphate layer. Mater Lett 61:2739–2743. doi: 10.1016/j.matlet.2006.06.092

45. Musse C, Sharma S, Madalena M, et al. (2016) New approaches towards composite and multilayer membranes for intermediate temperature-polymer electrolyte fuel cells and direct methanol fuel cells. J Power Sources 316:139–159.

46. Li X, Zhang H, Mai Z, et al.(2011) Ion exchange membranes for vanadium redox flow battery (VRB) applications. Energy Environ. Sci 4:1147. doi: 10.1039/c0ee00770f.

CHAPTER 5

DEVELOPMENT OF HIGH PERFORMANCE ANION EXCHANGE MEMBRANES BY CHEMICAL MODIFICATION OF POLYVINYL ALCOHOL FOR ELECTROCHEMICAL DEVICES

5.1 Introduction

There is widespread concern over the use of fossil fuels and other non-renewable energy resources due to the global environmental problems and also due to the fact that these resources are depleting at a fast rate. Hence the development of efficient energy storage/conversion devices like rechargeable batteries and fuel cells for the harvesting of renewable energy like solar and wind energy have received considerable attention in the recent years [1–8]. Ion-exchange membranes (IEMs) serve as a major component of these electrochemical devices. High ionic conductivity, excellent chemical stability and mechanical strength of the membranes are essential for ensuring sustainable and durable operation of these electrochemical devices. Several efforts have been made for the development of anion-exchange membranes due to potential advantages that hold over currently existing cation-exchange membranes [9]. Currently used anion-exchange membranes are based on poly(arylene-ether sulfone) [10], polyphenylene oxide [11], polyphenylene [5] polybenzimidazoles [12–14], polyethylene [15], polyvinylidene fluoride (PVDF) [16], ethylene–tetrafluoroethylene (ETFE) [3], polyether ether ketone(PEEK) [17], polysulfones [18], poly(arylene ether) and poly(ether imide) [10,17,19–22]. Commonly, AEMs are synthesized via chloro-methylation of the polymers and subsequent exposure to trimethylamine (TMA) to form the quaternary ammonium (QA) head-group [11]. But QA group is prone to Hoffmann degradation reaction in strong basic conditions and this reduces the long term performance of these membranes.

Recently, interesting works have been focused on non-QA AEMs to overcome afore mentioned problems. Investigation of guanidinium moieties as anion-exchange sites has given promising results. The high alkalinity of guanidine yields high

concentration of mobile hydroxide ions and thus makes the membrane highly conductive [10,23–25]. The charge delocalization from the resonance structures of guanidinium ion improves the chemical stability of such membranes [23] and avoid Hoffman degradation when used as AEMs [25,26].

Poly(vinyl alcohol) is an environmental friendly biopolymer [27]. AEMs based on PVA have potential applications due to its non toxicity, good film forming ability, low cost, good mechanical strength, chemical stability, high hydrophilic behavior and low methanol permeability. In addition to its uses in fibers, films and coatings, PVA also finds applications in modern technologies such as polyelectrolytes, hydrogels and biomaterials [28–31]. The chemical modification of polymers is an important method in the development of new AEMs with improved properties. Most chemical modifications of PVA have been done on the pendent hydroxyl groups because of its high reactivity [32]. PVA modification reactions commonly employed are esterification, etherification and acetylation of the hydroxyl groups [33,34]. Recently functionalization of PVA hydroxyl groups with azide group was reported by Gacal and co-workers [35].

Here, we report an effective and simple method for the synthesis of a novel anion-exchange membrane (AEMs) by chemical modification of polyvinyl alcohol to polyvinyl ketone using $KMnO_4$ [32,36] followed by guanidination and cross-linking with glutaraldehyde [37]. The viscous solution so obtained was used for membrane fabrication by solution casting method.

5.2. Experimental

5.2.1. Materials

Polyvinyl alcohol (PVA) (M_w 89,000-98000), guanidine hydrochloride, glutaraldehyde (25 wt% solution in water of analytical grade), potassium permanganate and hydrochloric acid were purchased from Merck.

5.2.2. Chemical modification of PVA

A 5 wt% PVA solution was prepared by dissolving 5 g PVA in 100 ml D. I. water at 80°C in a 500 ml reaction flask. Then 0.25 g of $KMnO_4$ in 10 ml water was added

drop wise and stirred for 1 h followed by 0.02 moles of guanidine hydrochloride and was stirred again for another 2 h at 60°C. Then glutaraldehyde solution (5 wt%) was added drop wise (2.5 wt% of PVA) into the mixture followed by three drops of 1M HCl as catalyst for cross-linking. The compositions of the membranes were varied by using different amount of guanidine hydrochloride (0.02moles, 0.01moles and 0.005 moles). The corresponding membranes are represented as PVAOG2, PVAOG1 and PVAOG0.5. The viscous solution was cast into membranes on a clean glass plate. The membranes were peeled from the glass plate after drying in vacuum oven at 50°C for 48 h. The membranes were 120±20µm thick. All the membranes were immersed in 1M NaOH solution for 1 day prior to testing. The synthetic route for the chemical modification of PVA polymer membrane is illustrated in **Fig.**60

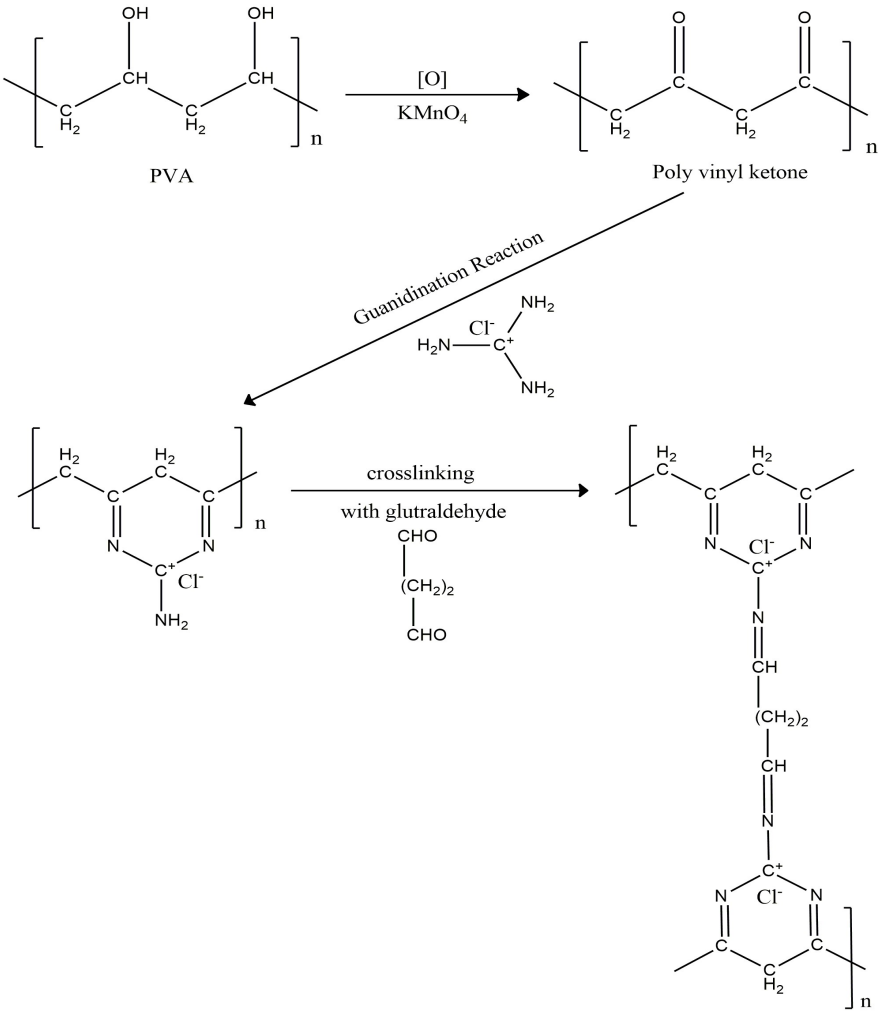

Fig. 60 Scheme of Chemical modification of PVA

5.2.3. Membrane Characterization

FT-IR spectra of the membrane and starting materials were recorded using Perkin Elmer instrument (Model L160000A) over a range of 4000-400 cm^{-1}. The morphology of the composite membrane was examined by a scanning electron microscope (JSM-5600, JEOL Company, Japan,). TGA thermograms of the composite membranes were recorded on a Shimadzu TGA-50H analyzer by heating the samples from room temperature to 700°C under a nitrogen atmosphere at a heating rate of 10°C/min. The water uptake of the membrane was determined by weighing both vacuum dried membranes and membranes that were fully equilibrated with water. The membranes were weighed under wet conditions after being equilibrated in distilled water for 24 h at room temperature. The samples were then dried in vacuum oven for two days. The water uptake was calculated as follows.

$$\text{Water uptake (\%)} = \frac{Wwet - W_{dry}}{W_{dry}} \times 100\%$$

Where W_{wet} is the mass of the water swollen membrane, and W_{dry} is the mass of the dry membrane.

The ion exchange capacities of the membranes were determined by double titration method. Membrane samples were accurately weighed and were immersed in 25 ml of 0.05M HCl solution for 48 h and the HCl solution was back titrated by 0.05M NaOH solution using phenolphthalein as indicator.

Ion exchange capacities of the samples were calculated using the equation:

$$\text{IEC} = \frac{n_1 - n_2}{M_{dry}}$$

Where n_1 and n_2 are the concentrations of (mmol) hydrochloric acid required before and after equilibrium respectively, and M_{dry} is the mass in g of the dried sample.

The average value of the three samples calculated from the above equation is the IEC value of the measured membrane.

Electrochemical impedance spectroscopy was used to measure the membrane conductivity using AUTOLAB 50519 PGSTAT instrument. Conductivity measurements were performed in a specially made two compartment cell using platinum electrodes [39,40]. The membrane and solution were held at the experimental temperature for at least 20 min prior to experimentation to ensure thermal equilibrium. AC impedance measurements were performed using frequency ranges from 100 Hz-1000 kHz and alternating potential amplitude of 10 mV. Fully hydrated membranes were placed in the conductivity cell and the cell was filled with 1M NaOH. The real impedance value at the intercept in the Nyquist plot was taken as the resistance of the membrane. The resistance of the membrane and solution (R_{total}) was measured. The resistance of the solution ($R_{solution}$) was measured without the membrane. Membrane resistance (R_{mem}) was obtained from the difference of the measured resistances ($R_{mem} = R_{total} - R_{solution}$). The thickness of the membrane was measured with a digital micrometer by placing the membrane between two glass slides to ensure both a planar surface and limited compression.

The conductivity of the membrane was calculated as follows $\sigma = L/RA$ Scm^{-1}, Where σ is the hydroxide conductivity in Scm^{-1}, R is the ohmic resistance of the membrane (Ω), L is the distance between the electrodes (in cm.), A is the cross sectional area of membrane samples (cm^2).

The tensile strength of the membranes were investigated with universal testing machine (UTM) (Zwick, Model 1446-60, Germany) [39,41]. For this test the samples were prepared according to ASTM-D882 standard. The films were then placed between the grips of the testing machine. The grip length was 5cm and speed of testing was set at the rate of 10 mm/min.

Methanol permeability through the membrane was measured with a homemade apparatus. The measurement is based on the Gasa method [42] which employed a permeation cell derived from Walker et al. [43]. Definite weight of methanol was sealed inside a permeation cell and allowed to diffuse through an opening of area $4cm^2$ covered

by a membrane. Measurements were conducted at room temperature. In fact, permeation process involves dissolution and diffusion of ethanol molecules in the membrane materials. The mass of methanol inside the vial as a function of time was measured and the permeability (P) of the membrane was given by the equation

$$P = \frac{N \times l}{V.P. \times A \times t}$$

where N is the number of moles of methanol lost (moles), l is thickness of the membrane, V.P is saturated vapor pressure of methanol at 25°C, A is the membrane area for methanol permeation in (cm^2), and t is time (days)

The chemical stability of anion-exchange membranes is an important parameter that affects the performance of electrochemical devices, especially at high pH and strong chemical environments. The alkaline stability was measured by immersing the composite membrane sample with a size of 3cm x 3cm in 2M NaOH at room temperature for 2 weeks. They were taken out, washed with D.I. water, wiped with tissue paper, and then studied using FT-IR technique to detect any degradation or changes in chemical structures. Loss of weight of the membrane was also measured [11,45]. The oxidative stability of membrane was determined by immersing the samples 3cm x 3cm into Fenton's reagent for 24 h (30 ppm $FeSO_4$ in 30% H_2O_2) at 25°C, which was evaluated by recording the weight loss of the membrane with time [46].

Performance of the prepared membrane as separator in all-iron flow battery

All-iron flow battery experiments were performed in the 36 cm^2 flow cell hardware with electrolyte flowing across two electrodes, separated by the membrane prepared [35]. All experiments were performed with electrolyte flow rates of 25 ml min^{-1}. Electrolyte for both positive and negative electrodes consisted of 1M $FeCl_2$ and 1.5M NH_4Cl. The electrodes were made from densified graphite with a cross-sectional area of 16 cm^2. The charging efficiency of the all-iron redox flow cell was determined by charging the cell at 100 mA cm^{-2} for 100 s followed by discharging at 50 mA cm^{-2} using AUTOLAB 50519 PGSTAT instrument. The cell performance is normally determined

by its coulombic efficiency (CE). CE is the ratio of discharge capacity (Q_{dis}) to charge capacity (Q_{ch}) of a cell.

5.3. Results and discussion

5.3.1. Structural analysis

Fig. 61(a-e) shows the FT-IR spectra of PVA, Guanidine chloride, and synthesized membranes respectively. **Fig.** 61 (a) shows the characteristic peaks of PVA in the region 3400-3100 cm^{-1} due to -OH stretching, band at 2920 cm^{-1} due to -CH stretching vibrations of polymer back bone and band at 1420 cm^{-1} is attributed to bending vibrations of $-CH_2$ group as reported in literature [47,48]. **Fig.** 61 (b) shows a strong band between 3400-3100 cm^{-1} which is attributed to the stretching vibrations of N-H groups in guanidinium group. The peak at 1654 cm^{-1} is a coupled vibration having contributions from both N-H in plane bending vibrations and symmetric stretching vibrations of C-N groups of guanidinium ion as reported in literature [25,49,50]. **Fig.** 61 (c-e) of the membranes show a strong band between 3400-3100 cm^{-1} which is attributed to the stretching vibrations of -OH group of bonded water molecules, –OH groups in PVA, and N-H stretching vibrations of guanidinium group [50]. The band at 2924 cm^{-1} is due to the stretching vibrations of -CH groups of PVA polymer back bone and band at 1420 cm^{-1} is due to bending vibrations of $-CH_2$ group [51]. The peak at 1654 cm^{-1} is a coupled vibration having contributions from both N-H in plane bending vibrations and asymmetric stretching vibrations of C-N groups of guanidinium ion [24,25,49,50]. The result shows that successful incorporation of guanidinium group into the PVA matrix has been achieved.

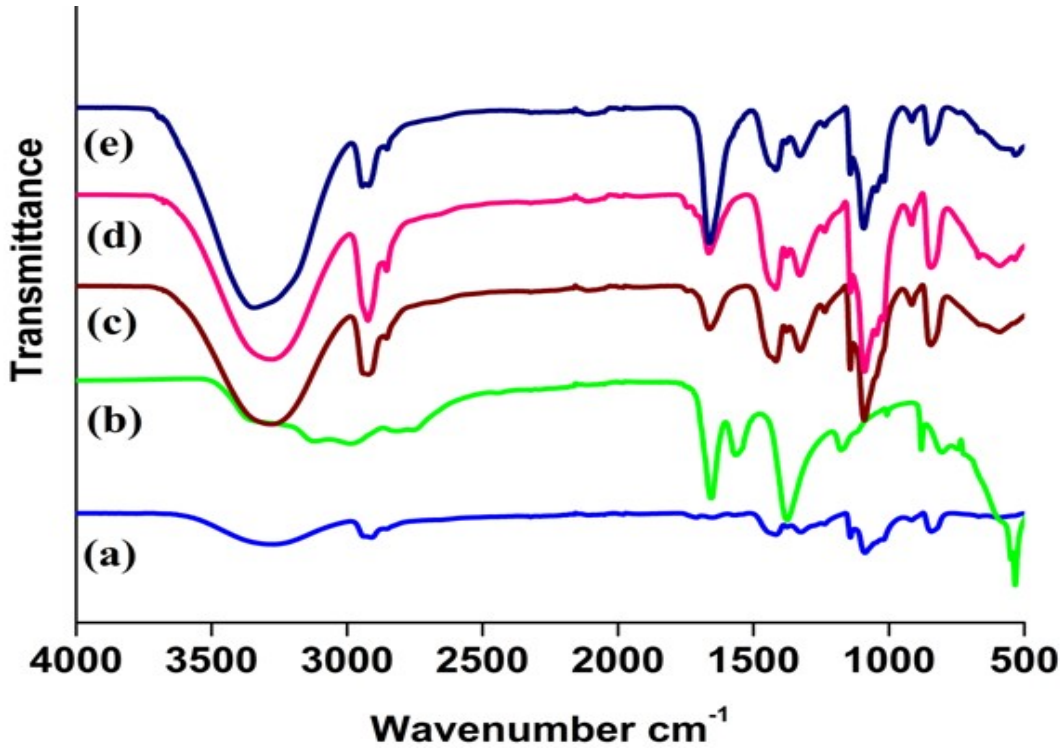

Fig. 61 FTIR spectra of the starting materials and membranes (a) PVA (b)Guanidine chloride (c)Membrane PVAOG0.5 (d)PVAOG1(e)PVAOG2

Fig. 62 Photograph of the PVAOG2 anion-exchange membrane

5.3.2. SEM analysis

Scanning electron microscopy (SEM) is used to investigate the microstructures of the membranes. **Fig.** 63 (a-b) present the SEM images of surface and cross-section of PVAGO2 membranes. The surface of the membrane was found to be smooth without any cracks or pinholes, indicating the fine quality of the membrane, which was further confirmed by cross-section image of the membrane. Cross-sectional SEM image of PVAOG2 membrane shows that the thickness of the membrane is about 120 ±20 μm. The fabricated PVAOG2 membrane appeared as a transparent film as shown in photograph **Fig.** 62.

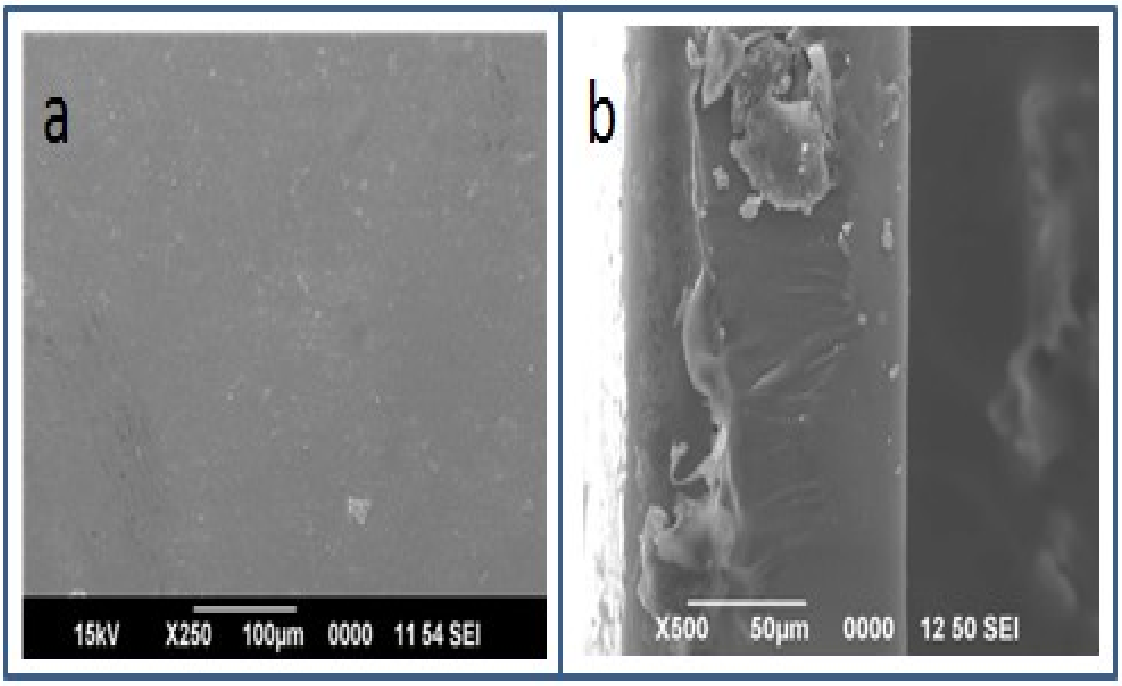

Fig.63 (a) SEM surface image (b) SEM cross-sectional image of PVAOG2 membrane

5.3.3. Water uptake

Water uptake is considered as one of the essential properties of anion-exchange membranes for practical applications. Presence of water molecules is considered mandatory for facilitated hydroxide (or any anion) transport. It dependence on the

hydrophilicity of the base polymer, the nature of ion exchange group and degree of cross linking [39]. Water uptake values of the newly fabricated membranes found to be lower than that of PVA membrane as shown in the **Fig.** 64. This indicates that cross-linked polymer matrix form a net work reducing the free volume between the polymer chains leading to a decrease in water uptake and improvement in dimensional stability of the membrane [26]. However, too high a water uptake can result in the deterioration of mechanical and chemical stabilities of the membranes [11,52].

5.3.4. Ion exchange capacity

IEC provides an indication of amount of exchangeable groups in the membrane [11,20]. As shown in **Fig.** 65 the IEC values increase with guanidine content up to 0.01moles and further addition of guanidine shows not much change in IEC value. The IEC of the PVAOG2 membrane was found to be 0.61 meq g^{-1}.

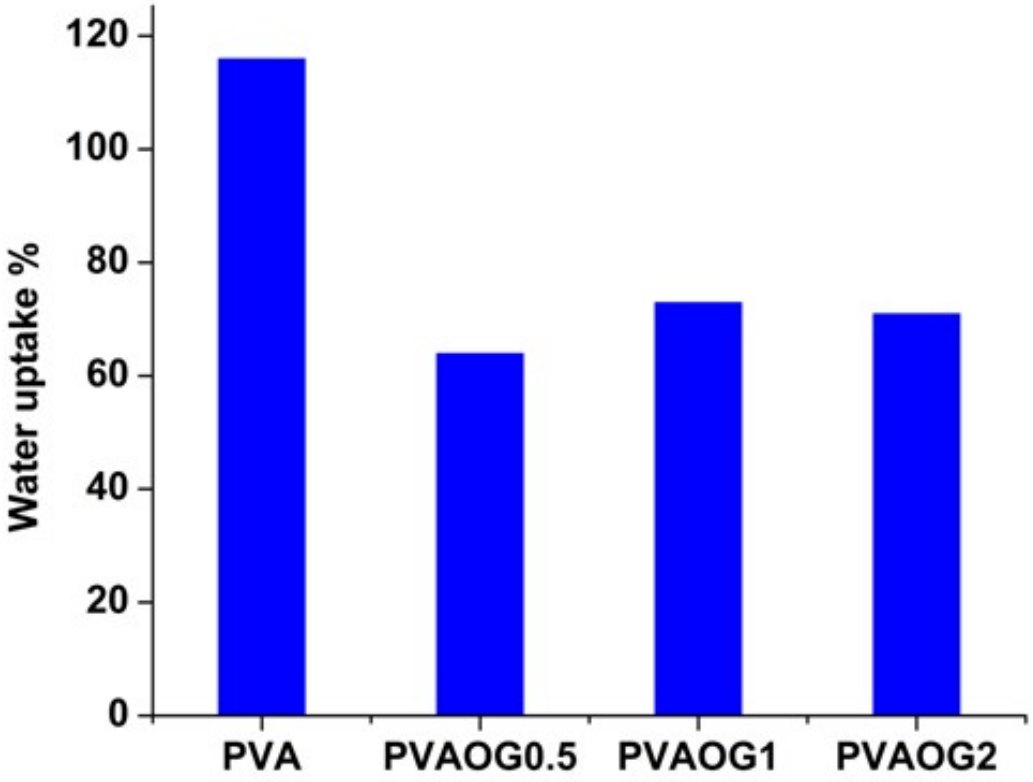

Fig. 64 Water uptake of membranes with varying guanidine content

IEC of the membranes increased from 0.2 meq g^{-1} for PVAOG0.5 to 0.61 meq g^{-1} for PVAOG2, Nafion has IEC 0.91 meq g^{-1} and conductivity 80–90 $mScm^{-1}$ at room temperature [20]. IEC is also highly dependent on the basicity of ion exchange groups. Strong basic groups lead to an augmentation of both the number of dissociated hydroxides and high IEC thus improves ionic conductivity of the membrane [25].

5.3.5. Electrical properties

The conductivity of the anion-exchange membrane is an important property for applications of membranes in electrochemical devices. Herein, the ionic conductivities were examined by electro-chemical impedance spectra (EIS) recorded in the frequency range of 100 Hz to 100 kHz and with signal amplitude of 10 mV. **Fig.** 66 shows that ionic conductivity of the membranes increases from 10 mS cm^{-1} for PVA upto 71 mS cm^{-1} for PVAOG2 membrane at room temperature with increase in guanidine content. The ionic conductivity of the membranes largely depends on the nature of ion-exchange group and hydrophilicity of the polymer matrix. The enhanced ionic conductivity of the chemically modified membrane compared to a PVA membrane can be attributed to the increase in the guanidinium groups of the membrane that interacts with anions in solution. Therefore, the higher alkalinity of the guanidinium groups has led to improvement in ionic conductivity [11]. The conduction of ions across an ion exchange membrane also depends on the water content of membrane matrix. Water content plays a decisive role in ionic conduction through increase of the hydrophilic domains, which provide larger ion-conductive channels within the membrane. In an ideal ion exchange membrane, the water content should be limited and the IEC to be maximized [52].

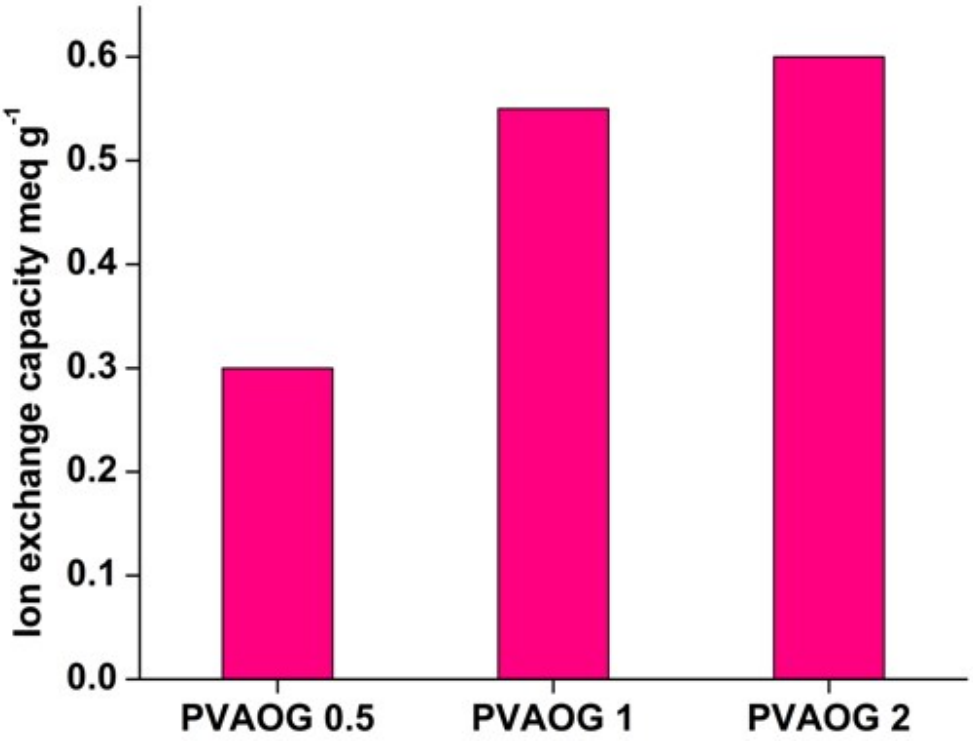

Fig. 65 IEC of membranes with varying guanidine content

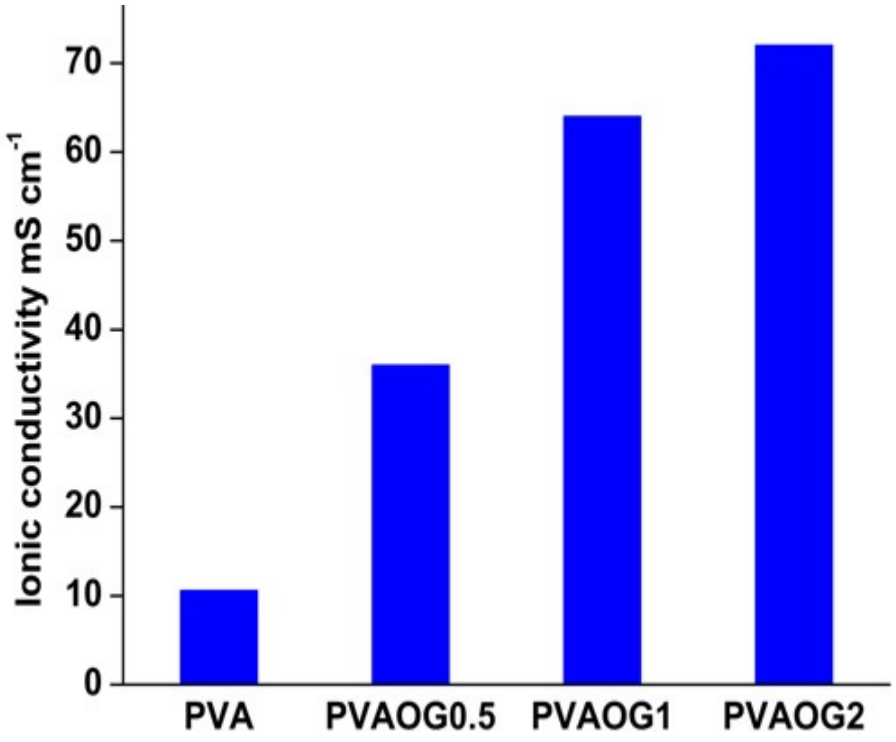

Fig. 66 Ionic conductivity of membranes with varying guanidine content

5.3.6 Thermo Gravimetric Analysis

Thermal stability is an important parameter for the use of membranes in high temperature electrochemical applications. **Fig.**67 shows TGA curves for (a) PVAOG2 membrane (b) PVA membrane, respectively. The samples were heated in the temperature range from 30°C to 750°C at a constant rate of 10°C/min under nitrogen atmosphere. The TGA curve of pure PVA film **Fig.** 67 (b) shows three major weight loss regions [53]. The first region at a temperature of 80-160°C was associated with the evaporation of weakly adsorbed water and the weight loss of the membrane is about 12.9%. The second region at about 250-350°C is due to the degradation of PVA polymer membrane and the weight loss of the membrane at this stage is about 61.6%. The peak of third stage at 450°C is due to the splitting of PVA chains into small segments associated with 87.7% weight loss of the membrane. **Fig.** 67(a) TGA curve of PVAOG2 membrane also exhibits three major weight loss regions. The first region at a temperature of 80-160°C is also due to the evaporation of weakly adsorbed water and the weight loss of the membranes is about 9.5%. The second region at 250-350°C is due to the decomposition of side chain of PVA, guanidine and glutaraldehyde in the membrane, the weight loss of the membrane is only about 45.5% for PVAOG2 membrane [11]. The peak of third stage at 450°C is due to the splitting of PVA chains into small segments associated with 75.1% weight loss of the membrane. TGA results as shown in **Fig.** 67 indicate that thermal degradation pattern of the newly fabricated membrane shifted towards higher temperatures compared to a pure PVA sample. This suggests that the chemical modification of PVA matrix by guanidination followed by its cross-linking with glutaraldehyde improved thermal stability of the newly fabricated membrane.

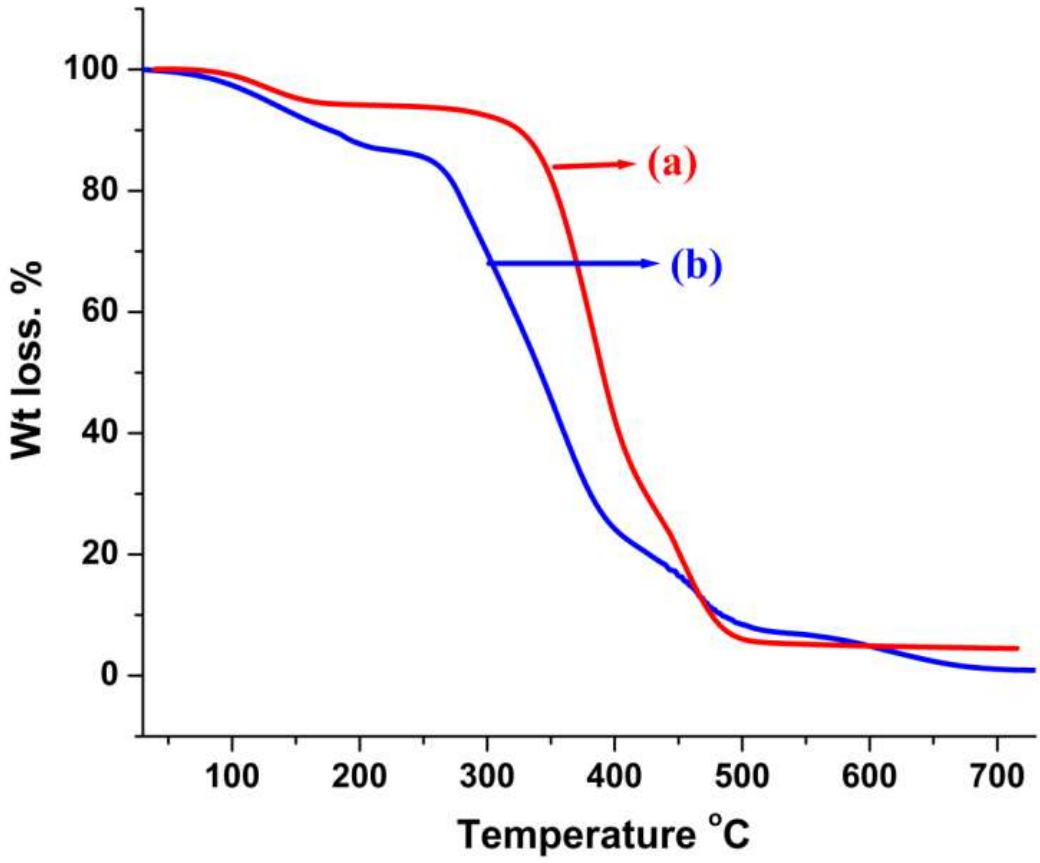

Fig. 67 The TGA curves of (a) PVAOG2 membrane (b) PVA membrane

5.3.7. Mechanical properties

Adequate mechanical and dimensional stability are required for membranes used in electrochemical devices. The membranes act as a carrier for ions and as a barrier to provide effective separation between two compartments. So the membranes must be thin for better ionic conduction at the same time mechanically robust to avoid damage during practical applications [54]. The tensile strength of the membranes was in the range of 32-37 MPa. Compared to tensile strength of Nafion-117 (34 MPa), the prepared membranes exhibited better values [55].

5.3.8. Methanol permeability

Methanol permeability is an important parameter used to evaluate the potential of ion exchange membranes for applications in direct methanol fuel cells [24]. The methanol permeability values of the synthesized membrane indicate very good methanol

barrier properties of this membrane. **Fig.**68 shows that methanol permeability increased with increasing temperature. This is due to the increase in mobility of both methanol and polymer chains with increasing temperature [38]. The membrane PVAOG2 possesses methanol permeability of 2.05×10^{-9} mol cm^{-1} day^{-1} Pa^{-1} at room temperature. For a comparison Nafion 117 exhibits methanol permeability of 3.5×10^{-7} mol cm^{-1} day^{-1} Pa^{-1} at room temperature [24].

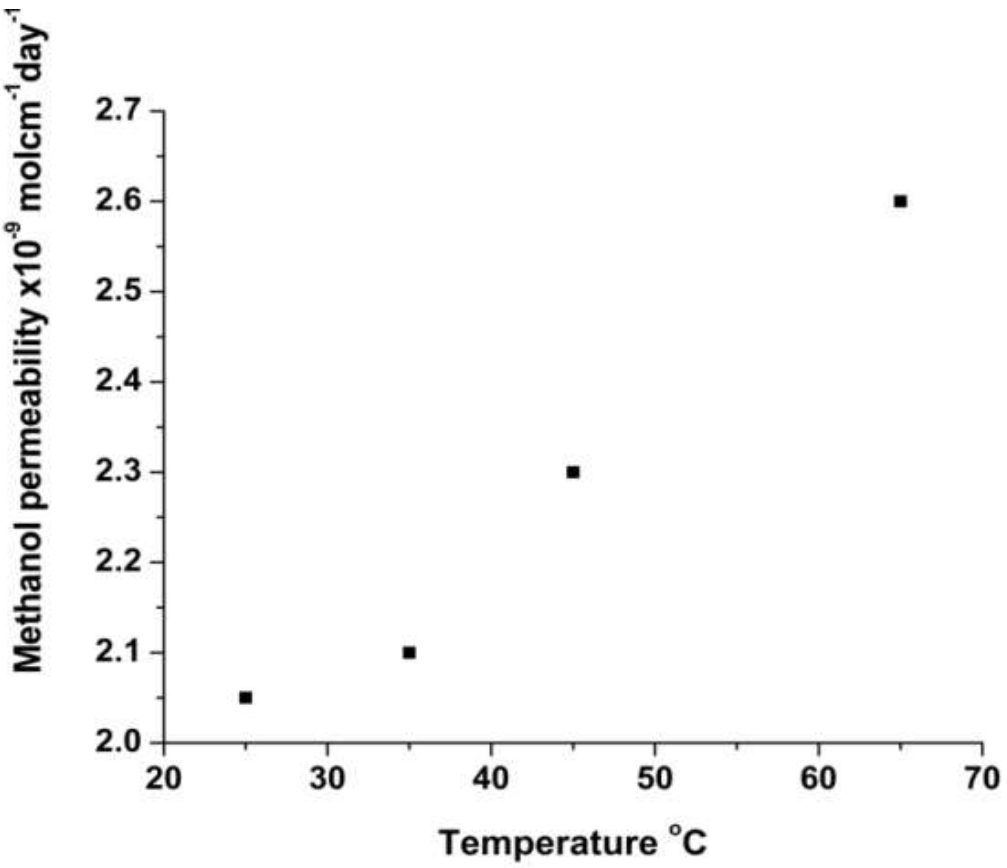

Fig. 68 Methanol permeability of PVAOG2 membrane at varying temperatures

5.3.9. Chemical stability

To meet the requirements of the practical applications in strong chemical environments, the prepared AEMs must have good chemical stability, especially in high pH environments. Here, the membrane exhibited excellent alkaline stability. The FT-IR spectrum of the membrane after alkaline stability test is presented in **Fig.**69. The spectra show no significant change in peak positions or their relative intensities even after an exposure of membrane in 2M aq. NaOH medium for 2 weeks. During the alkaline

stability test, the membranes did not show any loss of weight. Fenton's reagent is used to simulate and accelerate the harsh operation environment, in which the $OH^{\cdot}$ and $OOH^{\cdot}$ radicals formed from H_2O_2 can cause the degradation of the AEMs. All the membranes did not show any physical deformation, colour change and weight loss as shown in **Fig.**70. The membrane found to be good in chemical stability.

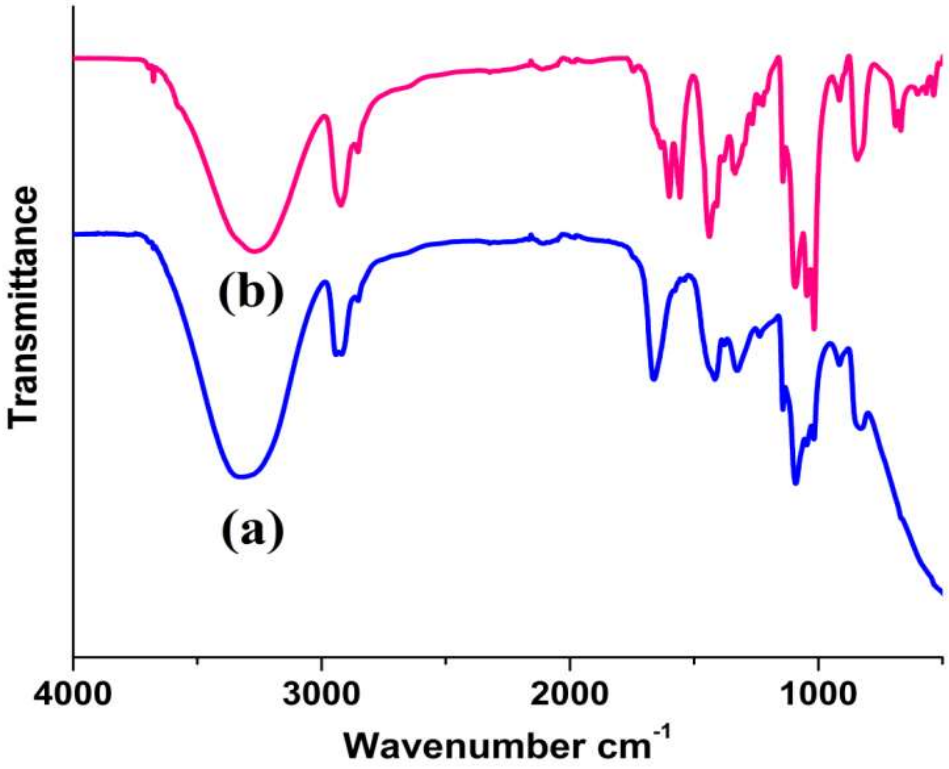

Fig. 69 FT-IR spectrum of the PVAOG2 membrane (a) before alkaline stability test (b) after alkaline stability test

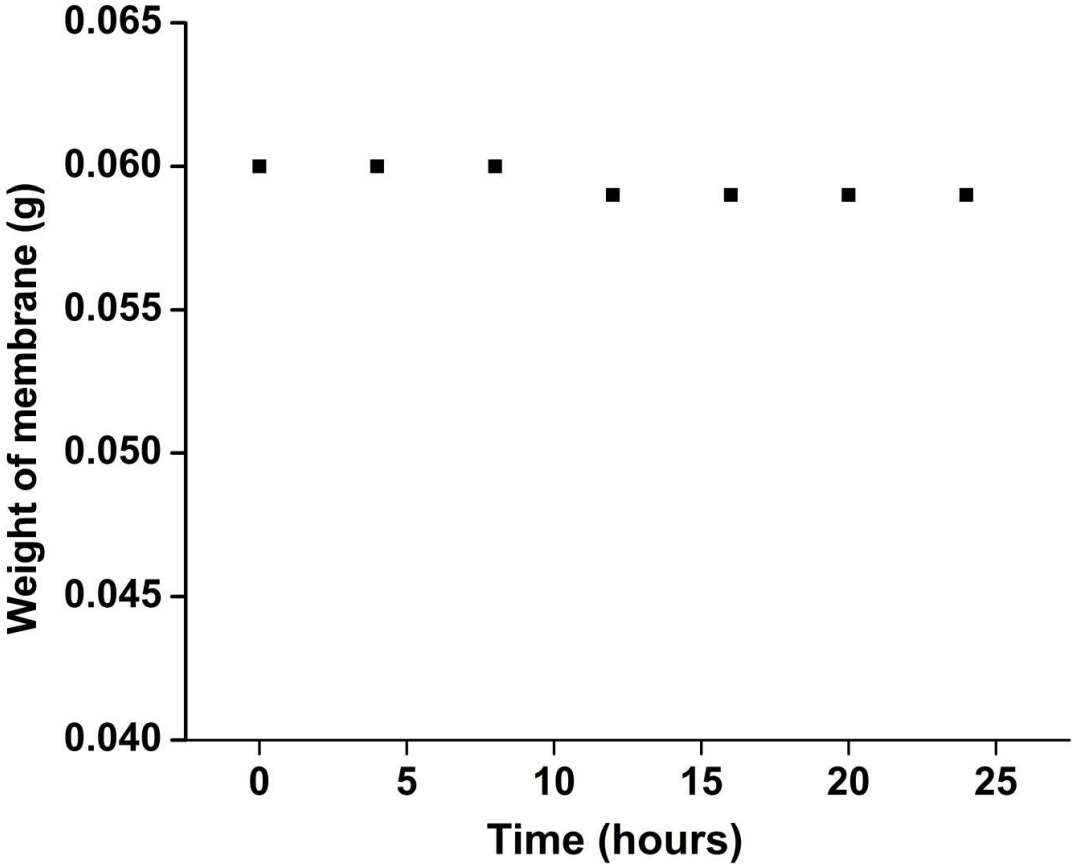

Fig. 70 Weight of membrane with time during Fenton's test

5.3.10. Performance of the prepared membrane as separator in all-iron flow battery

The cell voltage-time curve measured during the charging and discharging of an all-iron redox flow cell using the prepared membrane as separator is shown in **Fig.** 71. A constant current density of 100 mA cm^{-2} for charging and 50 mA cm^{-2} for discharging was used. Repeated charge-discharge measurement of the cell with high-efficiency electrolyte at 100 mA cm^{-2} demonstrated that high coulombic efficiency (> 75%) could be maintained over repeated cycles. Higher coulombic efficiency indicates low cross-mixing of ions [54]. These results confirm the viability of the new composite membrane as a separator in all-iron redox flow battery.

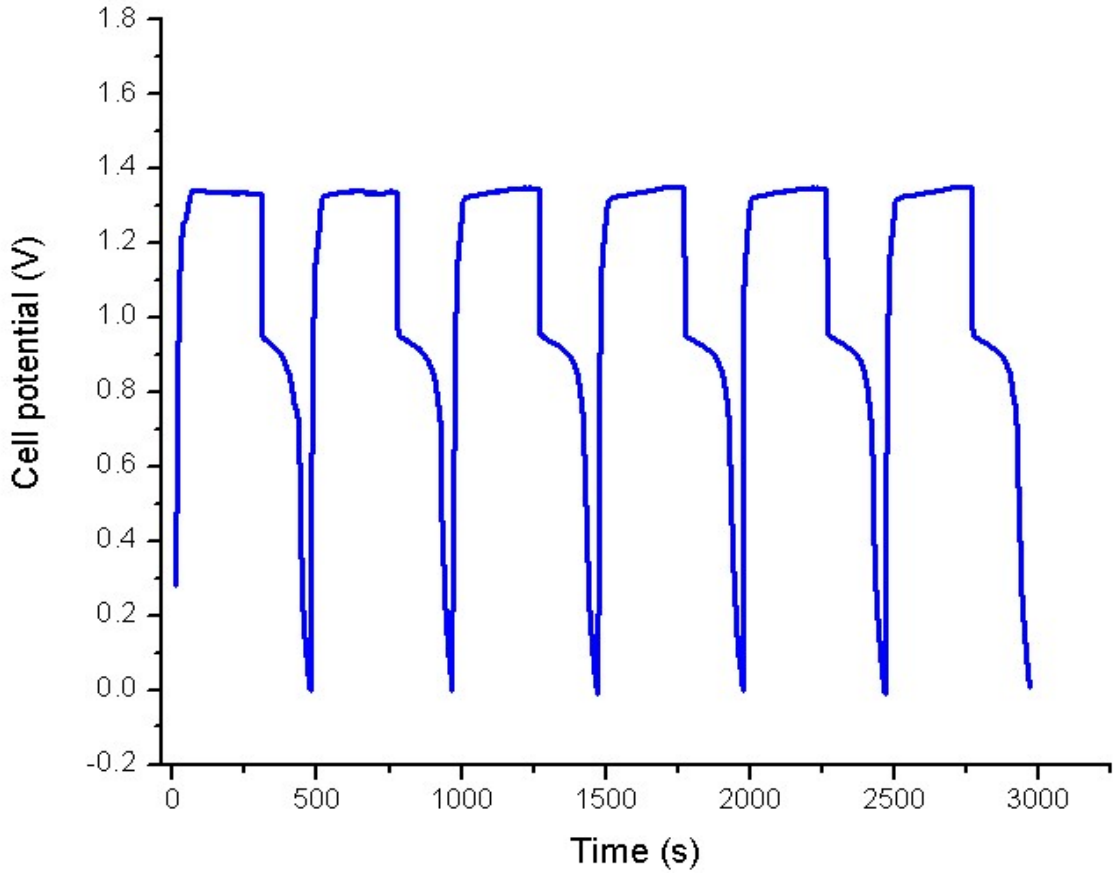

Fig. 71 The cell voltage-time curve of all- iron redox flow cell during galvanostatic charge-discharge experiment

5.4. Conclusions

In summary, we have demonstrated a facile and effective method for the preparation of AEMs functionalized with highly stable guanidinium ion exchange group. The membranes were prepared by chemical modification of polyvinyl alcohol. The resultant membranes are flexible and tough enough for potential use as AEM materials. The membrane exhibited the ionic conductivity of 71mS/cm at room temperature, excellent mechanical properties, thermal stability up to 150°C, this shows that these membranes are ideal for applications in that temperature range. These membranes exhibited good chemical stability in strong chemical environments. The fabricated membrane is a promising alternative to the existing commercial membranes.

5.5 References

[1] V. Pupkevich, V. Glibin, D. Karamanev, Phosphorylated polyvinyl lcohol membranes for redox Fe^{3+}/H_2 flow cells, J. Power Sources. 228 (2013) 300–307. doi:10.1016/j.jpowsour.2012.11.080.

[2] X. Li, H. Zhang, Z. Mai, H. Zhang, I. Vankelecom, Ion exchange membranes for vanadium redox flow battery (VRB) applications, Energy Environ. Sci. 4 (2011) 1147. doi:10.1039/c0ee00770f.

[3] J. Qiu, M. Li, J. Ni, M. Zhai, J. Peng, L. Xu, H. Zhou, J. Li, G. Wei, Preparation of ETFE-based anion exchange membrane to reduce permeability of vanadium ions in vanadium redox battery, J. Memb. Sci. 297 (2007) 174–180. doi:10.1016/j.memsci. 2007.03.042

[4] T. Sukkar, M. Skyllas-Kazacos, Modification of membranes using polyelectrolytes to improve water transfer properties in the vanadium redox battery, J. Memb. Sci. 222 (2003) 249–264. doi:10.1016/S0376-7388(03)00316-8

[5] C. N. Sun, Z. Tang, C. Belcher, T. A. Zawodzinski, C. Fujimoto, Evaluation of Diels-Alder poly(phenylene) anion exchange membranes in all-vanadium redox flow batteries, Electrochem. Commun. 43 (2014) 63–66. doi:10.1016/j.elecom.2014.03.010

[6] T. Mohammadi, M. Skyllas-Kazacos, Characterisation of novel composite membrane for redox flow battery applications, J. Memb. Sci. 98 (1995) 77–87. doi:10.1016/0376-7388(94)00178-2.

[7] T. Mohammadi, M. Skyllas-Kazacos, Use of polyelectrolyte for incorporation of ion-exchange groups in composite membranes for vanadium redox flow battery applications, J. Power Sources. 56 (1995) 91–96. doi:10.1016/0378-7753(95)80014-8.

[8] P. K. Leung, C. Ponce de León, F.C. Walsh, An undivided zinc-cerium redox flow battery operating at room temperature (295 K), Electrochem. Commun. 13 (2011) 770–773. doi:10.1016/j.elecom. 2011.04.011.

[9] T. Feng, B. Lin, S. Zhang, N. Yuan, F. Chu, M.A. Hickner, C. Wang, L. Zhu, J. Ding, Imidazolium-based organic-inorganic hybrid anion exchange membranes for fuel cell applications, J. Memb. Sci. 508 (2016) 7–14. doi:10.1016/j.memsci.2016.02.019.

[10] Q. Zhang, S. Li, S. Zhang, A novel guanidinium grafted poly(aryl ether sulfone) for high-performance hydroxide exchange membranes, Chem. Commun. 46 (2010) 7495–7497. doi:10.1039/c0cc01834a.

[11] X. Lin, L. Wu, Y. Liu, A.L. Ong, S.D. Poynton, J.R. Varcoe, T. Xu, Alkali resistant and conductive guanidinium-based anion-exchange membranes for alkaline polymer electrolyte fuel cells, J. Power Sources. 217 (2012) 373–380.

[12] S. Singha, T. Jana, Structure and Properties of Polybenzimidazole/Silica Nanocomposite Electrolyte Membrane: Influence of Organic/Inorganic Interface, ACS Appl. Mater. Interfaces. 6 (2014) 21286–21296.

[13] O. D. Thomas, K. J. W. Y. Soo, T. J. Peckham, M. P. Kulkarni, S. Holdcroft, A Stable Hydroxide-Conducting Polymer, J. Am. Chem. Soc. (2012) 10753–10756. doi:dx.doi.org/10.1021/ja303067t.

[14] S. Maity, S. Singha, T. Jana, Low acid leaching PEM for fuel cell based on polybenzimidazole nanocomposite with protic ionic liquid modified silica, Polymer (Guildf). 66 (2015) 76–85.

[15] M. Faraj, M. Boccia, H. Miller, F. Martini, S. Borsacchi, M. Geppi, New LDPE based anion-exchange membranes for alkaline solid polymeric electrolyte water electrolysis, Int.J. Hydrogen Energy. 37 (2012) 14992–15002.

[16] S. Singha, T. Jana, Effect of composition on the properties of PEM based on polybenzimidazole and poly(vinylidene fluoride) blends, Polymer (Guildf). 55 (2014) 594–601. doi:10.1016/j.polymer.2013.

[17] M. L. Di Vona, D. Marani, A. D'Epifanio, E. Traversa, M. Trombetta, S. Licoccia, A covalent organic/inorganic hybrid proton exchange polymeric membrane: Synthesis and characterization, Polymer (Guildf). 46 (2005) 1754–1758. doi:10.1016/j.polymer. 2004.12.033.

[18] M. L. Di Vona, R. Narducci, L. Pasquini, K. Pelzer, P. Knauth, Anion-conducting ionomers : Study of type of functionalizing amine and macromolecular, Int. J. Hydrogen Energy. 39 (2014) 14039–14049. doi:10.1016/j.ijhydene.2014.06.166.

[19] J. Zhou, M.Ünlü, I.Anestis-Richard, P.A. Kohl, Crosslinked, epoxy-based anion conductive membranes for alkaline membrane fuel cells, J. Memb. Sci. 350 (2010) 286–292.

[20] C. Qu, H. Zhang, F. Zhang, A high-performance anion exchange membrane based on bi-guanidinium bridged polysilsesquioxane for alkaline fuel cell application, J. Mater. Chem. 22 (2012) 8203–8207. doi:10.1039/c2jm16211c.

[21] Q. Duan, S. Ge, C. Wang, Water uptake, ionic conductivity and swelling properties of anion-exchange membrane, J. Power source. 243 (2013) 773–778. doi:10.1016/j.jpowsour. 2013.06.095.

[22] A. Amel, S. B. Smedley, D. R. Dekel, M. A. Hickner, Characterization and Chemical Stability of Anion Exchange Membrane Crosslinked with Polar Electron-Donating Linkers, J. Electrochem. Soc. 162 (2015) F1047–F1055. doi:10.1149/2. 0891509jes.

[23] Tsutomu ishikawa, Superbases for Organic Synthesis: Guanidines, Amidines, Phosphazenes and Related Organocatalysts, John Wiley & Sons, Ltd 2009. doi:10.1351/pac198860111627.

[24] S. D. Sajjad, D. Liu, Z. Wei, S. Sakri, Y. Shen, Y. Hong, F. Liu, Guanidinium based blend anion exchange membranes for direct methanol alkaline fuel cells (DMAFCs), J. Power Sources. 300 (2015) 95–103. doi:10.1016/j.jpowsour.2015.08.002.

[25] S. D.Sajjad, Y. Hong, F. Liu, Synthesis of guanidinium-based anion exchange membranes and their stability assessment, Polym. Adv. Technol. 25 (2014) 108–116. doi:10.1002/pat.3211.

[26] L. Zeng, T. S. Zhao, L. Wei, Y. K. Zeng, Z. H. Zhang, Highly stable Pyridinium-functionalized cross-linked anion exchange membranes for all vanadium redox flow batteries, J. Power Sources. 331(2016) 452–461. doi:10.1016/j.jpowsour.2016.09.065.

[27] K. Hu, J. Nie, J. Liu, J. Zheng, Separation of methanol from methanol/water mixtures with pervaporation hybrid membranes, J. Appl. Polym. Sci. 128 (2013) 1469–1475. doi:10.1002/app.38241.

[28] N. Takada, T. Koyama, M. Suzuki, M. Kimura, K. Hanabusa, Ionic conduction of novel polymer composite films based on partially phosphorylated poly(vinyl alcohol), Polymer (Guildf). 43 (2002) 2031–2047.

[29] F. Jianqi, G. Lixia, PVA/PAA thermo-cross linking hydro gel fiber: preparation and pH-sensitive properties in electrolyte solution, 38 (2002) 1653–1658.

[30] E. Fortunati, D. Puglia, M. Monti, C. Santulli, M. Maniruzzaman, J.M. Kenny, Cellulose nanocrystals extracted from okra fibers in PVA nanocomposites, J. Appl. Polym. Sci. 128 (2013) 3220–3230. doi:10.1002/app.38524.

[31] J. H. Yeum, B. C. Ji, C. Lee. etal Molecular Weight Poly(vinyl alcohol) Microfibrils in High Yields with the Low-Temperature Polymerization of Vinyl Pivalate in Tetrahydrofuran and saponification, J. Polym. Sci. Part A Polym. Chem. 40 (2002) 1103–1111. doi:10.1002/pola.10199.

[32] Y. L. Liu, Y. C. Chiu, Novel approach to the chemical modification of poly(vinyl alcohol): Phosphorylation, J. Polym.Sci. Part A Polym. Chem. 41 (2003) 1107–1113.

[33] C. Gaina, O. Ursache, V. Gaina, D. Ionita, C. Gaina, O. Ursache, V. Gaina, D. Ionita, Study on the Chemical Modification of Pol(Vinyl Alcohol) with 4-Maleimidophenyl Isocyanate, Polym. Plast.Technol. Eng. (2012) 37–41. doi:10.1080/03602559.2011.617404.

[34] S. Sangngern, S. Sahasithiwat, A. Kaewvilai, Chemical Preparation of chemical vapor sensing materials from composites of esterified poly(vinyl alcohol) and carbon black, Sensors Actuators B. Chem.156 (2011) 961–968. doi:10.1016/j.snb.2011.03.014.

[35] B. N. Gacal, B. Koz, B. Gacal, B. Kiskan, M. Erdogan, Y. Yag, Pyrene functional poly(vinyl alcohol) by “click” chemistry, J.Poly Sci. Pt. A Polym. Chem. 47 (2009) 1317–1326.

[36] M. A. Malik, M. Ilyas, Z. Khan, Kinetics of permanganate oxidation of synthetic macromolecule poly(vinyl alcohol), Indian J. Chem. 48A (2009) 189–193.

[37] D. J. Brown, United States Patent US 6,875,830 B2, 2005.

[38] P. Y. Xu, T. Y. Guo, C. H. Zhao, I. Broadwell, Q. G. Zhang, Q. L. Liu, Anion exchange membranes based on poly(vinyl alcohol) and quaternized polyethyleneimine for direct methanol fuel cells, J. Appl. Polym. Sci. 128 (2013) 3853–3860. doi:10.1002/app.38592.

[39] J. S. Koo, N. Kwak, T. Sung, Synthesis and properties of an anion-exchange membrane based on vinylbenzyl chloride–styrene –ethyl methacrylate copolymers, J. Memb. Sci. 423-424 (2012) 293–301. doi:10.1016/j.memsci.2012.08.024.

[40] W. E. Mustain, J. A. Vega, C. Chartier, W. E. Mustain, Effect of hydroxide and carbonate alkaline media on anion exchange membranes, J. Power Sources. 195 (2015) 7176–7180. doi:10. 1016/j.jpowsour.2010.05.030.

[41] M. Heydari, A. Moheb, M. Ghiaci, M. Masoomi, Effect of cross-linking time on the thermal and mechanical properties and pervaporation performance of poly(vinyl alcohol) membrane cross-linked with fumaric acid used for dehydration of isopropanol, J. Appl. Polym. Sci. 128 (2013) 1640–1651.

[42] J. V. Gasa, R. A. Weiss, M. T. Shaw, Ionic crosslinking of ionomer polymer electrolyte membranes using barium cations, J. Memb. Sci. 304 (2007) 173–180. doi:10.1016/j.memsci.2007.07.031.

[43] M. Walker, K. Baumgärtner, Barrier properties of plasma-poymerized thin films, Surf. Coatings Technol. 119 (1999) 996– 1000.

[44] A. Dorner-Reisel, C. Schürer, G. Irmer, E. Müller, Electrochemical corrosion behaviour of uncoated and DLC coated medical grade Co28Cr6Mo, Surf. Coatings Technol. 177-178 (2004) 830–837. doi:10.1016/j.surfcoat.2003.06.015.

[45] B. Lin, L. Qiu, J. Lu, F. Yan, Cross-linked alkaline ionic liquid-based polymer electrolytes for alkaline fuel cell applications, Chem. Mater. 22 (2010) 6718–6725. doi:10.1021/cm102957g.

[46] Y. Wu, C. Wu, T. Xu, F. Yu, Y. Fu, Novel anion-exchange organic-inorganic hybrid membranes: Preparation and characterizations for potential use in fuel cells, J. Memb. Sci. 321 (2008) 299–308. doi:10.1016/j.memsci.2008.05.003.

[47] E. D. Wang, T. S. Zhao, W. W. Yang, Poly(vinyl alcohol)/3-(trimethyl ammonium) propyl-functionalized silica hybrid membranes for alkaline direct ethanol fuel cells, Int. J. Hydrogen Energy. 35 (2010) 2183–2189. doi:10.1016/j.ijhydene.2009.12.179.

[48] A. M. AL-Sabagh, Z. Abdeen, Preparation and Characterization of Hydrogel Based on Poly(vinyl alcohol) Cross-Linked by Different Cross-Linkers Used to Dry Organic Solvents, J. Polym. Environ. 18 (2010) 576–583. doi:10.1007/s10924-010-0200-5.

[49] C. J. Antony, M. J. Bushiri, H. Tresa, C. Y. Panicker, M. Fleck, Spectroscopic properties of guanidinium zinc sulphate $[C(NH_2)_3]_2Zn(SO_4)_2$ and ab initio calculations of $[C(NH_2)_3]_2$ and $HC(NH_2)_3$, Spectrochim. Acta Part A Mol. Biomol. Spectrosc. 73 (2009) 942–945. doi:10.1016/j.saa.2009.04.024.

[50] M. S. Braiman, D. M. Briercheck, K. M. Kriger, Modeling Vibrational Spectra of Amino Acid Side Chains in Proteins : Effects of Protonation State , Counterion , and Solvent on Arginine C-N Stretch Frequencies, J. Phys. Chem. B. 103 (1999) 4744–50

[51] Y. Xiong, Q. . Liu, A. M. Zhu, S. M. Huang, Q. H. Zeng, Performance of organic–inorganic hybrid anion-exchange membranes for alkaline direct methanol fuel cells, J. Power Sources. 186 (2009) 328–333.

[52] S. Sharma, M. Dinda, C.R. Sharma, P.K. Ghosh, A safer route for preparation of anion exchange membrane from inter-polymer film and performance evaluation in electrodialytic application, J. Memb. Sci. 459 (2014) 122–131. doi:10.1016/j.memsci.2014.02.011.

[53] C. C. Yang, S. J. Chiu, W. C. Chien, S. S. Chiu, Quaternized poly(vinyl alcohol)/alumina composite polymer membranes for alkaline direct methanol fuel cells, J. Power Sources. 195 (2009) 2212–2219. doi:10.1016/j.jpowsour.2009.10.091.

[54] A. K. Manohar, K. M. Kim, E. Plichta, M. Hendrickson,S. Rawlings, S.R. Narayanan, A High Efficiency Iron-Chloride Redox Flow Battery for Large-Scale Energy Storage, J. Electro chem. Soc. 163 (2016) 5118–5125. doi:10.1149/2.0161601jes.

[55] H. Hou, S. Wang, W. Jin, Q. Jiang, L. Sun, L. Jiang, G. Sun, KOH modified Nafion112 membrane for high performance alkaline direct ethanol fuel cell, Int. J. Hydrogen Energy. 36 (2011) 5104 - 5109. doi:10.1016/j.ijhydene.2010.12.093.

CHAPTER 6

DEVELOPMENT OF ANION-EXCHANGE MEMBRANES FOR ELECTROCHEMICAL DEVICES BY CHEMICAL FUNCTIONALIZATION OF PHENOL-FORMALDEHYDE RESINS

6.1 Introduction

Polymer electrolyte membrane fuel cells and rechargeable batteries are considered as modern clean energy conversion/storage technologies due to their high energy conversion efficiencies, low local pollution levels, low noise and low maintenance costs. Anion-exchange membranes as separators in these devices have been extensively studied in recent years as they promise to overcome the disadvantages of Nafion-based proton exchange membrane fuel cells such as low CO tolerance, high electro kinetic over potentials, high fuel permeation and high catalyst cost [1–4]. Among the variety of methods used for AEM synthesis, a commonly used method is to modify the base polymer matrix, such as poly phenylene oxide [5], polyaryl ether sulfone ketones [1] and poly(ether ketone) (PEK) [6]. Usually ion-exchange groups are incorporated to the membranes via chloro-methylation of the polymers followed by exposure to trimethylamine (TMA) to form the corresponding trimethyl-type quaternary ammonium (QA) head-group [6]. But QA group is prone to Hoffmann degradation reactions in strong alkaline environments and this reduces the durability of these membranes [7]. The AEMs prepared by these methods also exhibit low ionic conductivity making them inadequate for practical applications [1]. Hence significant research efforts have been done to develop membranes having excellent chemical stability, ionic conductivity, and mechanical strength [8,9]. X. Lin et al. and C. Qu et al. have prepared a series of AEMs with pendant a guanidinium groups with improved alkaline stability and high ionic conductivity [4,10]. These improvements in properties of guanidinium functionalized AEMs arise from high basicity and resonance stabilized structure of the guanidinium functional groups [4,10]. The pKa of guanidine in aqueous medium is 13.6 and this high alkalinity yields high concentration of mobile hydroxide ions which is higher than that of trimethylamine [11,12].

In 1872 Von Bayer reported the formation of first synthetic resin by polycondensation of phenol and formaldehyde [13]. In 1910 Baekeland made the first plastic by the polycondensation of phenol and formaldehyde [13,14]. Ion exchange property of PF resin was discovered by Adams and Holmes in 1935 [15]. Around 1940, synthetic ion-exchange membranes based on phenol-formaldehyde condensation products were used in many industrial applications such as electrodialysis, electrodialytic concentration of seawater and desalination of saline water [13,14,16–18]. Polycondensation of sodium phenol sulfonate, phenol and formaldehyde was carried out in the presence of an alkali catalyst for the preparation of ion-exchange resins. Low molecular weight prepolymer was coated on a reinforcing fabric such as glass fiber and cured to complete the condensation reaction [17,18]. Anion-exchange membranes were also prepared by polycondensation of phenylenediamines, phenol and formaldehyde. The durability of such membranes, was not sufficient for long-term usage [16,18].

In the last two decades, remarkable progress has been made in the development of high performance polymers as matrices for membranes. Due to high mechanical strength, good chemical resistance, solubility in common solvents, and commercial availability, PVC polymers are widely used for the preparation of polymer membranes [19,20]. PVC based membranes are commercially employed as battery separators, ultra filtration membrane and as matrices in proton exchange membranes (PEM) for fuels [19,21]. J.W. Qian and et al. reported good performance for pervaporation of benzene/cyclohexane mixtures using blend membranes of PVC and EVA [21]. Sulfonated PVC membranes with high permeability and selectivity were developed as proton exchange membranes for fuel cells [19]. PVC blend membranes with high antifouling properties are fabricated by incorporating a novel zwitter ionic polymer into the PVC matrix [22]. Yongsheng Chen et al. fabricated PVC/Fe_2O_3 ultra filtration membranes with good performance [23]. Y. Jafarzadeh et al. developed PVC/PC blend membranes for ultrafiltration [24].

The present work deals with the development of anion-exchange resins by chemical functionalization of phenol-formaldehyde resins with guanidinium groups. First phenol and formaldehyde was condensed in basic medium and the resins obtained were condensed with guanidine hydrochloride in the presence of formaldehyde in basic medium resulting in the formation of cross-linked polymers. The membranes were made

by homogenizing ion-exchange resins and a binder polymer such as PVC in an appropriate solvent such as tetrahydrofuran (THF) followed by solution casting.

6.2. Experimental

6.2.1. Materials

Phenol, formaldehyde solution (37%), tetrahydrofuran (THF), guanidine hydrochloride, and ammonia solution were purchased from Merck. Commercial-grade PVC of high molecular weight was used.

6.2.2. Synthesis of anion–exchange material

Phenol and formaldehyde (40%) in the molar ratio of 1:2 was refluxed in basic medium (pH 9) till a yellow resin was separated from the above reaction mixture. It was taken out, washed with D. I. water and dried. The resin was finely powdered and dispersed in acetone and heated with 1 mole guanidine chloride solution for 2 h at 80°C. The final condensation product was separated from the reaction mixture, washed with water, filtered and dried.

6.2.3 Preparation of anion–exchange membrane

Heterogeneous anion-exchange membrane was prepared by solution casting method. Definite weight of anion–exchange material and PVC powder were stirred in an appropriate solvent such as tetrahydrofuran (THF) for about 8h at room temperature. The homogeneous suspension was cast onto a clean glass plate using a film applicator. Composite membranes were peeled from the glass plate after 48 h. The composite membranes were 80 μm thick. All the membranes were immersed in 2M NaOH solution for 24 h prior to testing. The compositions of the membranes were varied by using different amount of guanidine functionalized anion-exchange material (10 wt%, 20 wt%, 30 wt% and 40 wt %). The corresponding membranes are represented as P1, P2, P3 and P4.

6.2. 4 Characterization Techniques

The membranes were characterized by FT- IR spectroscopy using Perkin Elmer spectrum Two instrument (Model L160000A) over a range of 4000 - 400 cm^{-1}.

The surface morphologies of the composite membranes were examined by a scanning electron microscope (JSM-5600, JEOL Co., Japan). The samples were coated with a thin layer of gold by ion sputtering prior to microscopic examination. The SEM images of the anion-exchange membranes were transformed to a computer and evaluated with an image analysis system.

Thermal degradation experiments of the composite membranes were carried out in Shimadzu TGA-50 thermo gravimetric analyzer. Thermal analyses were completed on thin films having an average mass of 15 mg. The samples were heated from room temperature to 850°C under nitrogen atmosphere at a heating rate of 10°C /min [25].

Water uptake of the composite membranes was determined by weighing the membranes under wet conditions after being equilibrated in distilled water for 24 h at room temperature. The surfaces of the membranes were then carefully wiped with filter paper and the membranes were weighed immediately. The samples were vacuum dried for two days and weighed again.

The water uptake was calculated as follows.

$$Water\,uptake\ (\%) = \frac{W_{wet} - W_{dry}}{W_{dry}} \times 100\,\% \qquad (3)$$

Where W_{wet} is the mass of the water swollen membrane, and W_{dry} is the mass of the dry membrane.

The ion exchange capacities (IECs) of the composite membranes were determined by double titration method. Samples were accurately weighed and were

immersed in 25 ml of 0.05 M HCl solution for 48 h and the HCl solution was back titrated by 0.05M NaOH solution using phenolphthalein as indicator. IECs of the samples were calculated using the equation:

$$\text{IEC} = \frac{n_1 - n_2}{M_{dry}}$$

Where n_1 and n_2 are the amounts of (mmol) hydrochloric acid required before and after equilibrium respectively, and M_{dry} is the mass in g of the dried sample. The average value of the three samples calculated from the above equation is the IEC value of the membrane.

Electrochemical impedance spectroscopy (EIS) techniques were used to evaluate ionic conductivity of the membranes, using AUTOLAB 50519 PGSTAT instrument. Impedance measurements of the membranes were performed in a two electrode setup where the membranes were clamped between two platinum electrodes and the cell was thermostated at 25±0.1°C for at least 20 minutes to ensure thermal equilibrium. Impedance measurements were performed in the frequency range 100 Hz-1000 kHz using an alternating potential of amplitude 10 mV. Fully hydrated membranes were placed in the conductivity cell and it was filled with 1M NaOH. The resistance of the membrane and solution was measured (R_{total}). The resistance of the solution was measured without the membrane ($R_{solution}$). Membrane resistance (R_{mem}) was obtained from the difference of the measured resistances ($R_{mem} = R_{total} - R_{solution}$). Thickness of the membrane was measured with a digital micrometer by placing the membrane between two glass slides to ensure both a planar surface and limited compression. The conductivity of the membrane was calculated as follows $\sigma = L/RA$ mS cm^{-1}, Where σ is the hydroxide conductivity in mS cm^{-1}, R is the ohmic resistance of the membrane (Ω), L is the thickness of the membrane (in cm), A is the cross sectional area of membrane samples (cm^2).

Methanol permeability through the membrane was measured with a homemade apparatus. The measurement is based on the Gasa method [26] which employed a permeation cell derived from Walker et al. [27]. Definite weight of methanol was sealed inside a permeation cell and allowed to diffuse through a hole of area 4 cm^2 covered by a

membrane. Measurements were conducted at room temperature. In fact, permeation process involves dissolution and diffusion of methanol molecules in the membrane materials. The mass of methanol inside the vial as a function of time was measured and the permeability (P) of the membrane was given by the equation:

$$P = \frac{N \times l}{V.P. \times A \times t}$$

where N is the number of moles of methanol lost (moles), l is thickness of the membrane, V. P. is saturated vapor pressure of methanol at 25^{o}C, A is the membrane area for methanol permeation in (cm^2), and t is time (days).

The alkaline stability was measured using 2M aq. NaOH at room temperature. For this purpose, the composite membrane sample was immersed in 2M NaOH at room temperature for 2 weeks. They were taken out, washed with D.I. water, wiped with tissue paper, and then studied using FT-IR technique to detect any degradation or changes in chemical structures. Loss of weight of the membrane was also measured [4,28].

The oxidative stability of membrane was determined by immersing the samples 3cm x 3cm into Fenton's reagent (30 ppm FeSO4 in 30% H_2O_2) for 24 h at 25°C, which was evaluated by recording the weight loss of the membrane with time [29].

All-iron flow battery experiments

All-iron flow battery experiments were performed in a flow cell hardware with electrolyte flowing across two electrodes, separated by the membrane prepared [30]. All experiments were performed with electrolyte flow rates of 25 ml min^{-1}. Electrolyte for both positive and negative electrodes consisted of 1M $FeCl_2$ and 1.5M NH_4Cl. The electrodes were made from graphite plates with a cross-sectional area of 16 cm^2. The charging efficiency of the all-iron redox flow cell was determined by Charging the cell at 100 mA cm^{-2} for 100 s followed by discharging at 50 mA cm^{-2} using AUTOLAB 50519 PGSTAT instrument. The cell performance is determined by its columbic efficiency (CE). CE is the ratio of a cell's discharge capacity (Q_{dis}) to its charge capacity (Q_{ch}).

6.3. Results and Discussion

6.3.1 Structural analysis

Fig. 72(a-e) shows the FT-IR spectra of (a) Guanidinium chloride (b) Anion-exchange material (c) pvc membrane (d) Membrane P2 (e) MembraneP4 respectively. The spectrum (a) of Guanidinium chloride shows broad band in the region 3100-3400 cm^{-1}, due to the stretching vibration of N-H bonds of guanidinium [31]. The peak at 1654 cm^{-1} is attributed to the coupled vibrations of N-H in plane bending vibrations and asymmetric stretching vibrations of C-N group of the guanidinium group [32,33]. The peak at 1198 cm^{-1} is assigned to N-H bending vibration of guanidinium group [32,33]. The spectrum (b) of anion-exchange material shows band in the region 3100-3400 cm^{-1} attributed to the stretching vibrations of N-H groups and O-H stretching vibrations. The absorption peak in the region of 3100-3400 cm^{-1} of the anion-exchange material is weaker, which indicates that the majority of functional groups such as $–NH_2$ offered by guanidine and –OH group of phenol were subjected to condensation reaction with formaldehyde. The peak at 1654 cm^{-1} is a coupled vibration having contributions from both N-H in plane bending vibrations and asymmetric stretching vibrations of C-N groups of guanidinium ion. The absorption peaks at 1504 cm^{-1} is attributed to the vibration of aromatic ring of benzene in phenol [34,35]. The peak at 1078 $cm^{-1}$is assigned to C-O-C ether links formed during condensation reactions with formaldehyde [35]. The spectrum (c) of PVC membrane shows strong signals at 1425 cm^{-1}, 1340 cm^{-1}, 1200 cm^{-1}, 1050 cm^{-1}, 950 cm^{-1} and at 690 cm^{-1}.These correspond to the C-C, C-H and C-Cl vibrations found within the PVC polymer [19,36]. The peak at 1600 cm^{-1}, 1505 cm^{-1} is due to C-C aromatic stretching vibrations of phenyl group [35]. The spectra (d), (e) correspond to that of the membranes (P2 and P4) with increasing amounts of anion-exchange material. In the spectra (d,e) of the membranes show peak in the region of 3000-3400cm^{-1} are corresponding to the stretching vibrations of N-H groups of guanidine and stretching vibrations of O-H groups. The band at 2917 cm^{-1} could be assigned to stretching vibrations of C-H group groups of polymer back bone and band at 1450 cm^{-1} is attributed to bending vibrations of $-CH_2$ group [34]. The peaks at 1600 cm^{-1} and 1505 cm^{-1} are corresponding to C-C aromatic stretching vibrations of phenyl group. The above spectral observations suggest the successful incorporation of anion-exchange material into the polymer matrix [34,37].

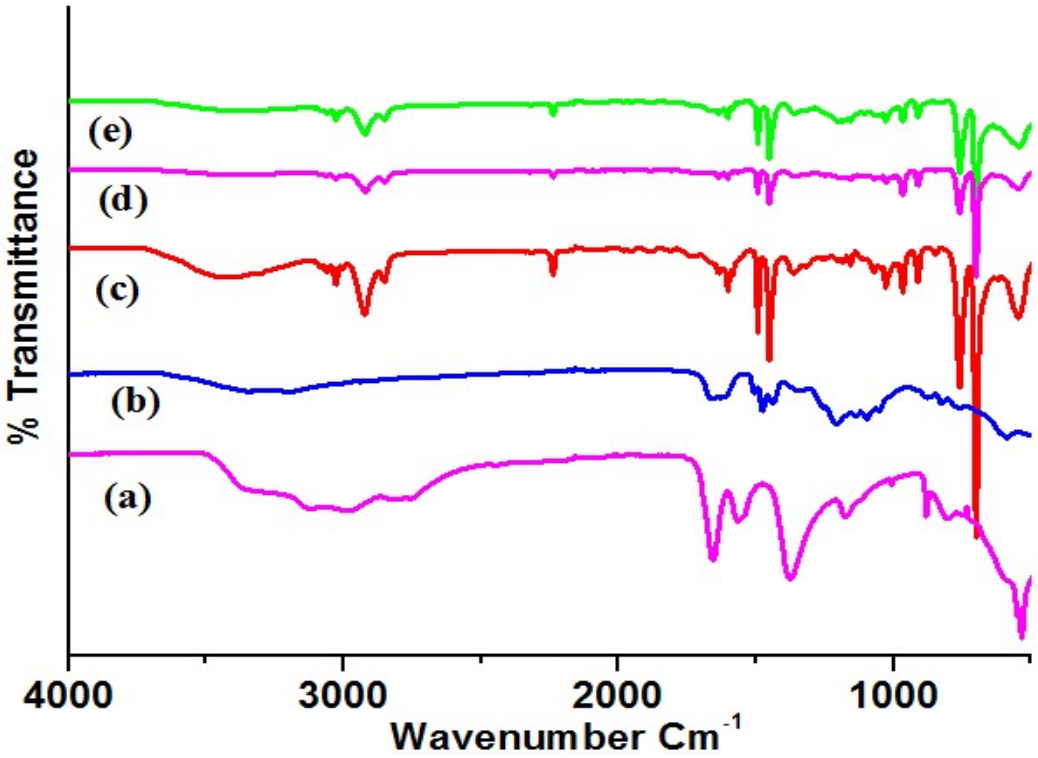

Fig. 72 FT-IR spectrum of (a) Guanidinium chloride (b) anion-exchange material (c) PVC polymer (d) Ion-exchange membrane P2 (e) Ion-exchange membrane P4

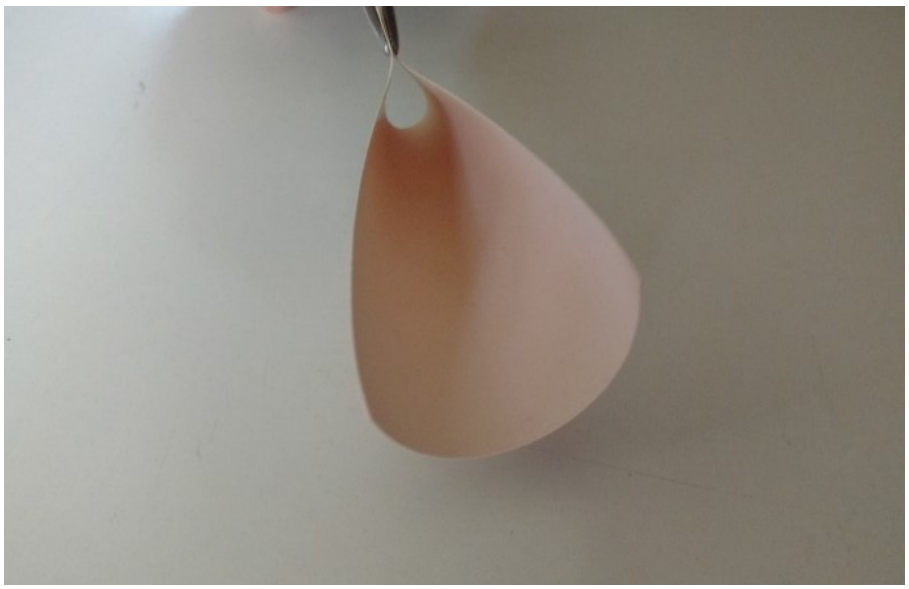

Fig. 73 Photograph of the prepared Ion-exchange membrane P4

6.3.2 SEM analysis

Scanning electron microscopy (SEM) is used to investigate the microstructures of the membranes. **Fig.** 74 (a) shows the SEM image of PVC membrane which presents a smooth and defect free surface of the membrane without any cracks or pinholes, indicating the fine quality of the membrane. **Fig.** 74 (b-c) shows the surface morphology of composite membrane P4 using 40% anion exchange material at different magnifications. Anion exchange materials are found to be uniformly distributed in the polymer matrix, which establishes the connectivity of the composites which enhances compatibility between the matrix and the anion-exchange material. However, some agglomerates can be observed in the composite membranes. **Fig.** 74(d) shows the cross-sectional image of membrane P4 and the thickness of the membrane was 120 μm. The anion-exchange membraneP4 found to be flexible as shown in photograph **Fig.** 73.

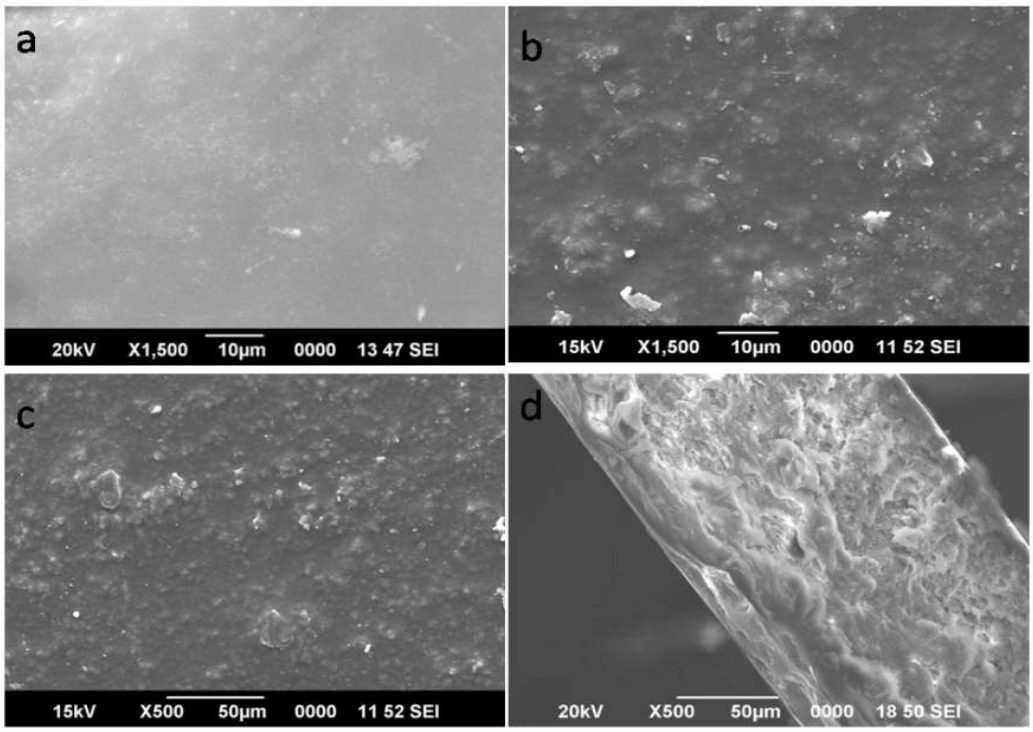

Fig. 74 SEM images of membranes: (a) PVC membrane (b&c) composite membraneP4, using 40% anion exchange material at different magnifications and (d) cross-sectional image of membrane P4.

6.3.3. Water uptake

The water uptake values of the membranes with different contents of anion-exchange material are shown in **Fig.**75. water uptake of AEM is a key factor which determines the performance of electrochemical devices. Higher water uptake values will facilitate hydroxide transport by generating solvated ionic species and broadening ion transport channels, to maintain high ionic conductivity of the materials [38]. Water uptake primarily depends on the microstructure of the membrane and functional groups of ion exchange groups attached to the polymer chains. The water uptake of these membranes, increased moderately with increase in the content of ion-exchange material. This indicates that the water uptake strongly depends on the amount of ion-exchange material. However, excessive water uptake may lead to the deterioration of the AEMs mechanical properties. An ideal AEM should exhibit proper water uptake, high conductivity, and excellent mechanical properties. In these membranes the guanidinium ion exchange group is also thought to participate in absorbing water due to hydrogen bonding capacity.

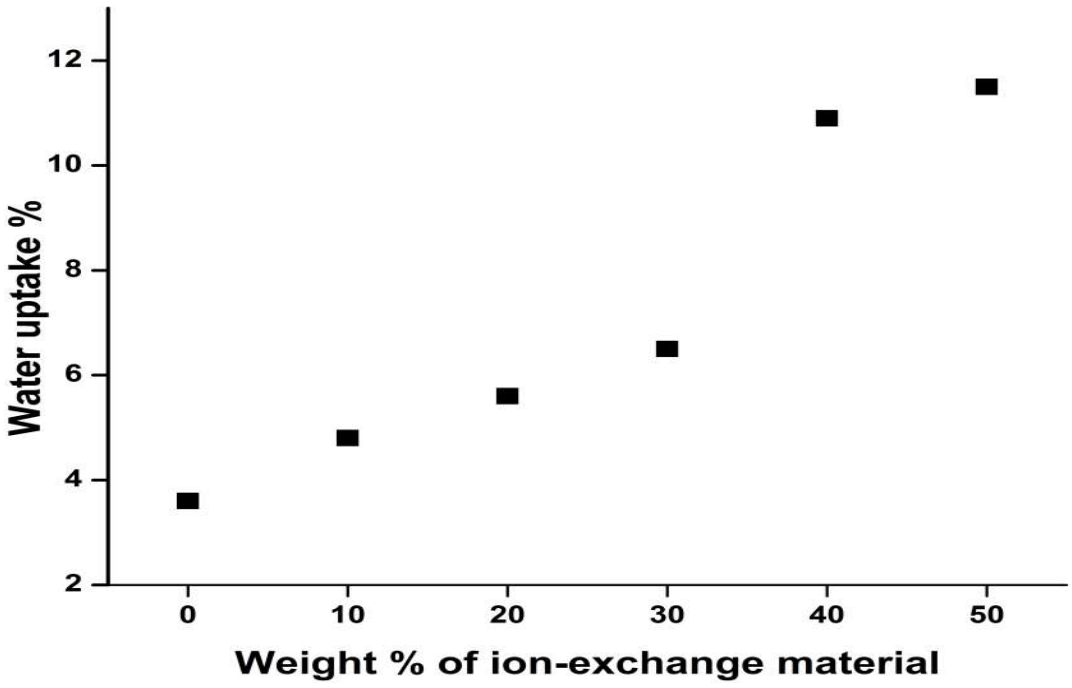

Fig. 75 Water uptake of membranes with varying anion-exchange material content

6.3.4 Ion exchange capacity

The IEC values of the membranes with different contents of anion-exchange material are shown in **Fig.** 76. The IEC gives the amount of the exchangeable groups in the membrane matrix. The IEC values of membranes increased from 0.51 to 1.23 mmol g^{-1}. The IEC value of the membrane found to be increasing with increase in wt% of anion-exchange material. The IEC value of Nafion 117 is 0.90 mmol g-1 [10]. High IEC is attributed to the strong basicity of the guanidinium cation present in the membrane [4]. Higher IEC values facilitate hydroxide ion transport, by generating interconnected ionic conductive channels [2,39]. This will contribute to efficient hydroxide ion conduction through the membrane matrix [40].

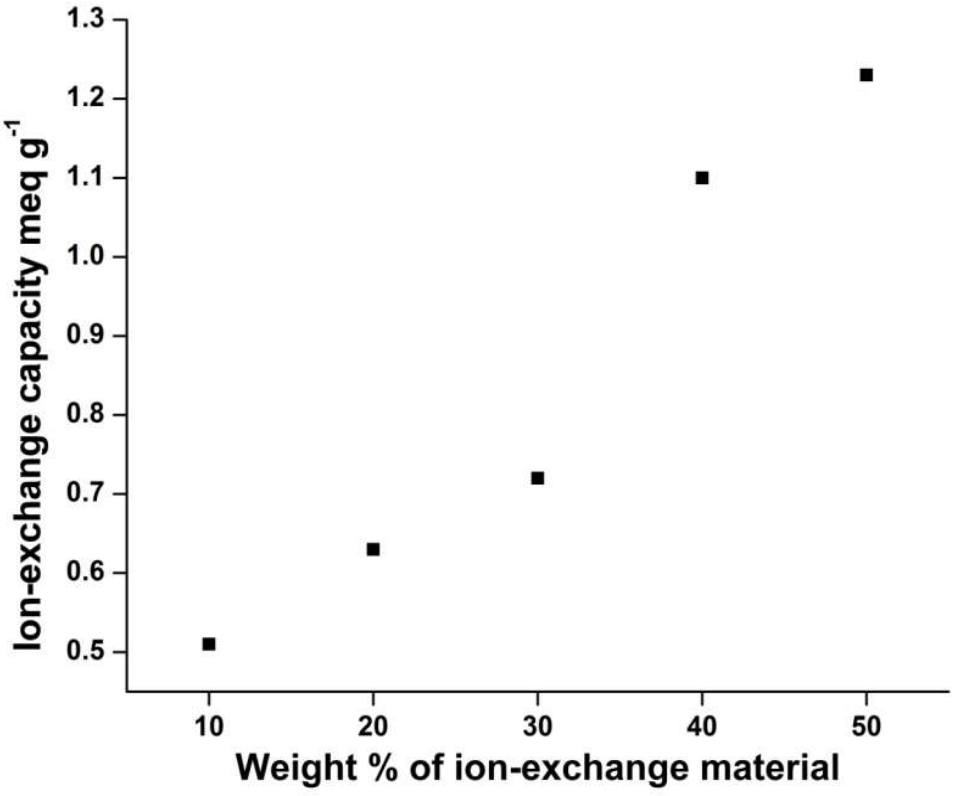

Fig. 76 Ion exchange capacity of membranes with varying anion-exchange material content

6.3.5 Electrical properties

The ionic conductivity of the AEMs is a key factor which determines the performance of electrochemical devices. Herein, the ionic conductivities were examined by electrochemical impedance spectra (EIS recorded in the frequency range of 100 Hz to 1000 kHz and with signal amplitude of 10mv). Nyquist plot for the AEM is presented in **Fig.** 77. The membrane resistance was obtained from the intercept on the Z' axis in the high-frequency region of the Nyquist plot. The ionic conductivities of the AEMs are shown in **Fig.** 78. Conductivities of AEMs increased from 11 to 71 mS cm^{-1} with increase in wt% of ion-exchange material from 10 to 40%.

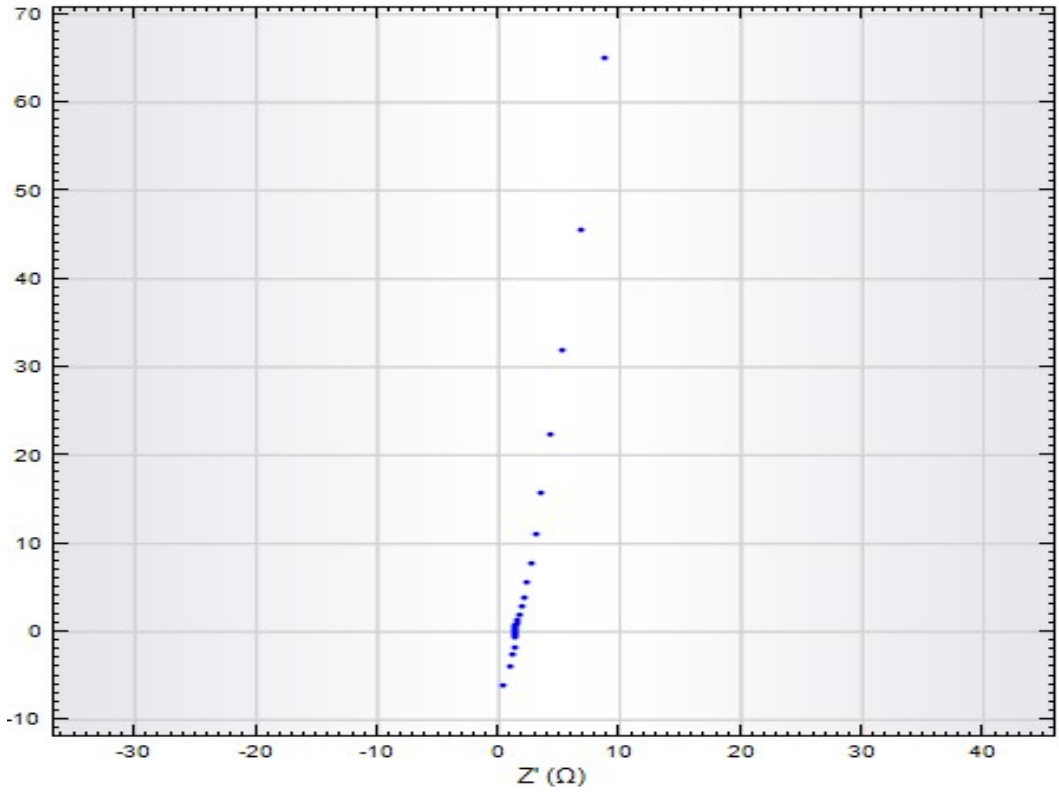

Fig. 77 Nyquist plot for the AEM P4 from AC impedance spectroscopy measurements at room temperature

As shown in **Fig.**78 the ionic conductivity of the fabricated membranes increases with increasing content of ion-exchange material. It can be seen that the appropriate amount of ion-exchange material contributes to the improvement of the conductivity of the composite membranes. Well-distributed hydrophilic guanidine functionalized ion exchange material leads to wider hydrated ion transport channels for the conduction of anions in the membrane. The higher alkalinity of the guanidinium groups has led to the

improvement in ionic conductivity [31]. These are supported by the fact that the increase in ion-exchange material leads to increased water uptake and an increase in ionic conductivity. Hydroxide conduction mainly occurs through the Grotthuss mechanism by the formation and cleavage of the bonds as it diffuses through the hydrogen-bonded network of water molecules [38]. The hydroxyl groups on the solvated guanidinium ion exchange groups will lead to a further increase in the formation and cleavage of bonds of the diffusing hyper-coordinating water molecule. As shown in **Fig.**79 the ionic conductivity of the fabricated membranes decreases with increase in thickness of the membrane.

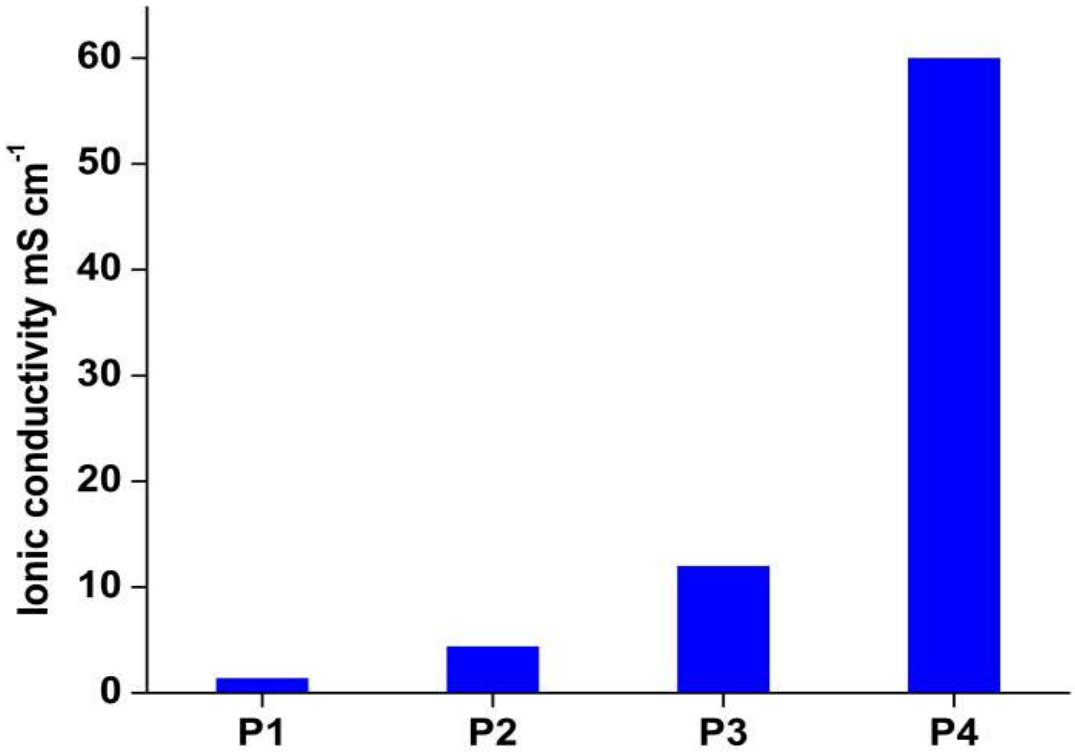

Fig. 78 Ionic conductivity of composite membranes Vs anion-exchange material wt%

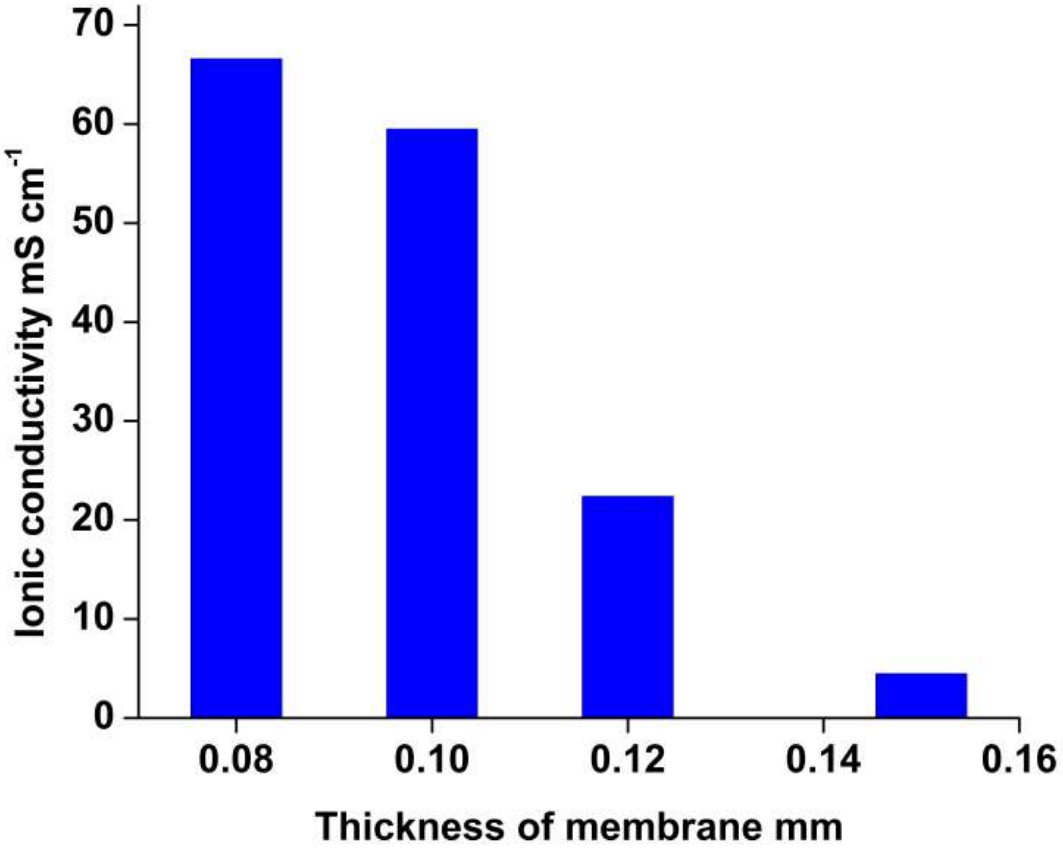

Fig. 79 Ionic conductivity of the composite membranes Vs thickness

6.3.6 Thermo-gravimetric analysis

The thermal stability of the membranes was evaluated using TGA under a nitrogen flow at a heating rate of 10°C min^{-1} from room temperature to 750°C. **Fig.** 80 (a-c) shows TGA curves of (a) pvc membrane, (b) Membrane P2 and (c) Membrane P4. In **Fig.** 80 (a) first weight loss stage of less than 7% occurred from room temperature to 350°C, which was due to the evaporation of absorbed water from the sample and due to the loss of pendant chloride as HCl, leaving residual polyethylene backbone structure. The second weight loss stage appeared from 420 to 450°C, could be attributed to the thermal degradation of the polymer backbone [19]. In **Fig.** 80 (b&c) of P2 and P4 membranes show similar degradation patterns. The first weight loss stage of less than 7% occurred from room temperature to 250°C, which was due to the evaporation of absorbed water from the sample. The second weight loss stage appeared from 420 to 450°C, and could be attributed to the thermal degradation of phenyl groups and the

decomposition of guanidinium groups in the membranes [4]. The third weight loss stage occurred above 500°C and was caused by the decomposition of the polymer's backbone. All the membrane exhibited weight losses of less than 7% below 200°C, indicates the good thermal stability of the fabricated membranes, suitable for practical applications. All the membrane exhibited weight losses of less than 7% below 200°C, indicates the good thermal stability of the fabricated membranes, suitable for practical applications.

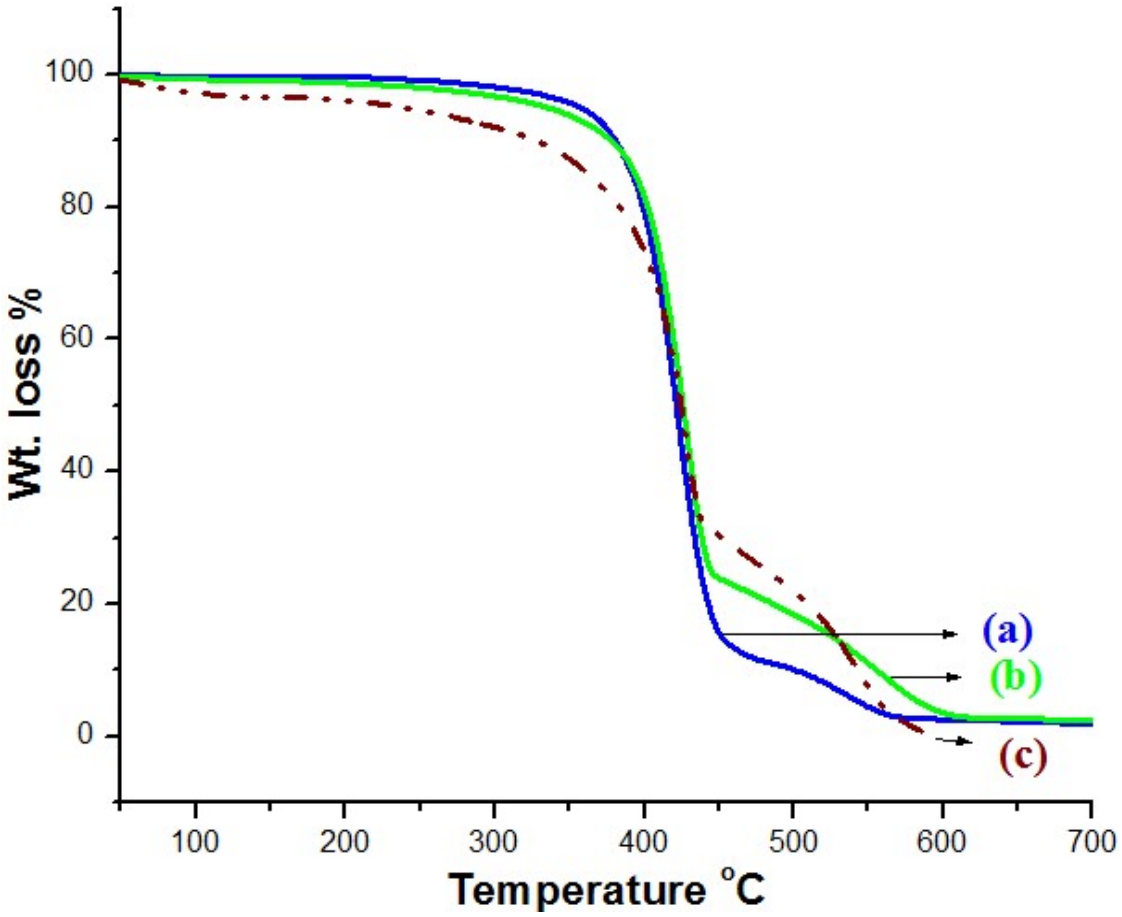

Fig. 80 TGA curves for (a) PVC membrane (b) Membrane P2 and(c) Membrane P4

6.3.7. Chemical stability

The chemical stability of anion-exchange membranes is an important parameter that affects the performance of electrochemical devices, especially at high pH and strong chemical environments. All the membranes retained their shape and flexibility during the alkaline stability test in 2M aqueous NaOH solution for 2 weeks. The conductivity of the membranes do not exhibited any decline after the alkaline stability test. There was no

obvious degradation or weight loss has been took place, the membranes maintained integrity.

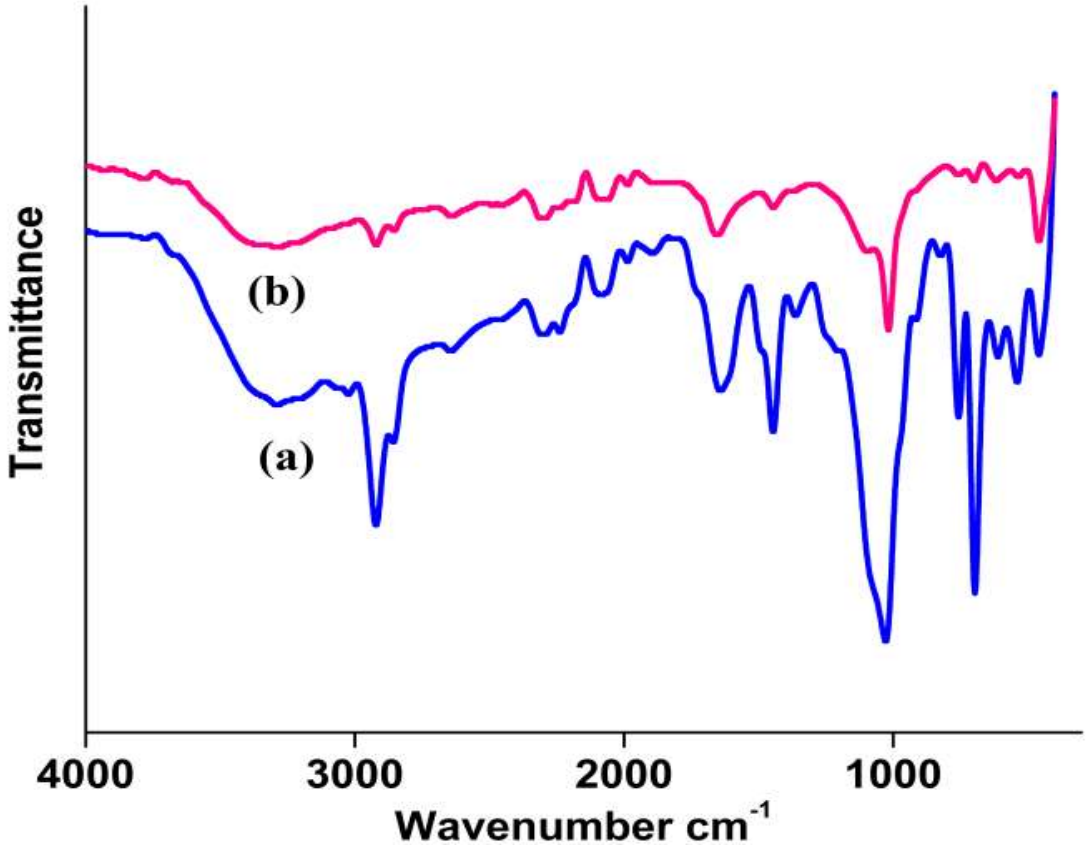

Fig. 81 FT-IR spectrum of the membrane P4 (a) before (b) after alkaline stability test

The comparison of FT-IR results for the membrane before and after alkaline stability test in 2M aqueous NaOH provides further evidence supporting its excellent alkaline stability. As shown in **Fig.** 81, there is no obvious variation in intensity of absorption bands of C-N and -OH groups were observed after 2 weeks of testing in 2 M aqueous NaOH .

The oxidative stability is always a concern for polymer electrolyte membranes which are used in electrochemical devices due to the harsh chemical environments. Hence Fenton's reagent is used to simulate and accelerate the harsh operational environment, in which the $OH^{\cdot}$ and $OOH^{\cdot}$ radicals formed from H_2O_2 can cause the degradation of the AEMs. All the membranes did not show any physical deformation or colour change. These results show good oxidation stability of the membranes.

6.3.8. Methanol permeability

Methanol permeability of membranes at room temperature is shown in **Fig.** 82. It can be seen that the methanol permeability is gradually reduced with increase in the content of ion-exchange material in the membrane. However, the methanol permeability of the synthesized membranes are much lower than that of the Nafion N117 and Tokuyama A201 membrane at room temperature [31]. Hence the fabricated membranes have generally good methanol barrier properties

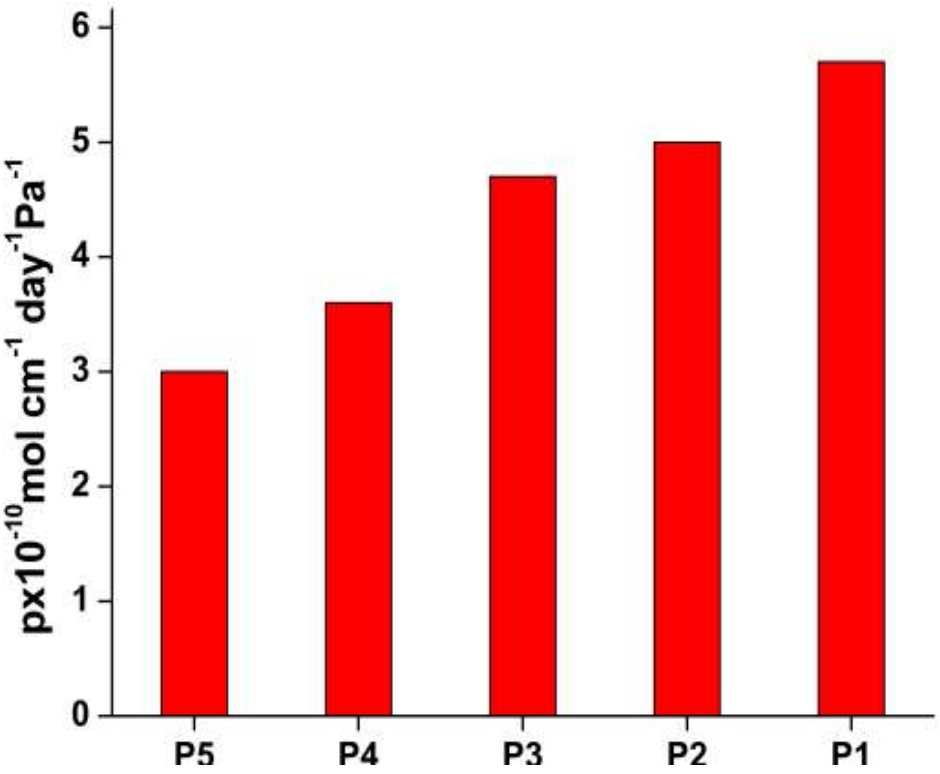

Fig. 82 Methanol permeability values of different membranes

6.3.9. All iron Flow battery studies

The cell voltage-time curve measured during the charging and discharging of an all-iron redox flow cell using the prepared membrane as separator is shown in **Fig.** 83. A constant current density of 100 mA cm^{-2} for charging and 50 mA cm^{-2} for discharging is used. Repeated cycling of the cell with the high-efficiency electrolyte at 100 mA cm^{-2} demonstrated that high columbic efficiency (> 75%) could be maintained over repeated cycles. Higher columbic efficiency indicates low cross-mixing of ions [41]. These results confirm the viability of the new composite membrane as a separator in all-iron redox flow battery.

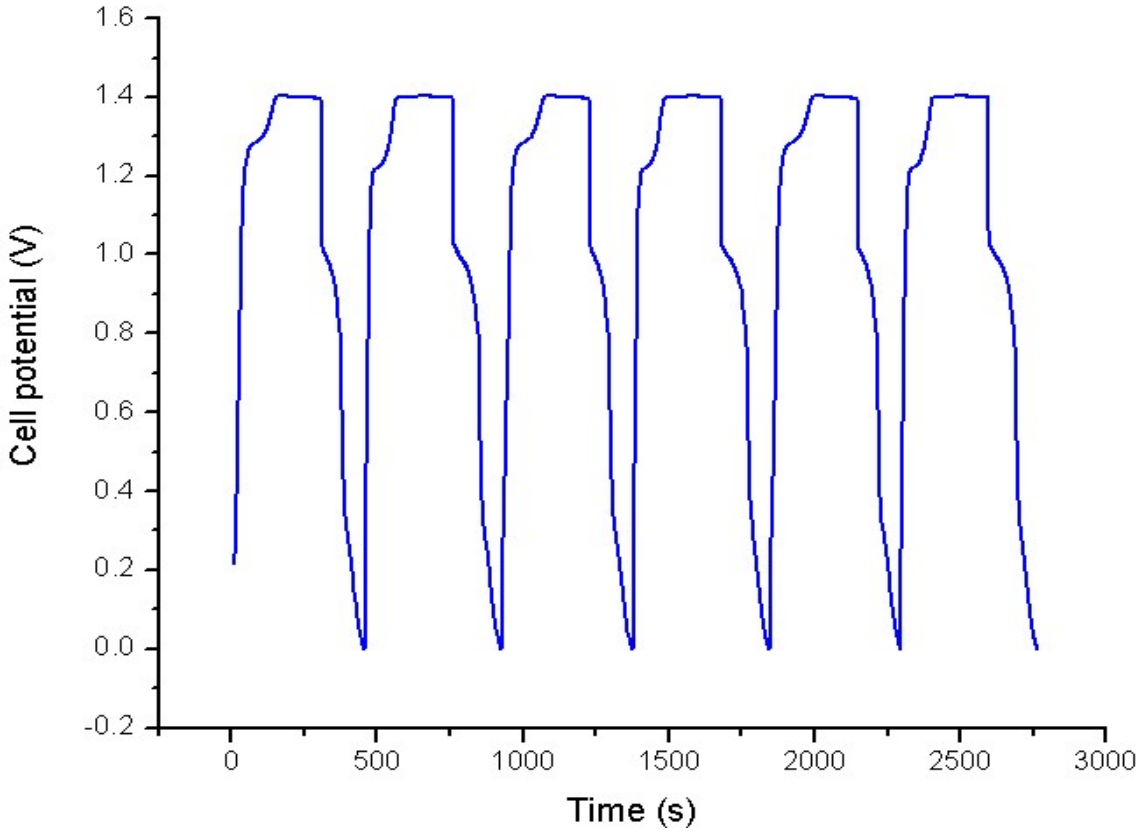

Fig. 83 The cell voltage-time curve of all- iron redox flow cell during galvanostatic charge-discharge experiment

6.4 Conclusions

In summary, we developed a simple and facile method to prepare AEMs with high alkaline stability and enhanced ionic conductivity. The facile nature of the technique offers an attractive alternative to traditional approaches. This method avoids the use of chloromethyl methyl ether, the carcinogenic reagent generally used for AEMs preparation. SEM images of membranes showed a relatively uniform surface for the membranes. The increase of ion-exchange material wt% in casting solution led to an improvement in water content, Ion exchange capacity, and electrical conductivity. In this method the carcinogenic and toxic reagent chloromethyl methyl ether commonly used for AEMs preparation is completely avoided. The TGA analysis of the membranes revealed thermal stability up to 150°C this shows that these membranes are ideal for applications in that temperature range. The composite membranes exhibited enhanced chemical stability in strong chemical environments and this can be attributed to the resonance stabilized guanidine group as anion-exchange site. By considering the AC impedance data, the conductivity measurements showed a marked enhancement in conductivity by increasing the content of ion-exchange material. The electrochemical performance of an all-iron redox flow cell was studied using galvanostatic charge-discharge tests using the above membrane as separator and the system exhibited a columbic efficiency of 80% during the repeated charge-discharge cycles. The results of this study offer an attractive alternative to the traditional approaches for the synthesis of AEMs.

6.5 References

[1] J. Zheng, Q. Zhang, H. Qian, B. Xue, S. Li, S. Zhang, Self-assembly prepared anion exchange membranes with high alkaline stability and organic solvent resistance, J. Memb. Sci. 522 (2017) 159–167. doi:10.1016/ j.memsci.2016.09.021.

[2] L. Liu, C. Tong, Y. He, Y. Zhao, C. Lü, Enhanced properties of quaternized graphenes reinforced polysulfone based composite anion exchange membranes for alkaline fuel cell, J. Memb. Sci. 487 (2015) 99–108. doi:10.1016/j.memsci.2015.03.077.

[3] T. Feng, B. Lin, S. Zhang, N. Yuan, F. Chu, M.A. Hickner, C. Wang, L. Zhu, J. Ding, Imidazolium-based organic-inorganic hybrid anion exchange membranes for fuel cell applications, J. Memb. Sci. 508 (2016) 7–14. doi:10.1016/j.memsci.2016.02.019.

[4] X. Lin, L. Wu, Y. Liu, A.L. Ong, S.D. Poynton, J.R. Varcoe, T. Xu Alkali resistant and conductive guanidinium-based anion-exchange membranes for alkaline polymer electrolyte fuel cells, J. Power Sources. 217 (2012) 373–380.

[5] Y. Liu, B. Zhang, C.L. Kinsinger, Y. Yang, S. Seifert, Y. Yan, C. Mark Maupin, M.W. Liberatore, A.M. Herring, Anion exchange membranes composed of a poly(2,6-dimethyl-1,4-phenylene oxide) random copolymer functionalized with a bulky phosphonium cation, J. Memb. Sci. 506 (2016) 50–59. doi:10.1016/j.memsci. 2016.01.042.

[6] C. M. Tuan, D. Kim, Anion-exchange membranes based on poly(arylene ether ketone) with pendant quaternary ammonium groups for alkaline fuel cell application, J. Memb. Sci. 511 (2016) 143–150. doi:10.1016/j.memsci.2016.03.059.

[7] J. Ran, L. Wu, Y. He, Z. Yang, Y. Wang, C. Jiang, L. Ge, T. Xu, Ion exchange membranes: New developments and applications, J. Memb. Sci. 522 (2017) 267–291.

[8] S. Maurya, S.-H. Shin, Y. Kim, S.-H. Moon, A review on recent developments of anion exchange membranes for fuel cells and redox flow batteries, RSC Adv. 5 (2015) 37206–37230.

[9] G. Merle, M. Wessling, K. Nijmeijer, Anion exchange membranes for alkaline fuel cells : A review, J. Memb. Sci. 377 (2011) 1–35. doi:10.1016/j. emsci.2011.04.043.

[10] C. Qu, H. Zhang, F. Zhang, B. Liu, A high-performance anion exchange membrane based on bi-guanidinium bridged polysilsesquioxane for alkaline fuel cell application, J. Mater. Chem. 22 (2012) 8203–8207. doi:10.1039/c2jm16211c.

[11] Q. Zhang, S. Li, S. Zhang, A novel guanidinium grafted poly(aryl ether sulfone) for high-performance membranes, Chem. Commun. 46 (2010) 7495–7497. doi:10.1039/ c0cc01834a.

[12] Tsutomu Ishikawa, Superbases for Organic Synthesis: Guanidines, Amidines, Phosphazenes and Related Organocatalysts, John Wiley & Sons, Ltd 2009. doi:10.1351/pac198860111627.

[13] Brydson J., Plastics materials, Butterworth - Heinemann Ltd, Linacre House, Jordan Hill , Oxford OX2 8DP, 1966.

[14] W. Hesse, L. Jürgen, Phenolic resins, Ullmann's Encycl. Ind.Chem (2011) 1129–1147. doi:10.1002/14356007.a19_371.pub.

[15] M. Luqman, Ion exchenge technology Springer, 2013. doi:10.1007/978-94-007-1700-8.

[16] S. D. Alexandratos, Ion-Exchange Resins : A Retrospective from Industrial and Engineering Chemistry Research, Ind. Eng. Chem. Res. 48 (2009) 388-398. doi:10.1021/ie801242v.

[17] Y. Wang, T. Xu, Ion exchange membranes, Encycl. Membr. Sci. Technol. (2013) 1–58.

[18] T. Sata, Ion Exchange Membranes Preparation, Characterization, Modification and Application, The Royal Society of Chemistry, Thomas Graham House, Science Park, Milton Road, Cambridge CB4 OWF, UK 2002.

[19] J. T. S. Allan, L. E. Prest, E. B. Easton, The sulfonation of polyvinyl chloride : synthesis and characterization for proton conducting membrane applications, J. Memb. Sci. (2015). doi:10.1016 /j.memsci.2015.03.093

[20] Z. Maghsoud, M. Pakbaz, M. Hossein, N. Famili, S.S. Madaeni, New Polyvinyl chloride/Thermoplastic Polyurethane Membranes with Potential Application in Nanofiltration, J. Memb. Sci. (2017). doi:10.1016/j.memsci.2017.07.001.

[21] Q. F. An, J. W. Qian, H. B. Sun, L. N. Wang, L. Zhang, H. L. Chen, Compatibility of PVC/EVA blends and the pervaporation of their blend membranes for benzene/cyclohexane mixtures, J. Memb. Sci. 222 (2003) 113–122. doi:10.1016/S0376-7388(03)00260-6.

[22] L. Fang, S. Jeon, Y. Kakihana, B. Zhu, H. Matsuyama, Improved antifouling properties of polyvinyl chloride blend membranes by novel phosphate based-zwitterionic polymer additive, J. Memb. Sci. (2017). doi:10.1016/j.memsci.2017.01.044.

[23] E. Demirel, B. Zhang, M. Papakyriakou, S. Xia, Y. Chen, Fe_2O_3 nanocomposite PVC membrane with enhanced properties and separation performance, J. Memb. Sci. 529 (2017) 170–184. doi:10.1016/j.memsci.2017.01.051.

[24] A. Behboudi, Y. Jafarzadeh, R. Yegani, Polyvinyl Chloride/poly carbonate blend ultrafiltration membranes for water treatment, J. Memb. Sci. (2017). doi:10.1016/j.memsci. 2017.04.011.

[25] M. L. Di Vona, R. Narducci, L. Pasquini, K. Pelzer, P. Knauth, Anion-

conducting ionomers : Study of type of functionalizing amine and macromolecular, Int. J. Hydrogen Energy. 39 (2014) 14039–14049. doi:10.1016/j.ijhydene.2014.06.166.

[26] J. V. Gasa, R. A. Weiss, M. T. Shaw, Ionic crosslinking of ionomer polymer electrolyte membranes using barium cations, J. Memb. Sci. 304 (2007) 173–180. doi:10.1016/j.memsci.2007.07.031.

[27] M. Walker, K. Baumgärtner, Barrier properties of plasma-polymerized thin films, Surf. Coatings Technol. 119 (1999) 996–1000. doi:10.1016/S0257-8972(99)00216-9.

[28] B. Lin, L. Qiu, J. Lu, F. Yan, Cross-linked alkaline ionic liquid-based polymer electrolytes for alkaline fuel cell applications, Chem. Mater. 22 (2010) 6718–6725. doi:10.1021/cm102957g.

[29] T. Wang, F. Sun, H. Wang, S. Yang, L. Fan, Preparation,properties of pore-filling membranes based on sulfonated copolyimides and porous polyimide matrix, Polymer (Guildf). 53 (2012) 3154–3162. doi:10.1016/j.polymer.2012.05.049.

[30] A. K. Manohar, K. M. Kim, E. Plichta, M. Hendrickson, S. Rawling, S.R. Narayanan, A High Efficiency Iron-Chloride Flow Battery for Large-Scale Energy Storage, J. Electrochem. Soc. 163 (2016) 5118–5125. doi:10.1149/2.0161601jes.

[31] S. D. Sajjad, D. Liu, Z. Wei, S. Sakri, Y. Shen, Y. Hong, F. Liu, Guanidinium based blend anion exchange membranes for direct methanol alkaline fuel cells (DMAFCs), J. Power Sources. 300 (2015) 95–103. doi:10.1016/j.jpowsour.2015.08.002.

[32] C. J. Antony, M. J. Bushiri, H. Tresa, C. Y. Panicker, M. Fleck, Spectroscopic properties of guanidinium zinc sulphate $[C(NH_2)_3]_2Zn(SO_4)_2$ and ab initio calculations of $[C(NH_2)_3]_2$ and $HC(NH_2)_3$ C.J., Spectrochim. Acta Part A Mol. Biomol. Spectrosc. 73 (2009) 942–945. doi:10.1016/j.saa.2009.04.024.

[33] M. S. Braiman, D. M. Briercheck, K. M. Kriger, Modeling Vibrational Spectra of Amino Acid Side Chains in Proteins : Effects of Protonation State, Counterion, and Solvent on Arginine C-N Stretch Frequencies, J. Phys. Chem. B. 103 (1999) 4744–4750.

[34] L. Yanshan, W. Shujun, L. Hongyan, M. Fanbin, M. Huanqing, Preparation and characterization of melamine/formaldehyde/ polyethylene glycol crosslinking copolymers as solid – solid phase change materials, Sol. Energy Mater. Sol. Cells. 127 (2014) 92–97. doi:10.1016/j.solmat.2014.04.013.

[35] I. Poljanšek, M. Krajnc, Characterization of Phenol-Formaldehyde Prepolymer Resins by In Line FT-IR Spectroscopy, Acta Chim. Slov. 52 (2005) 238–244.

[36] S.H.M. R.Q. Fu, J. J. Woo, S. J. Seo, J. S. Lee, Sulfonated poly styrene/polyvinyl chloride composite membranes for PEMFC applications, J. Memb. Sci. 309 (2008) 156–164.

[37] H. Zhao, Q. Li, A Facile Route for Nitrogen-Doped Hollow graphitic Carbon Spheres with Superior Performance in Supercapacitors, J. Mater. Chem. 48 (2012) 1–8.

[38] G. Merle, M. Wessling, K. Nijmeijer, Anion exchange membranes for alkaline fuel cells : A review, J. Memb. Sci. 377 (2011) 1–35. doi:10.1016/j.memsci.2011.04.043.

[39] W. Chen, X. Yan, X. Wu, S. Huang, Y. Luo, X. Gong, G. He, Tri-quaternized poly(ether sulfone) anion exchange membranes with improved hydroxide conductivity, J. Memb. Sci. 514 (2016) 613–621. doi:10.1016/j.memsci.2016.05.004.

[40] S. Sharma, M. Dinda, C. R. Sharma, P. K. Ghosh, A safer route for preparation of anion exchange membrane from inter-polymer film and performance evaluation in electrodialytic application, J. Memb. Sci. 459 (2014) 122–131. doi:10.1016/j.memsci.2014.02.011.

[41] X. Li, H. Zhang, Z. Mai, H. Zhang, I. Vankelecom, Ion exchange membranes for vanadium redox flow battery (VRB) applications, Energy Environ. Sci. 4 (2011) 1147. doi:10.1039/c0ee00770f.

CHAPTER 7

SUMMARY AND CONCLUSION

The first chapter in this thesis presents a description about the classification of ion-exchange membranes, transport mechanisms in anion-exchange membranes, chemical stability of anion-exchange membranes, strategies for improving the chemical stability of anion-exchange membranes, anion-exchange membrane preparation methods and the applications of anion-exchange membranes as separators in electrochemical devices like flow batteries and fuel cells.

Chapter 2 of this thesis describes various experimental techniques and methods used for the characterization of the anion-exchange materials and prepared membranes. Characterizations were done using FT-IR, SEM, TEM, XRD and EDAX techniques. The properties of the membranes such as ion-exchange capacity, water uptake, alkaline stability, oxidative stability, methanol permeability, tensile strength, impedance and ionic conductivity were also measured.

Chapter 3 of this thesis describes the synthesis of inorganic anion- exchange material, calcium titanate (perovskite) nanopowder by precipitating mixed oxalate and hydroxide of calcium and titanium $[CaTi(OH)_x(C_2O_4)_y]$ from a solution of potassium titanyl oxalate and calcium chloride in ammoniacal medium followed by calcination. The XRD pattern revealed the formation of phase pure orthorhombic calcium titanate. The crystalline nature of the particles was revealed by HRTEM image, and the shapes of the particles were found to be spherical, with an average size of 200 nm. Selected area electron diffraction (SAED) pattern revealed the crystalline nature of the material and the rings in the SAED pattern corresponds to the crystal planes of calcium titanate. Morphological features were investigated with SEM, and the $CaTiO_3$ particles were found to be spherical with a diameter of approximately 200 nm.

Chapter 4 of this thesis includes the development of polyvinyl alcohol/calcium titanate nanocomposite anion-exchange by incorporating calcium titanate nanoparticles ($CaTiO_3$) into polyvinyl alcohol matrix. The PVA/$CaTiO_3$ nanocomposite membranes

30 wt% $CaTiO_3$ were found to have an ionic conductivity of 66 mS cm^{-1} at room temperature. The electrochemical performance of an all-iron redox flow cell was studied using galvanostatic charge-discharge tests using the above membrane as separator and the system exhibited a coulombic efficiency of 75% during the charge-discharge cycles.

Chapter 5 in this thesis describes a novel approach for the synthesis of highly stable guanidinium functionalized homogeneous membrane based on PVA prepared by the oxidation of PVA to polyvinyl ketone using $KMnO_4$ followed by guanidination and cross-linking. The resultant membranes were flexible and tough enough for electrochemical applications. The membranes showed ionic conductivity of 70 mS cm^{-1} at room temperature, excellent tensile strength, thermal stability and good chemical stability in strong chemical environments. The electrochemical performance of an all-iron redox flow cell were studied using galvanostatic charge-discharge tests using the above membrane as separator and the system exhibited columbic efficiency above 75%.

Chapter 6 of this thesis includes the synthesis of anion-exchange material by condensation of phenol and formaldehyde in basic medium followed by condensation reaction with guanidine chloride. The anion-exchange material was dispersed in PVC polymer matrix for membrane preparation. The membranes with 40 wt% ion-exchange resin content possess ionic conductivity of 67 mS cm^{-1} at room temperature. The anion-exchange membranes exhibited good thermal stability up to 150°C and this shows that these membranes are ideal for applications in that temperature range. Membranes showed excellent chemical stability and mechanical properties without any loss of ion conductivity under alkaline and oxidative conditions. The electrochemical performance of an all-iron redox flow cell was studied using galvanostatic charge-discharge tests using the above membrane as separator and the system exhibited a columbic efficiency of 80% over the repeated charge-discharge cycles.